MAGNETIC ORDERING IN SYSTEMS OF REDUCED DIMENSIONALITY

Stuart Purdie

A Thesis Submitted for the Degree of PhD
at the
University of St Andrews

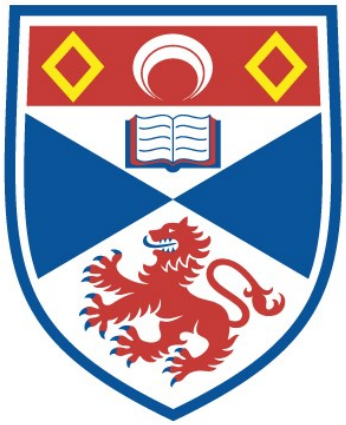

2005

Magnetic ordering in systems of reduced dimensionality

A thesis presented to the
University of St Andrews for the
degree of Doctor of Philosophy

Stuart Purdie

November, 2004

ProQuest LLC.
789 East Eisenhower Parkway
P.O. Box 1346
Ann Arbor, MI 48106 – 1346

Abstract

The magnetic behaviour of thin films of (111) FCC structures and (0001) corundum structed materials were studied by the mean field analysis and some Monte Carlo simulation. These models were conditioned on a mapping from first principles calculcations to the Ising model. The effect of the sugested octopolar reconstruction for the polar (111) surfaces of FCC was also examined.

Declarations

I, Stuart Purdie, hereby certify that this thesis, which is approximately 35000 words in length, has been written by me, that it is the record of work carried out by me and that it has not been submitted in any previous application for a higher degree.

Date 30/11/04 Signature of candidate

I was admitted as a research student in September 2000 and as a candidate for the degree of Ph.D. in july 2001; the higher study for which this is a record was carried out in the University of St Andrews between 2000 and 2003.

Date 30/11/04 Signature of candidate

I hereby certify that the candidate has fulfilled the conditions of the Resolution and Regulations appropriate for the degree of Ph.D. in the University of St Andrews and that the candidate is qualified to submit this thesis in application for that degree.

Date 30/11/04 Signature of supervisor

In submitting this thesis to the University of St Andrews I understand that I am giving permission for it to be made available for use in accordance with the regulations of the University Library for the time being in force, subject to any copyright vested in the work not being affected thereby. I also understand that the title and abstract will be published, and that a copy of the work may be made and supplied to any bona fide library or research worker.

Date 30/4/04 Signature of candidate

Contents

Chapter 1

Introduction

Thin films of magnetic materials have technological relevance, particularly in giant magneto-resistance devices, and in spintronic systems. Giant magneto-resistance (GMR) devices [1, 2] consist of many layers of material that would be ferromagnetic in bulk, intercalated with layers of a diamagnetic material. These systems have an antiparallel ordering of the magnetic layers, for a specific range of spacer thicknesses. An applied magnetic field can override this coupling, and cause the magnetic moments to align. This process causes a change in the electrical resistance of the GMR device. By selection of materials for the ferromagnetic and diamagnetic layers, and the thickness and number of each layer, the properties of the device can be tuned. These devices show great promise for use as sensors of magnetic field, in applications such as hard disk read heads.

A spin valve, defined here as a system that exploits the spin of an electron, generally works by pulling electrons into a semiconductor, through a ferromagnetic layer [3]. These devices are also sensitive to magnetic fields,

although they operate at lower applied fields, and have a smaller magnetoresistance than GMR devices. However, spin valves offer potential for spintronic devices, which are defined as "devices where the direction that the spin of the electron is pointing is at least as important as the charge of the electron", a definition first coined by Lucent technologies [4].

The typical method of construction for a spin valve is with two layers of a ferromagnetic material, separated by a diamagnetic spacer. One layer is made magnetically "hard", generally by pinning it with an antiferromagnetic layer. The other layer is then magnetically "soft", and can respond to applied fields. Figure 1.1 shows a schematic of a typical spin valve system.

Although the properties of these devices as assemblies are understood, the properties of each film in isolation have not been subject to much scrutiny.

The first hurdle in the experimental examination of a surface or thin film is to prepare that surface. A semi-infinite surface is simply a sample where the surface properties are studied, and the thickness of the system is large compared to the surface effects. These are theoretically distinct from the thin films, but are related in terms of the experimental techniques used to study them.

Compared with bulk material, the desire to examine different crystallographic surfaces is an immediate complicating factor. One of the more desirable methods of producing a semi-infinite surface is by cleaving a sample, to produce the desired face [5, 6]. Surfaces can be examined by cutting to that plane and polishing [7]. To finish, the surface it is sputtered under UHV, and then annealed in oxygen. The major deficiency with this technique is that surfaces so produced often tend to facet during the preparation.

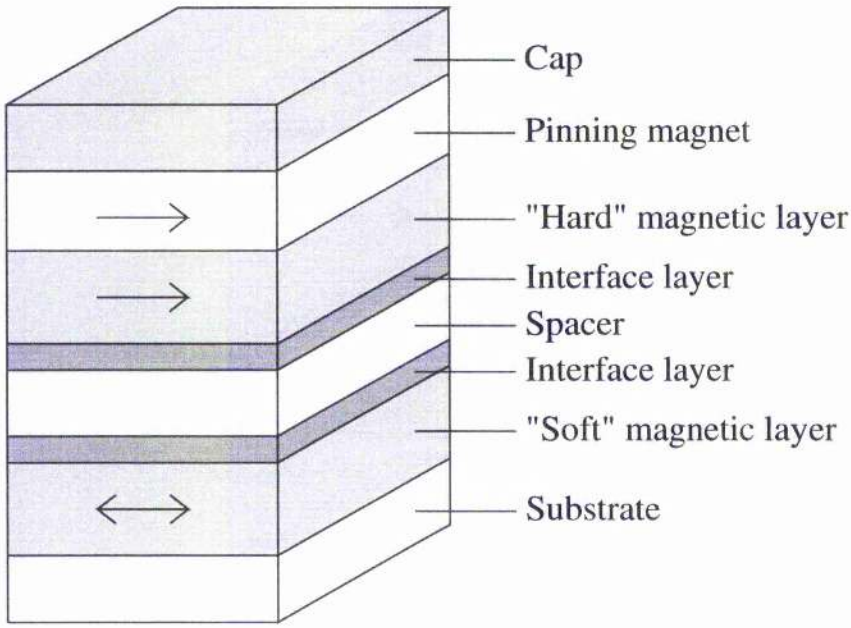

Figure 1.1: A schematic of a typical spin valve. The interfacial layers prevent chemical interaction of the magnetic layers and the spacer. The substrate and cap are not functional parts of the system.

The most common method of preparation of thin films of oxides is to grow them on a suitable substrate. Most substrates will be a stable, semi-infinite surface. One simple way is to prepare a metal surface, and oxidise the surface in a controlled manner, to grow an oxide film. The orientation of the film produced depends on the orientation of the substrate, and the quality of the film depends on lattice mismatch between the film and the substrate. A number of films have been produced by this method [8], including FeO on Fe [9] and NiO on Ni [10], although it is not suitable for all oxides. Occasionally

use of an alloy substrate is better suited to growth of the oxide film, such as Al_2O_3 on NiAl [11], in this case due to the greater melting point of the alloy. If direct growth is not possible, then more sophisticated methods exist, such as chemical vapour methods [12], sol-gels [13] and solution based methods [14]. Heteroepitaxial growth, by depositing a metal and then oxidising, has also been reported, such as FeO on Pt [15]. Hematite films have been grown by use of molecular beam epitaxy [16, 17] on sapphire.

The most significant problem with surface or film preparation comes from the unstable surfaces. Such surfaces are difficult to prepare in controlled form for study. One major group of unstable surfaces are the dipolar surfaces. As shown by Lacman [18], this is because of the infinite surface energy of the dipolar surfaces, due to the macroscopic dipole moment of the film. Tasker [19] classified surfaces into three types, of which the first two have zero dipole moment perpendicular to the surface, and a third type surface which has a non-zero dipole moment, and thus is unstable. The electrostatic energy of a slab with such a surface [20] is given in equation 1.1, where N is the number of bilayers, d is the separation between the two charged layers in a bilayer, and σ is the charge per layer.

$$E = 2\pi N d\sigma^2 \tag{1.1}$$

Clearly, the energy increases with the number of bilayers, N, increases, and for macroscopic thicknesses the energy tends to ∞. Thus as systems get thicker, this dipolar energy would dominate the system, unless the system is very thin, or stabilised by some method.

The most common method of surface stabilistion is by reconstruction, to quench the dipole moment. For NiO(111) on Ni(100), no reconstruction was found [21], but other substrates for NiO(111) [22, 23] all show a p(2x2) pattern in low energy electron diffraction (LEED) analysis. The most likely candidate for this p(2x2) reconstruction is the octopolar reconstruction [24], where 75% of the outermost layer is removed, and 25% of the layer beneath, which results in {100} nanofacets in the surface. Both oxygen and metal terminated surfaces have been observed in NiO(111), as opposed to CoO(111) on Co(0001) [25], where only oxygen terminated surfaces have been observed. The CoO(111) surfaces appear to be stabilised by hydroxyl groups, which obscure investigation of any reconstruction. FeO(111) grown on Fe(110) and Fe(111) [26] shows a p(2x2) reconstruction, like NiO(111). MgO films have been produced [27], and show a number of reconstructions, of which a p(2x2) is one [28].

For a theoretical study on magnetic oxides, a high degree of accuracy is required, as the individual magnetic interactions are very much smaller than the electrostatic interactions. The first ab initio study was done in 1993 [29], on VO, MnO and NiO compared to the non-magnetic CaO, by the unrestricted Hartree-Fock (UHF) method. Structural optimisations were carried out, and the calculated lattice parameters were found to be within 2.5% of the experimental value, except for the case of VO, which is always defective. This error is similar to that found for a wide range of other ionic oxides. Local magnetic moments were found to be in good agreement with the experimental values and the systems were found to be high spin antiferromagnetic insulators, in agreement with experiment. A further study [30] showed that

the difference in energies between ferromagnetic and antiferromagnetic states in MnO and NiO agree with the differences in Néel temperature between the two oxides. The effect of magnetostriction, a distortion in the system perpendicular to the isomagnetic planes was found to be in close agreement with the experimental values. When described as the deviation from the cubic angle, the theory predicted 0.47°and 0.075°for MnO and NiO respectively, as compared to experimental values of 0.62°[31] and 0.1°[32].

Two magnetic transition metal oxides with the corundum structure have also been studied by UHF. The first of these studies, on α-Fe_2O_3 (hematite) [33], showed that the experimental magnetic ordering ($R\bar{3}$) was predicted by theory, whilst the second on Cr_2O_3[34] showed that its different experimental magnetic ordering (R3c) was also predicted by UHF calculations. A later paper extended this study to the hypothetical Co_2O_3 and Ni_2O_3 [35], predicting the same magnetic ground state as for hematite.

A combined theoretical and experimental study [36] using X-ray diffraction data, for both semi-infinite surfaces and films, found an octopolar reconstruction in NiO(111) surfaces. One interesting aspect is that magnetic moments on the oxygen sites were observed, at the surface. A grazing incidence x-ray diffraction (GIXD) study on similar surfaces [37] also shows the octopolar reconstruction. Both studies show only Ni termination for the semi-infinite surfaces. Studies on other materials, however, such as MgO(111) [28] show other reconstructions, namely as $(\sqrt{3}x\sqrt{3})R30°$and $(2\sqrt{3}x2\sqrt{3})R30°$.

GIXD studies [38] on MgO(111) showed the existence of an oxygen terminated octopolar reconstruction, but also other surface terminations, depending on the surrounding atmosphere. In particular it proposed a surface

reconstruction that is chemically favoured over the octopolar reconstruction in oxygen poor environments, being a layer of (0001) Mg over an oxygen terminated octopolar surface, called α-Mg/OMg. A similar reconstruction has been seen in other rocksalt structures, depending on the ambient conditions.

A major theme of this thesis is the modeling of magnetic ordering, using a next nearest neighbour Ising model, where the values of the coupling constants are derived from some more complete model. These two constants are J_d, the nearest neighbour coupling constant, and J_{se}, the next nearest neighbour constant. For MnO (and NiO), a UHF study [30] found a value of 0.05 meV for J_d and 2 meV for J_{se}, both favouring antiparallel alignment, and for NiO a J_d of 1.5 meV and J_{se} of 7 meV, again both favouring antiparallel alignment.

Moreira et al [39] used a large number of different quantum mechanical formulations to evaluate the behaviour of NiO, including its magnetic exchange constants. In addition to Hartree-Fock and LDA DFT (with Dirac-Slater local exchange, and the LDA correlation functionals), a number of hybrid functionals were utilised. Mixing 50% Hartree-Fock exchange energy and 50% Dirac-Slater local exchange, with the LDA correlation functional (Fock-50), and 35% Hartree-Fock exchange energy and 65% Dirac-Slater local exchange, again with the LDA correlation functional (Fock-35), gave a range of functionals with a smooth progression. Although called LDA, it is more correct to refer to the DFT functionals as local spin density (LSD) formulations. The popular B3LYP functional was also used. As well as these, a series of cluster based CI calculations were performed, giving a wide range of computational conditions. The LDA approach was noted to predict a metal-

lic state for NiO, as was previously known, but all the other calculations predicted a magnetic insulator. All schemes disagreed with experimental observations for some physical parameter, although it was noted that Fock-35 seemed to give best all round agreement. The calculated coupling constants are sumarised in table 1.1.

In an attempt to improve the LSD approximation, a correction for its self-interaction can be applied. This leads to the SIC-LSD (self interaction correction) calculation schema. A study on NiO [40] calculated exchange constants both in the bulk and on the (100) surface, where the surface values were calculated for a 7 layer and an 11 layer film. Two different sets of constants were considered, those in the plane, and those out of the plane, and the values for the outermost layers are given in the table. The film calculations were performed with the additional basis, and showed an enhancement of the out of plane superexchange coupling of around 40%, with a slight decrease in in-plane coupling.

A cluster CI calculation [41] calculated values for the superexchange coupling constant only, in the bulk and at the (100) surface of NiO, and found that the value at the surface was around 20% that of the bulk. Two CI methods were used - complete active space self consistent field (CASSCF), and complete active space second order perturbation (CASPT2), which used CASSCF as the zeroth order term in a perturbation expansion, to correct for dynamic electron correlation. These calculations were also performed with additional basis functions between the atom locations, which was referred to as extended active space (EAS) calculation.

Experimental determination of the coupling constants is difficult, not

least given the small values they have, compared to other aspects of the system. There have been a number of determinations, from various methods, for NiO.

Magnetic susceptibility [42] data as a function of temperature was used with a random phase approximation Greens function theory [43] to give estimates of the coupling constants. An earlier study [44] used low temperature powder susceptibility data for J_{se} and susceptibility at the Néel point for J_d found that J_d was antiferromagnetic in character, in contradiction to the consensus.

Inelastic neutron scattering [45] has been used to measure spin-wave dispersions, from which the coupling can be estimated. Although the values were strictly for a Heisenberg spin Hamiltonian, the Ising model is a simpler decomposition of the Heisenberg model for the case of co-linear spins.

An analysis of weak peaks in Raman scattering of NiO [46] attributes some peaks to a four magnon process. Making the assumption that J_d is 0 allows an estimate of J_{se} to be made.

A band theory based theoretical approach [47] was used to evaluate various parameters for the three systems MnO, MnS and NiO. The authors noted that the calculation of the coupling constants, within a Heisenberg model, were too large by a factor of around three, although qualitatively correct. NiO was estimated to have a J_d of 5.3 meV and J_{se} of 106 meV, giving a ratio of 0.05. For MnO, J_d was predicted to be 2.61 meV and antiferromagnetic in character, and a J_{se} of 2.57, giving a ratio of -1.01. With MnS, both constants were again antiferromagnetic in character with J_d 0.86 meV and J_{se} 2.32, the ratio being -0.37.

Method	J_d (meV)	J_{se} (meV)	Ratio $\frac{J_d}{J_{se}}$	Source
Magnetic susceptibility	2.9	17.4	0.17	[42]
Magnetic susceptibility	-1.4	17.3	-0.08	[44]
Spin wave dispersion	1.4	19.0	0.08	[45]
Raman scattering	0	19.8	0	[46]
Periodic UHF	0.05	0.2	0.25	[30]
Periodic UHF	1.0	5.4	0.19	[39]
Periodic Fock-50	2.2	12.9	0.17	[39]
Periodic Fock-35	2.4	21.9	0.11	[39]
Periodic B3LYP	3.2	29.2	0.11	[39]
Periodic LDA DFT	8.7	93.6	0.09	[39]
CASCI Cluster CI	0.4	4.4	0.09	[39]
CASSCF Cluster CI	0.5	5.0	0.10	[39]
CASPT2 Cluster CI	1.2	16.7	0.07	[39]
DDCI2 Cluster CI	1.2	12.6	0.10	[39]
DDCI3 CLuster CI	1.8	16.3	0.11	[39]
Periodic SIC-LSD	2.3	12	0.19	[40]
Periodic SIC-LSD (extra basis)	1.8	11	0.16	[40]
7 layer SIC-LSD - IP	1.66	9.52	0.17	[40]
7 layer SIC-LSD - OOP	2.09	15.6	0.13	[40]
11 layer SIC-LSD - OOP	2.08	14.71	0.14	[40]
CASSCF CI	-	3.3	-	[41]
CASPT2 CI	-	11.7	-	[41]
CASSCF-EAS CI	-	4.5	-	[41]
CASPT2-EAS CI	-	13.5	-	[41]
CASSCF CI - (100)	-	2.7	-	[41]
CASPT2 CI - (100)	-	9.8	-	[41]
CASSCF-EAS CI - (100)	-	13.5	-	[41]
CASPT2-EAS CI - (100)	-	11.2	-	[41]

Table 1.1: Summary of measured and calculated magnetic coupling constants from literature for NiO. Positive J_d indicates favouring a parallel alignment, and positive J_{se} indicates favouring antiferromagnetic alignment. The abbreviation "IP" should be read as "surface in place", and "OOP" as "surface out of plane".

Spin wave dispersion data, collected by inelastic neutron scattering [48] for MnO also found both coupling constants to be antiferromagnetic in character. The ratio of constants was -0.87, with J_d of 0.78 meV and J_{se} of 0.90 meV. Another experimental measurement of MnO [43], this time from magnetic susceptibility measurements was in agreement with the nature of the constants, both favouring antiparallel alignment, and found a J_d of 0.86 meV and J_{se} of 0.95 meV, which give a ratio of -0.90. This is similar to values found by Coles et al [49], who measured paramagnetic resonance of Mn ions in MgO, and found a J_d and J_{se} of 2.4 meV, both antiferromagnetic in character, and thus a ratio of -1.

In wustite, $Fe_{1-x}O$, experimental work with inelastic neutron scattering [50] measured the strengths of interatomic magnetic coupling constants in terms of a Heisenberg spin model. A value of J_d of 0.459 meV, or 0.256 meV depending on orientation relative to magnetostriction effects, and favouring ferromagnetic behaviour was found. The corresponding J_{se} was measured as 0.808 meV, and favoured antiparallel alignment of spins.

However, there are cases where the application of the Ising model breaks down. A recent hybrid density functional study on VO [51] found that J_d was around 5 times larger than J_{se} over the range of Hamiltonians used with both favouring antiparallel alignment, which would predict an AF3 ordering. However, direct calculation predicted that AF1 ordering was favoured. This discrepancy is due to changes in the electronic structure with the different spin alignments, such as a shift in the O($2p$) band occupancy of about 0.5e between AF1 and AF3 magnetic orders.

Chapter 2

Theory

Throughout this thesis there are four theoretical methods used, being Hartree-Fock and Density Functional Theory methods for electronic structure, the statistical mechanical method of Monte Carlo simulation, and mean field analysis.

This chapter will outline the basic principles of these methods, and the relevant equations, approximations and simplifications where applicable.

2.1 Hartree-Fock theory

The Hartree-Fock calculations within this thesis were all performed using the CRYSTAL 98 program, which performs linear combination of atomic orbital (LCAO) self consistent field (SCF) periodic Hartree-Fock calculations, and thus implementation details specified will be from that package.

The electronic structure of an N-electron system can be calculated from solutions to the N-electron Schrödinger equation (2.1). This describes N

electrons moving in the Columbic field of M nuclei of charges Z_a.

$$H(1,...,N)\Psi(1,...,N) = E\Psi(1,...,N) \tag{2.1}$$

If Born-Oppenheimer approximation [52] can be applied to the system under study, H(1,...,N) is given by (2.2), in atomic units. This approximation states that as the motion of the electrons is significantly faster than the nuclear motion, and the mass of the nucleii is significantly greater than the mass of the electrons, the nucleii can be considered to be static. This results in the electronic structure being decoupled from the nuclear dynamics.

$$H = \sum_{i}^{N}\left(-\frac{1}{2}\nabla_i^2 - \sum_{a}^{M}\frac{Z_a}{|\mathbf{r_i}-\mathbf{R_a}|} + \sum_{j>1}^{N}\frac{1}{|\mathbf{r_i}-\mathbf{r_j}|}\right) \tag{2.2}$$

Equation (2.2) has the terms $\mathbf{r_i}$ and $\mathbf{R_a}$ which are the electronic and fixed nuclear position vectors, respectively. The N electron wavefunction, $\Psi(1,...,N)$, is then functionally dependent on $\mathbf{r_i}$ and parametrically dependent on $\mathbf{R_a}$. The kinetic term is the first single electron term, and the nuclear attraction energy is the second, whilst the two electron term is the repulsive interactions between electrons.

Solutions to the N electron Schrödinger equation must invoke approximations to $\Psi(1,...,N)$, as its exact functional form is not known. The simplest, and most general, of these is the single particle approximation, wherein it is assumed that the N electron wavefunction can be written as a product of N single particle wavefunctions. Such an approximate wavefunction, $\Omega(1,...,N)$ may be defined as

$$\Omega(1,...,N) = \Pi_i^N \chi_i \tag{2.3}$$

This, however, does not take into account the anti-symmetric nature of electrons, and so $\Omega(1,...,N)$ must be modified. A very common way to do this is to define the function in terms of Slater determinants of single particle wavefunctions, θ_k, each anti-symmetric with respect to interchange of electrons which gives equation (2.4), where C_k is a constant.

$$\Omega(1,...,N) = \sum_k C_k \theta_k \tag{2.4}$$

The Hartree-Fock method is a self consistent method that produces the best possible single determinant of single particle wavefunctions, θ_0. The variational principle is used to determine θ_0, where the expectation value of $H(1,...,N)$ is varied with respect to a trial determinantal wavefunction θ_0 until a minimum is obtained, equation (2.5), subject to the orthonormality constraint of equation (2.6).

$$E_0 = min\,\{\langle\theta_0|H(1,...,N)|\theta_0\rangle\} \tag{2.5}$$

$$\langle\theta_0|\theta_0\rangle = N \tag{2.6}$$

The expection value, E, is a minimum when

$$\frac{\partial E}{\partial \theta_0} = 0 \tag{2.7}$$

which, as θ_0 is a product of N individual wavefunctions, can be replaced by N coupled conditions,

$$\frac{\partial E}{\partial \psi_i} = 0; \forall 1 \leq i \leq N \tag{2.8}$$

subject to the orthonormality constraints

$$\langle \psi_i | \psi_j \rangle = \delta_{ij} \tag{2.9}$$

These two equations contain the Hartree-Fock equations in their most general form. Combining the expression for the Hamiltonian, equation 2.2, and the definition of θ_0, leads to an expression for E given by equation (2.10).

$$E = \sum_{i=1}^{N} \left(h_i + \sum_{i<j}^{N} J_{ij} - K_{ij} \right) \tag{2.10}$$

The one electron term, h_i, is of the form

$$h_i = \left\langle \psi_i \left| \hat{h}_i \right| \psi_i \right\rangle \tag{2.11}$$

$$h_i = \left\langle \psi_i \left| -\frac{1}{2}\nabla^2 - \sum_{a}^{M} \frac{Z_a}{|\mathbf{r}_i - \mathbf{R}_a|} \right| \psi_i \right\rangle \tag{2.12}$$

$$= \int d\tau(1) \psi_i^*(1) \left(-\frac{1}{2}\nabla^2 - \sum_{a}^{M} \frac{Z_a}{|\mathbf{r}_i - \mathbf{R}_a|} \right) \psi_i(1) \tag{2.13}$$

where (1) indicates that the integral is over the total coordinates of electron (1). Similarly, the two electron terms J_{ij} and K_{ij} are given by

$$J_{ij} = \left\langle \psi_i \psi_j \left| \frac{1}{r_{ij}} \right| \psi_i \psi_j \right\rangle \tag{2.14}$$

$$= \int \int d\tau(1) d\tau(2) \psi_i^*(1) \psi_j^*(2) \left| \frac{1}{r_{ij}} \right| \psi_i(1) \psi_j(2) \tag{2.15}$$

$$K_{ij} = \left\langle \psi_i \psi_j \left| \frac{1}{r_{ij}} \right| \psi_j \psi_i \right\rangle \tag{2.16}$$

$$= \int \int d\tau(1) d\tau(2) \psi_i^*(1) \psi_j^*(2) \left| \frac{1}{r_{ij}} \right| \psi_i(2) \psi_j(1) \tag{2.17}$$

The N electron Hamiltonian as given in 2.2 does not contain any explicit spin dependency, i.e there are no spin orbit terms. Thus the single particle wavefunctions, ψ_i, are formally functions of space and spin, and may be separated into space only, ϕ_i, and spin only, σ_i functions,

$$\psi_i = \phi_i \times \sigma_i \tag{2.18}$$

with the separated orthonormality constraints,

$$\langle \phi_i | \phi_j \rangle = \delta_{ij} \tag{2.19}$$

$$\langle \sigma_i | \sigma_j \rangle = \delta_{ij} \sigma_i \tag{2.20}$$

With the separation of the spin and space parts, the one and two electron terms become

$$h_i = \left\langle \phi_i | \hat{h}_i | \phi_j \right\rangle \tag{2.21}$$

$$J_{ij} = \left\langle \phi_i \phi_j \left| \frac{1}{r_{ij}} \right| \phi_i \phi_j \right\rangle \tag{2.22}$$

$$K_{ij} = \left\langle \phi_i \phi_j \left| \frac{1}{r_{ij}} \right| \phi_j \phi_i \right\rangle \delta_{\sigma_i \sigma_j} \tag{2.23}$$

It is convenient to write the two electron integrals in terms of operators. The first integral can be replaced by the Coloumb operator, $\hat{J}_i$, and the other integral is replaced by the exchange operator, $\hat{K}_i$. The expectation values of these operators are used to express J_{ij} and K_{ij}.

$$\hat{J}_i(2)\chi(1) = \left(\int d\tau(2) \frac{|\phi_i(2)|^2}{r_{12}} \right) \chi(1) \tag{2.24}$$

$$\hat{K}_i(2)\chi(1) = \left(\int d\tau(2) \frac{\phi_i^*(2)\chi(2)}{r_{12}} \right) \phi_i(1) \tag{2.25}$$

With these operators, E can now be written in operator form,

$$E = \sum_{i=1}^{N} \left(h_i + \sum_{i>j} \left[J_{ij} - K_{ij} \delta_{\sigma_i \sigma_j} \right] \right) \tag{2.26}$$

$$= \sum_i \left\langle \phi_i \left| \hat{h}_i + \sum_{i>j} \left[\hat{J}_j - \hat{K}_j \delta_{\sigma_i \sigma_j} \right] \right| \phi_i \right\rangle \tag{2.27}$$

$$= \sum_i \left\langle \phi_i \left| \hat{F}_i \right| \phi_i \right\rangle \tag{2.28}$$

$$= \sum_i F_i \tag{2.29}$$

where $\hat{F}_i$ is the Fock operator, and is defined by

$$\hat{F}_i = \hat{h}_i + \sum_{i>j} \left(\hat{J}_j - \hat{K}_j \delta_{\sigma_i \sigma_j} \right) \tag{2.30}$$

Given that $J_{ii} = K_{ii}$ for all i, the subscript on the sums can be simplified to

$$\hat{F}_i = \hat{h}_i + \sum_{j} \left(\hat{J}_j - \hat{K}_j \delta_{\sigma_i \sigma_j} \right) \tag{2.31}$$

The Hartree-Fock equations 2.8 and 2.9 can now be written as

$$\frac{\partial E}{\partial \psi_i} = \partial \sum_i \left\langle \phi_i \left| \hat{F} \right| \phi_i \right\rangle = 0 \tag{2.32}$$

subject to

$$\sum_i \langle \phi_i | \phi_j \rangle = \delta_{ij} \; \forall i, j \tag{2.33}$$

Applying the constraints with the method of Lagrange multipliers then results in the canonical Hartree-Fock equations,

$$\hat{F}_i \phi_i = \epsilon_i \phi_i \tag{2.34}$$

Therefore the optimum set of single particle functions, $\{\phi_i\}$, are eigenfunctions of the Fock operator. In the case of atoms, the radial Hartree-Fock equations can be derived. These are solvable by numerical integration, and can be exact, as the radial and spherical components of ϕ are separable.

For molecular and crystalline systems, however, the corresponding equa-

tions cannot be evaluated numerically, and so a further approximation is required, namely the linear combination of atomic orbitals (LCAO) approximation. This assumes that each single particle wavefunction can be expressed as the sum of orbitals centred at atomic positions,

$$\phi_i = \sum_r c_{ir}\varphi_r \tag{2.35}$$

$$\phi = \mathbf{c}\varphi \tag{2.36}$$

This changes the problem from determining the set of eigenfunctions of the Fock operator, into one of finding the set of expansion coefficients, $\{c_{ir}\}$ or $\mathbf{c}$ in matrix notation. The formulation of the Hartree-Fock equations in terms of these expansion coefficients was done by Roothaan and a slight variation based on the single particle density matrix of his analysis now follows. The single particle density matrix, $\mathbf{P}$, is defined by

$$\mathbf{P} = \mathbf{C}\mathbf{C}^{\dagger} or P_{rs} = \sum_{i=1}^{N} C_{ri}C_{is}^{*} \tag{2.37}$$

with the differential being

$$\delta P_{rs} = \sum_i (\delta C_{ri}C_{is}^{*} + C_{ri}\delta C_{is}^{*}) \tag{2.38}$$

In the case of closed shell systems with 2N electrons, where the populations of both spin types will be equal, the total energy is described in operator form by equation (2.39).

$$E = 2\sum_{i=1}^{N} \left\langle \phi_i \left| \hat{h}_i + \hat{J}_i - \frac{1}{2}\hat{K}_i \right| \phi_i \right\rangle \tag{2.39}$$

Substituting in equation (2.36) and then expressing in terms of the density matrix $\mathbf{P}$ gives,

$$E = Tr\mathbf{Ph} + \frac{1}{2}Tr\mathbf{PG}[\mathbf{P}] \tag{2.40}$$

Here, $\mathbf{h}$ represents the matrix of monoelectronic energies and $\mathbf{G}$ is the matrix of bielectronic interaction energies, which is a functional of the density matrix $\mathbf{P}$.

$$\mathbf{G}[\mathbf{P}] = \mathbf{J}[\mathbf{P}] - \frac{1}{2}\mathbf{K}[\mathbf{P}] \tag{2.41}$$

$$J_{rs}[\mathbf{P}] = \sum_{t,u} P_{tu} \int\int dr_1 dr_2 \varphi_r^*(r_1)\varphi_u^*(r_2)\frac{1}{r_{12}}\varphi_s(r_1)\varphi_t(r_2) \tag{2.42}$$

$$K_{rs}[\mathbf{P}] = \sum_{t,u} P_{tu} \int\int dr_1 dr_2 \varphi_r^*(r_1)\varphi_u^*(r_2)\frac{1}{r_{12}}\varphi_t(r_1)\varphi_s(r_2) \tag{2.43}$$

As before, the energy is mimimised by the use of the variational principle, so the variation in the density matrix is,

$$\delta\mathbf{P} = \delta\mathbf{C}\mathbf{C}^\dagger + \mathbf{C}\delta\mathbf{C}^\dagger \tag{2.44}$$

which results in the variation in the total energy of

$$\delta E = Tr\delta\mathbf{P}\mathbf{h} + \frac{1}{2}Tr\delta\mathbf{P}\mathbf{G}[\mathbf{P}] + \frac{1}{2}Tr\mathbf{P}\mathbf{G}[\delta\mathbf{P}] \tag{2.45}$$

$$\delta E = Tr\delta\mathbf{P}\mathbf{h} + Tr\delta\mathbf{P}\mathbf{G} \tag{2.46}$$

$$\delta E = Tr\delta\mathbf{P}\mathbf{F} \tag{2.47}$$

Substituting out $\mathbf{P}$ and writing in terms of C leads to

$$\delta E = \sum_{i,s} \left(\delta C_{ri} C^*_{is} + C_{ri}\delta C^*_{is}\right) F_{sr} \tag{2.48}$$

$$= \sum_{i,s} \left(C_{is} F_{rs} \delta C^*_{ri} + \delta C^*_{is} F_{sr} C^*_{ri}\right) \tag{2.49}$$

The atomic orbital basis set, $\{\varphi_r\}$, is multicentred which results in the orthogonality constraint on each φ_r is

$$\langle\varphi_s|\varphi_r\rangle = S_{rs} \tag{2.50}$$

where the set of all $S_r s$ are the elements of the overlap matrix $\mathbf{S}$. Applying this constraint with the method of Lagrangian multipliers gives, in matrix form, equation (2.52).

$$\sum_{s,r} \left(F_{sr} c_{sa} - S_s r \sum_i c_{ri}\epsilon_{ia} \right) = 0 \tag{2.51}$$

$$\mathbf{F}\mathbf{C} = \epsilon\mathbf{S}\mathbf{C} \tag{2.52}$$

The coefficients of the atomic orbitals, in the form of the matrix, $\mathbf{C}$, are

determined from solution of these equations by an iterative process which is repeated until self consistency is reached. In practice, repeated until some specified tolerance is reached. The density matrix is constructed, initially from some estimate, typically from atomic densities, and then the matrix G is calculated, and then the Fock matrix. This is then diagonalised to give the total energy, and a new density matrix to repeat the process with. As written, the space functions for doubly occupied orbitals are fixed to be equal, a procedure sometimes called restricted Hartree-Fock (RHF). For open shell systems the Hartree-Fock equations are essentially the same, save that the constraint is removed, resulting in the unrestricted Hartree-Fock (UHF) procedure. The Slater determinant θ_0 now must have two different spin states, α and β, which results in the total energy being given by equation 2.53.

$$\begin{aligned} E = \; & \sum_k \left\langle \psi_k^\alpha \left| \hat{h} + \tfrac{1}{2}\left(\hat{J} - \hat{K}^\alpha\right) \right| \psi_k^\alpha \right\rangle + \\ & \sum_m \left\langle \psi_m^\beta \left| \hat{h} + \tfrac{1}{2}\left(\hat{J} - \hat{K}^\beta\right) \right| \psi_m^\beta \right\rangle \end{aligned} \tag{2.53}$$

In the LCAO approximation,

$$\psi_k^\alpha = \sum_k \varphi_q C_{qk}^\alpha \tag{2.54}$$

$$\psi_k^\beta = \sum_k \varphi_q C_{qk}^\beta \tag{2.55}$$

This leads to the definition of two density matrices, one for each spin state, defined as before.

$$P^{\alpha}_{rs} = \sum_{k}^{n_\alpha} \left(C^{\alpha}_{rs}\right)^* C^{\alpha}_{rk}, \quad \text{or matrix form, } \mathbf{P}^{\alpha} = \mathbf{C}^{\alpha}\mathbf{C}^{\alpha\dagger} \tag{2.56}$$

$$P^{\beta}_{rs} = \sum_{k}^{n_\beta} \left(C^{\beta}_{rs}\right)^* C^{\beta}_{rk}, \quad \text{or matrix form, } \mathbf{P}^{\beta} = \mathbf{C}^{\beta}\mathbf{C}^{\alpha\dagger} \tag{2.57}$$

$$\tag{2.58}$$

From this pair of matrices, the total electron density matrix, $\mathbf{P}^{tot}$, and the net spin density matrix, $\mathbf{P}^{spin}$ can be defined.

$$\mathbf{P}^{tot} = \mathbf{P}^{\alpha} + \mathbf{P}^{\beta} \tag{2.59}$$

$$\mathbf{P}^{spin} = \mathbf{P}^{\alpha} - \mathbf{P}^{\beta} \tag{2.60}$$

Defining the total energy, E, in terms of these matrices gives,

$$\begin{aligned} E = & \quad Tr\mathbf{P}^{\alpha}\mathbf{h} + \tfrac{1}{2}Tr\mathbf{P}^{\alpha}\mathbf{J}\left[\mathbf{P^{tot}}\right] - \tfrac{1}{2}\mathbf{P}^{\alpha}\mathbf{K}\left[\mathbf{P}^{\alpha}\right] + \\ & \quad Tr\mathbf{P}^{\beta}\mathbf{h} + \tfrac{1}{2}Tr\mathbf{P}^{\beta}\mathbf{J}\left[\mathbf{P^{tot}}\right] - \tfrac{1}{2}\mathbf{P}^{\beta}\mathbf{K}\left[\mathbf{P}^{\beta}\right] \end{aligned} \tag{2.61}$$

$$= Tr\mathbf{P}^{tot}\mathbf{h} + \frac{1}{2}Tr\mathbf{P}^{tot}\mathbf{J}\left[\mathbf{P^{tot}}\right] - \frac{1}{2}\mathbf{P}^{\alpha}\mathbf{K}\left[\mathbf{P}^{\alpha}\right] - \frac{1}{2}\mathbf{P}^{\beta}\mathbf{K}\left[\mathbf{P}^{\beta}\right] \tag{2.62}$$

Application of the variational principle, and introducing the orthonormality constraints, equation 2.50, via Lagrangian multipliers, the equations for the two spin states are,

$$\mathbf{F}^{\alpha}\mathbf{C}_i^{\alpha} = \epsilon_i^{\alpha}\mathbf{S}\mathbf{c}_i^{\alpha} \tag{2.63}$$

$$\mathbf{F}^{\beta}\mathbf{C}_i^{\beta} = \epsilon_i^{\beta}\mathbf{S}\mathbf{c}_i^{\beta} \tag{2.64}$$

where the spin dependent Fock operators are,

$$\mathbf{F}^{\alpha} = \mathbf{F} - \mathbf{Z}; \quad \mathbf{F}^{\beta} = \mathbf{F} + \mathbf{Z} \tag{2.65}$$

where the operators are defined as

$$\mathbf{F} = \mathbf{h} + \mathbf{G} \tag{2.66}$$

$$\mathbf{G} = \mathbf{J}\left[\mathbf{P}^{tot}\right] - \frac{1}{2}\mathbf{K}\left[\mathbf{P}^{tot}\right] \tag{2.67}$$

$$\mathbf{Z} = \frac{1}{2}\mathbf{K}\left[\mathbf{P}^{spin}\right] \tag{2.68}$$

The description above applies to non-periodic (i.e. molecular) systems. Extension to periodic systems is possible by exploiting the associated translational symmetry. The unit cell of the direct lattice is spanned by a set of basis translation vectors, a_1, a_2, a_3, from which any general lattice point relative to the unit cell position, r_0, is given by the three integers N_1, N_2 and N_3.

$$\mathbf{R_0} = \mathbf{r_0} + N_1\mathbf{a_1} + N_2\mathbf{a_2} + N_3\mathbf{a_3} \tag{2.69}$$

The space group is a set of symmetry operations that describe the sym-

metry present in a unit cell of the crystal system. This set consists of point operations, p, translational vectors, $\mathbf{t}$, or fractional translational vectors, $\mathbf{v}$. The complete set of translations, $\mathbf{t}$, form an Abelian group, which means that the operations commute. The irreducible representations of the group are indexed by a wave vector, $\mathbf{k}$, such that the operation $\mathbf{t_n}$ can be expressed as $e^{i\mathbf{k}\cdot\mathbf{t_n}}$. Periodic boundary conditions apply, so the $\mathbf{k}$ vectors form a lattice, which is known as the reciprocal lattice in $\mathbf{k}$ space. In this reciprocal lattice, the equivalent of the unit cell of the direct lattice is known as the first Brilloiun Zone (BZ). Any general reciprocal lattice vector, $\mathbf{K}$ is given by

$$\mathbf{K} = n_1\mathbf{b_1} + n_2\mathbf{b_2} + n_3\mathbf{b_3} \tag{2.70}$$

where the reciprocal basis set, $\{\mathbf{b_i}\}$ is defined by

$$\mathbf{b_1}\mathbf{b_2} = 2\pi\delta_{ij} \tag{2.71}$$

and must satisfy the condition,

$$e^{i\mathbf{K}\cdot\mathbf{t_n}} = 1 \quad \forall\mathbf{t_n} \tag{2.72}$$

For periodic systems, the spin orbitals of equation (2.18), which are appropriately called crystalline orbitals in this context, and expressed as linear combinations of Bloch functions, $\{\chi_j(\mathbf{r},\mathbf{k})\}$, where the Bloch functions are written as linear combinations of the local atomic orbitals, $\{\phi_j\}$, centered at atomic positions.

These local atomic orbitals, as in the case of molecular calculations, can

be built up from a number of basis sets. Whilst Gaussian basis sets are popular, the inherent translational symmetry present in plane waves lend themselves to crystalline calculations. With whatever complete basis set is used, a matrix equation equivalent to equation (2.52) can be written as,

$$\mathbf{F}^{\sigma}(\mathbf{k})\mathbf{C}^{\sigma}(\mathbf{k}) = \mathbf{S}(\mathbf{k})\mathbf{C}^{\sigma}(\mathbf{k})\epsilon(\mathbf{k}) \tag{2.73}$$

for any $\mathbf{k}$ point in the BZ. $\mathbf{F}^{\sigma}(\mathbf{k})$ is the Fock operator in reciprocal space, $\mathbf{S}(\mathbf{k})$, similar to the molecular case, is the overlap matrix spanning the Bloch functions, and $\epsilon(\mathbf{k})$ is the diagonal energy matrix. The Fock operator in reciprocal space can be converted to the corresponding real space operator by a straight forward Fourier transform. Working through the algebra, an expression for the density matrix for a periodic system can be derived as,

$$\mathbf{P}^{\sigma}_{ij}(\mathbf{t}) = \sum_{a} \frac{1}{V_b} \int_{BZ} d\mathbf{k} c^{\sigma}_{ai}(\mathbf{k})^{*} c^{\sigma}_{ai}(\mathbf{k}) e^{i\mathbf{k}\cdot\mathbf{t}} \mathcal{V}\left[E_f - \epsilon^{\sigma}_{a}(\mathbf{k})\right] \tag{2.74}$$

where $c^{\sigma}_{ai}(\mathbf{k})$ is the coefficient of the j^{th} Bloch function of the a^{th} crystalline orbit at the point $\mathbf{k}$ with corresponding eigenvalue, $\epsilon^{\sigma}_{a}(\mathbf{k})$, $\mathcal{V}$ is a step function, which takes the value of 1 if $\epsilon^{\sigma}_{a}(\mathbf{k}) < E_f$, the Fermi energy, otherwise zero. The Fermi energy is the energy beneath which all the electron states are filled, at zero temperature. It can be determined by imposing the condition that N/2 crystalline orbits exist such that their eigenvalues are less than the Fermi energy. The Fermi energy can then be described by equation (2.75), where q is the number of electrons present in a unit cell.

$$q = \frac{2}{N} \sum_{a} \sum_{k} \mathcal{V} \left[E_f - \epsilon_a^{\sigma}(\mathbf{k}) \right] = \frac{2}{V_B} \sum_{a} \int_{BZ} d\mathbf{k} \mathcal{V} \left[E_f - \epsilon_a^{\sigma}(\mathbf{k}) \right] \qquad (2.75)$$

Integration over the reciprocal space must be carried out at each cycle, in order to determine the Fermi energy, and then a reconstruction of the one electron density matrix. This is performed over a number of $\mathbf{k}$ points belonging to a lattice known as the Monkhorst net [53]. The Monkhorst net has basis vectors $\{\mathbf{b_i}/si\}$, where $\{\mathbf{b_i}\}$ is the set of reciprocal lattice basis vectors, and the integers $\{s_i\}$ are known as the shrinking factors. The number of nonequivalent sample points is given by the product of shrinking factors and the order of the point group.

2.2 Density Functional Theory

One of the major computational overheads of wavefunction based methods is due to the non-local nature of the description, so that calculation of properties of a system in from a wavefunction based description required integrating over all space. If the properties of part of a system could be described in a more local fashion, where only the vicinity of a point need be examined to evaluate some operator at that point, that would suggest a significant computational saving.

Since the inception of quantum mechanics, there has been a movement to try and model situations using the electron density $\rho(\mathbf{r})$ as a fundamental descriptor. Initially, this was guided by intuition, before being proved that

the ground state properties are functionals of the electron density [54].

Hohenberg and Kohn showed that the electronic charge density is a unique functional of the external potential (i.e. external to the electron gas), and vice versa, and also that the total energy of a system of interacting electrons can be written as a functional of the charge density. It was also shown that the energy obeys a variational principle with respect to the charge density.

The major difficulty with this method is that the form of the functional is not known. A common assumption is that the functionals for exchange and for correlation are separable, and an early form of the functionals was typically the Thomas-Fermi [55, 56] functional for the kinetic and Columb energies, and the Dirac [57] functional for exchange. These functionals are purely local, relying only on the energy density at a point, and thus computationally attractive. The predictive power of these functionals was not great - in some circumstances they were acceptable, but for others, such as a molecular bond, they gave poor (disagreeing with observation) descriptions. Modern functionals have their root in Slaters $X\alpha$ method [58], which was an exchange functional developed as an approximation to the Hartree-Fock method. The modern implementation of density functional methods are based of the formalism developed by Kohn and Sham [59].

The basic principle of the method is to describe the total energy of the system as a functional of the electron density, $n(\mathbf{r})$, as in equation 2.76 within the Born-Oppenhimer approximation, where $T[n(\mathbf{r})]$ is the kinetic energy of non-interacting electrons, $V_N[n(\mathbf{r})]$ is the electron-nuclei interaction and $U_{ee}[n(\mathbf{r})]$ is the Columbic interaction between electrons. The final term $E_{xc}[n(\mathbf{r})]$ is a functional that includes the exchange and correlation effects.

$$E_{tot}[n(\mathbf{r})] = T[n(\mathbf{r})] + V_N[n(\mathbf{r})] + U_{ee}[n(\mathbf{r})] + E_{xc}[n(\mathbf{r})] \tag{2.76}$$

Equation 2.76 is formally exact, if the exact form of $E_{xc}[\rho]$ is used. The form of this functional is not known, so approximations are made to it. The Kohn-Sham procedure works very much like the Hartree-Fock procedure. A set of wavefunction-like orbitals, the Kohn-Sham orbitals, are generated, and from them a total electron density is produced. This allows the kinetic energy to be calculated from the wavefunctions, where it is straightforward.

A functional $F[n(\mathbf{r})]$, which describes the total energy of a system may be expressed as in (2.77).

$$F[n(\mathbf{r})] = T[n(\mathbf{r})] + \frac{e^2}{2}\int d\mathbf{r}\int d\mathbf{r}'\frac{n(\mathbf{r})n(\mathbf{r}')}{|\mathbf{r}-\mathbf{r}'|} + E_{xc}[n(\mathbf{r})] \tag{2.77}$$

Kohn and Sham used a wave function gradient method to derive a set of single particle equations that describe non-interacting particles moving in an effective potential that can be represented as a functional of the charge density,

$$\epsilon_i\psi_i(\mathbf{r}) = \left\{-\frac{\hbar}{2m}\nabla^2 + V_ks[n(\mathbf{r})]\right\}\psi_i(\mathbf{r}) \tag{2.78}$$

in which the effective single particle Kohn Sham potential is given as,

$$V_{ks}[n(\mathbf{r})] = V_{ext}(\mathbf{r}) + e^2\int d\mathbf{r}'\left(\frac{n(\mathbf{r}')}{|\mathbf{r}-\mathbf{r}'|} + \frac{\delta E_{xc}[n(\mathbf{r})]}{\delta n(\mathbf{r})}\right) \tag{2.79}$$

where $V_{ext}(\mathbf{r})$ is the external potential, typically just the potential defined

by the nuclear positions. The last term in equation (2.79) is a functional derivative that defines the exchange-correlation potential. The charge density $n\mathbf{r}$ is given by,

$$n(\mathbf{r}) = \sum_i |\psi_i(\mathbf{r})|^2 \tag{2.80}$$

and the total many electron energy can be evaluated as,

$$E = \sum_{i=1}^{N} \epsilon_i - \frac{e^2}{2} \int d\mathbf{r} \left(\int d\mathbf{r}' \frac{n(\mathbf{r})n(\mathbf{r}')}{|\mathbf{r} - \mathbf{r}'|} + E_{xc}[n(\mathbf{r})] \right) - \int d\mathbf{r} V_{xc}[n(\mathbf{r})]n(\mathbf{r}) \tag{2.81}$$

These equations define the Kohn Sham DFT method. In an analogous fashion to the Hartree-Fock method, an initial set of trial wavefunctions is constructed. From these, an initial charge density is constructed and inserted into equation (2.79) to give the Kohn Sham potential. From this, the set of single particle equations can be solved, to give the next set of wavefunctions, and the process repeated until a self consistency is achieved. Typically, this is measured by examination of the total energy (2.81).

Clearly, as described above, the method would be unable to handle spin polarised systems. Extension to open-shell systems proceeds in a manner analogous to the adaption of the Hartree Fock method to open shell systems, and results in the total electronic energy being a functional of two electron densities, each of opposing spin,

$$E[n_\uparrow(\mathbf{r}), n_\downarrow(\mathbf{r})] \tag{2.82}$$

Extension to crystalline systems follows the same steps as for the Hartree-Fock method.

The two most frequently used families of functionals are the Local Density Approximation (LDA), and the Generalised Gradient Approximation (GGA). The LDA methods make the approximation that the exchange-correlation energy for an electron at a position $\mathbf{r}$ in the electron gas is the equal to the exchange-correlation energy per electron of the homogeneous electron gas with the same density as the true electron gas at the position $\mathbf{r}$. This simple approximation ignores any inhomogeneities in the local charge density at the point $\mathbf{r}$. However, despite this, LDA methods have been surprisingly effective in many cases. The main flaw with the method is in regions of low electron density. The exact form of the the functional for such regions is known to be a power law dependence, whilst the LDA predicts an exponential fall off with electron density. This is particularly noticeable in molecules, where the difference in energy between two systems whose electron distributions have different 'surface areas' is in error, and results in overbinding of the molecule.

The extension of LDA to open shell systems follows straight forward principles, and is sometimes called Local Spin Density, or LSD.

The next major group of functionals are the GGA functionals where the parameterisation of the exchange-correlation energy includes the gradient of the charge density at a point, as well as the charge density. These correct many of the problems with LDA methods. These methods are perhaps best described as 'semi-local', in that taking the gradient at a point implies a dependence on the space around a point, in contrast to the truly local LDA.

These are quite distinct from the non-local Hartree-Fock method, where the energy for any given point in space depends on all other point in space also.

A more recent development has been the use of hybrid functionals, combining the Hartree-Fock exchange energies with some exchange and correlation functionals from DFT methods, in a weighted mean. First introduced by Becke [60], these functionals tend to be semi-empirical - in that the contributions to the weighted mean are chosen to reproduce some set of experimental values. In the case of Becke's B3LYP functional, it has found to be useful outside the data it was conditioned upon, being principly atomisation and ionisation energies of first and second row elements.

2.3 Lattice Spin Hamiltonians

For many problems, the rigors of the quantum mechanical methods are not required, or maintain too much unwanted computational overhead. Additionally, these methods become prohibitally expensive for temperatures above absolute zero, and so examination of temperatures above this, such as room temperature, is not feasible. In these cases, it is desirable to use a simpler model that can be related to the quantum mechanical descriptions. One particular case is for studies on the magnetic behaviour of systems.

For magnetic systems a major quest is to determine the temperatures that magnetic phase changes occur at, and the nature of any magnetic ordering. Additionally, there are long range correlation effects that occur in magnetic systems, with an infinite correlation length at the phase boundaries. Whilst this can be handled by calculations for finite size systems,

followed by extrapolation to infinity, the calculation time would, again, be prohibitive for a quantum mechanical description. Finally, it has been found that simpler models, parameterised from quantum mechanical calculations, give good results for a fraction of the time it would take for quantum mechanical calculations.

There are a number of lattice spin Hamiltonians in use for this purpose, with the two most common being the Ising spin Hamiltonian and Heisenberg spin Hamiltonian. These Hamiltonians correspond to simplified descriptions of the magnetism, from which solutions can be derived by a number of methods.

2.3.1 Heisenberg Hamiltonian

The Heisenberg model [61] considers that each spin in the lattice may point in any direction in space. For a lattice of N_L sites, a Heisenberg spin Hamiltonian may be defined as

$$\hat{H}_{spin} = -\frac{1}{2} J_d \sum_{i}^{N_L} \sum_{j}^{(nn)} \hat{\sigma}_{\mathrm{i}} \cdot \hat{\sigma}_{\mathrm{j}} + \frac{1}{2} J_{se} \sum_{i}^{N_L} \sum_{j}^{(nnn)} \hat{\sigma}_{\mathrm{i}} \cdot \hat{\sigma}_{\mathrm{j}} \qquad (2.83)$$

where the summations $\sum_j^{(} nn)$ and $\sum_j^{(} nnn)$ run over the lattice sites which are the nearest neighbours (nn) and next-nearest neighbours (nnn) to the i^{th} site respectively. $\hat{\sigma}_{\mathrm{i}}$ and $\hat{\sigma}_{\mathrm{j}}$ are the total spin operators at the i^{th} and j^{th} sites respectively, and are unit vectors within this model. J_d and J_{se} are coupling energies, and correspond to the direct and super-exchange interactions respectively, while $\hat{H}_{spin}$ is the spin Hamiltonian for the entire lattice. The sign convention is such that parallel nearest neighbours and anti-

parallel next-nearest neighbour spins lead to negative energies, i.e. stable alignments, when the coupling constants are positive. The fraction of J_d or J_{se} contributed by each interaction is determined by the scaler product of the spins vectors, giving maximum effect with they are co-linear, and no effect when they are orthogonal.

2.3.2 Ising spin Hamiltonian

The Ising spin Hamiltonian, $\hat{H}_{spin}$ is the simplest spin only Hamiltonian. It is, in fact, more general than just spin problems, and has application outside of magnetic studies. It can be used as a model in any system where an entity can be in one of two states, and there is an interaction between neighbouring entities. One example of this is for modeling binary alloys [62]. Despite this generality, in notation it shall be assumed, for simplicity and clarity, that the Ising Hamiltonian refers to spins.

$\hat{H}_{spin}$ is a phenomenological Hamiltonian, first proposed by Ising [63], which considered interactions between a spin and its neighbours. It was proposed as a model for ferromagnetic systems, and in the original formulation dealt only with one type of interaction, with the extension to two interaction types occurring later, as superexchange mechanisms were understood [64, 65]. The spin associated with each lattice point is considered to be in one of two states, referred to as "up" or "down", representing aligned with, or against, an applied field. A term for an applied field can be included in the Hamiltonian, although will not be here.

$$\hat{H}_{Ising} = -\frac{1}{2} J_d \sum_{i}^{N_L} \sum_{j}^{(nn)} \hat{\sigma}_i \hat{\sigma}_j + \frac{1}{2} J_{se} \sum_{i}^{N_L} \sum_{j}^{(nnn)} \hat{\sigma}_i \hat{\sigma}_j \tag{2.84}$$

Comparison with the Heisenberg Hamiltonian, above, shows the similarities. The sign convention for J_d and J_{se} following that for the Heisenberg Hamiltonian presented above. The corresponding total spin energy, E_{Ising} is given by,

$$E_{Ising} = -\frac{1}{2} J_d \sum_{i}^{N_L} \sum_{j}^{(nn)} \sigma_i \sigma_j + \frac{1}{2} J_{se} \sum_{i}^{N_L} \sum_{j}^{(nnn)} \sigma_i \sigma_j \tag{2.85}$$

The spin eigenvalues σ_i and σ_j can take values of ± 1. Equation 2.85 can be rewritten, to separate out the sum over lattice sites.

$$E_{Ising} = \sum_{i}^{N_L} \sigma_i \left(-\frac{1}{2} J_d \sum_{j}^{(nn)} \sigma_j + \frac{1}{2} J_{se} \sum_{j}^{(nnn)} \sigma_j \right) \tag{2.86}$$

$$= \sum_{i}^{N_L} \epsilon_i \tag{2.87}$$

where ϵ_i can be considered as the spin energy on the i^{th} site. Clearly,

$$\epsilon_i = \sigma_i \left(-\frac{1}{2} J_d \sum_{j}^{(nn)} \sigma_j + \frac{1}{2} J_{se} \sum_{j}^{(nnn)} \sigma_j \right) \tag{2.88}$$

The average spin energy per site is then $\frac{E_{Ising}}{N_L}$, or $\frac{1}{N_L} \sum_i^{N_L} \epsilon_i$, and is written as $\langle \epsilon_i \rangle$ or ϵ.

For specified, ordered, bulk spin alignments S, at zero temperature, where, for face centred cubic lattices S corresponds to FM, AF1, AF2, ..., orders,

the summations $\sum_j^{(nn)} \sigma_j$ and $\sum_j^{(nn)} \sigma_j$ may be written in terms of fixed whole numbers, $N_{nn}^{\uparrow\uparrow}(S)$, $N_{nn}^{\uparrow\downarrow}(S)$, $N_{nnn}^{\uparrow\uparrow}(S)$ and $N_{nnn}^{\uparrow\downarrow}(S)$, where $N_{nn}^{\uparrow\uparrow}(S)$ is the number of nearest neighbour interactions between spins that are aligned parallel at a site, within the ordering S. There will be a set of these four number for each type of site within a lattice. If, as is common, and is the case for rocksalt type structures, there is only one type of site, then all ϵ_i will be identical, so that the average spin energy per site, $\epsilon(S)$ can be written in terms of the numbers introduced above.

$$\epsilon(S) = -\frac{1}{2} J_d \left[N_{nn}^{\uparrow\uparrow}(S) - N_{nn}^{\uparrow\downarrow}(S) \right] + \frac{1}{2} J_s e \left[N_{nnn}^{\uparrow\uparrow}(S) - N_{nnn}^{\uparrow\downarrow}(S) \right] \tag{2.89}$$

$$= \frac{1}{2} \left[-J_d \Delta N_{nn}(S) + J_{se} \Delta N_{nnn} \right] \tag{2.90}$$

$$= \frac{1}{2J_{se}} \left[-x \Delta N_{nn}(S) + \Delta N_{nnn} \right] \tag{2.91}$$

where $x = \frac{J_d}{J_{se}}$ and ΔN_{nn} is the difference between the number of spin aligned and spin opposed nearest neighbours, with ΔN_{nnn} the same for the next nearest neighbours. Table 2.1 lists the relevant value for $N^{\uparrow\uparrow}$ etc for the bulk FCC lattice, from which the energies for the six ordered spin alignments can be calculated. The label FM is applied to the ferromagnetic state, while the other states are antiferromagnetic, and are given a number that is arbitrary in assignment.

	Symbol	FM	AF_1	AF_2	AF_3	AF_4	AF_5
Nearest neighbours	$N_{nn}^{\uparrow\downarrow}$	0	8	6	8	6	4
	$N_{nn}^{\uparrow\uparrow}$	12	4	6	4	6	8
Next nearest neighbours	$N_{nnn}^{\uparrow\downarrow}$	0	0	6	2	4	2
	$N_{nnn}^{\uparrow\uparrow}$	6	6	0	4	2	4

Table 2.1: Local magnetic environments of atoms for various magnetic orders in the rocksalt structure. Values taken from Hines et al [66].

$$E_{FM} = E_0 - 6J_d + 3J_{se} \tag{2.92}$$

$$E_{AF1} = E_0 + 2J_d + 3J_{se} \tag{2.93}$$

$$E_{AF2} = E_0 \qquad - 3J_{se} \tag{2.94}$$

$$E_{AF3} = E_0 + 2J_d + J_{se} \tag{2.95}$$

$$E_{AF4} = E_0 \qquad - J_{se} \tag{2.96}$$

$$E_{AF5} = E_0 - 2J_d - J_{se} \tag{2.97}$$

From these it can been seen that for $-\infty < J_d < \infty$ and $-\infty < J_{se} < \infty$, only the ferromagnetic and AF1, AF2 and AF3 states are possible at a temperature, T, of 0K. For different values of J_d and J_{se}, it is clear that the favoured (lowest energy) state can change. The boundary between these areas can be found by equating the two expressions for the energy. For example, for the boundary between FM and AF2 phases,

$$E_{FM} = E_{AF2} \tag{2.98}$$

$$E_0 + 6J_d - 3J_{se} = E_0 + 3J_{se} \tag{2.99}$$

$$J_d = J_{se} \tag{2.100}$$

Repeating this process builds a set of relationships, which can be expressed diagrammatically, in figure 2.1. The phases AF4 and AF5 do not appear, as there is no point where they are favoured over all other phases.

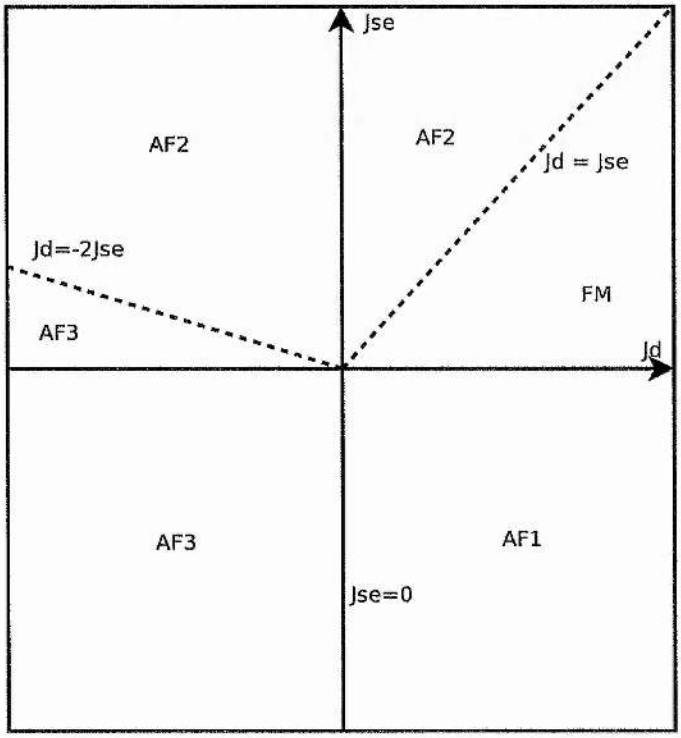

Figure 2.1: 0K phase diagram for Ising model rocksalt structures.

It is well observed that surfaces can have significant effect upon the mag-

netic ordering near the surface. Schweika *et al* [67] present a case were the surface layers are ordered above the bulk Néel temperature, noting that it is more common for surfaces to disorder, rather than order at a surface [68]. In addition to surface effects, the presence of a surface can have a dramatic effect on the behaviour of a system as a whole as noted by Alders et al [69] who observed reduction in the Néel temperature of films of NiO. The Ising Hamiltonian is also used in looking at wetting phenomena where there is some additional interaction characterised by a magnetic field applied to only the surface layer [70].

The same energetic analysis used for the bulk, above, can be applied thin films oriented in a specific direction, α, which can be specified in terms of the usual Miller indices, (100), (110), (111) etc. The set of numbers, $N^{\uparrow\downarrow}_{(nn)}(S)$ etc, are projected onto the film plane, giving corresponding numbers for a film $N^{\uparrow\downarrow}_{(nn)}(S_\alpha)$. These are best specified in terms of the total interactions within a plane, between a plane and the plane above, a plane and the next plane above, etc. In the case of (111) films, there are only interactions in the plane, and between adjacent planes, and are specified in table 2.2. As shown later, this has important consequences for the mean field treatment of the order-disorder phase transition.

The simplest case, geometrically speaking, after that of the infinite bulk, is a monolayer. However, the monolayer of (111) contains no next nearest neighbour interactions. This is a special case, as it is not possible to describe the system in terms of the ratio J_d/J_{se}, and is a simple hexagonal lattice with just a single interaction. The mean field description has a phase boundary at $J_d = 0$. With a ferromagnetic J_d, the system will align ferromagnetically,

	Spin state	FM	AF_2	AF_3
Out of plane (above)				
Nearest neighbours	Opposed	0	3	2
	Parallel	3	0	1
Next nearest neighbours	Opposed	0	3	1
	Parallel	3	0	2
In plane				
Nearest neighbours	Opposed	0	0	4
	Parallel	6	6	2
Out of plane (below)				
Nearest neighbours	Opposed	0	3	2
	Parallel	3	0	1
Next nearest neighbours	Opposed	0	3	1
	Parallel	3	0	2

Table 2.2: Local magnetic environments of atoms for various magnetic orders in the rocksalt structure, projected onto a (111) film.

and with a negative J_d, the system will order with a series of stripes. This gives a mean field reduced Néel temperature of $3J_d$ for positive J_d, and $1J_d$ for a negative J_d.

The next simplest system is the bilayer, which does contain next nearest neighbour interactions. Expressions can be written for the ground state energies at 0K. The notation $E(S)_n$ indicates the total energy for a system on n layers, in magnetic state S.

$$E(FM)_2 = E_0 - 9J_d + 3J_{se} \tag{2.101}$$

$$E(AF2)_2 = E_0 - 3J_d - 3J_{se} \tag{2.102}$$

$$E(AF3)_2 = E_0 + 3J_d + 1J_{se} \tag{2.103}$$

By equating and eliminating, the boundary between FM and AF2 is found to be at x = 1, and between AF2 and AF3 at x = -$\frac{2}{3}$. Similarly, for a trilayer system, the 0K energies are

$$E(FM)_3 = E_0 - 15J_d + 6J_{se} \tag{2.104}$$

$$E(AF2)_3 = E_0 - 3J_d - 6J_{se} \tag{2.105}$$

$$E(AF3)_3 = E_0 + 5J_d + 2J_{se} \tag{2.106}$$

Again, equating and eliminating gives the FM:AF2 boundary at x = 1, and AF2:AF3 boundary is at x = -1. Due to the manner in which the interactions are defined, all internal layers are identical in terms of numbers of interactions added (that is - there is no difference between an even or an odd numbered layer). Addition of a further layer to the FM state adds $3J_{se}$ -6 J_d to the total energy, in AF2 state it adds -3 J_{se} and in the AF3 state it adds $2J_d$ + J_{se}. Accordingly, expressions for the ground state energies as a function of n, the number of layers, are given by,

$$E(FM)_n = E_0 - (9 + 6(n-2))J_d + (3 + 3(n-2))J_{se}; n > 2 \tag{2.107}$$

$$E(AF2)_n = E_0 - 3J_d \qquad - (3 + 3(n-2))J_{se}; n > 2 \tag{2.108}$$

$$E(AF3)_n = E_0 + (3 + 2(n-2))J_d + (1 + 1(n-2))J_{se}; n > 2 \tag{2.109}$$

Equation of these formulae give the boundaries between phases, as a function of the number of layers. Rewriting these in terms of x gives

$$AF3 : AF2 => (2n-1)x + (n-1) = -3x - (3n-3) \tag{2.110}$$

$$x = \frac{4-4n}{2+2n} = \frac{2(1-n)}{1+n} \tag{2.111}$$

$$AF2 : FM => -3x - (3n-3) = -(6n-3)x + (3n-3) \tag{2.112}$$

$$x = \frac{6n-6}{6n-6} = 1 \tag{2.113}$$

These show that the AF3:AF2 phase boundary moves, as a function of temperature. In the limit of infinitely thick layered systems, which is the same as a bulk system, the phase boundary tends to the bulk vale of $x = -2$. The AF2:FM phase boundary is independent of the film thickness. This is is shown diagrammatically in figure 2.2.

Values for the coupling constants can be obtained from experimental measurements, or by calculation within some more complete model of electronic structure. Within the realm of quantum mechanical calculation it is not possible to calculate J_d and J_{se} directly, as they do not correspond to any physical observable variables, i.e. there are no $\hat{\mathbf{J}}_d$ or $\hat{\mathbf{J}}_{se}$ operators. To extract values of J_d and J_{se} from quantum mechanical calculations, a mapping is performed by writing expressions for the total energies of a system in the Ising Hamiltonian, and equating these to the energy given by quantum mechanical calculations. Thus, the E_0 term in the energy expressions represents the spin independent contribution to the total energy. As quantum mechanical calculations are implicitly at zero temperature, this mapping is exact, if the system is represented well by the Ising model.

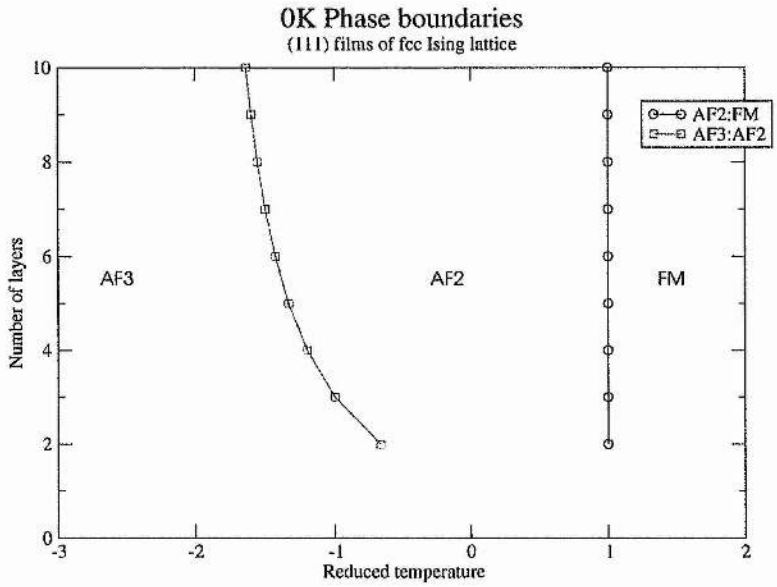

Figure 2.2: 0K phase diagram for Ising model rocksalt structures, projected onto a (111) film, over a range of film thicknesses.

2.4 Meanfield theory

The ideal method to investigate the properties of the Ising model is to evaluate the partition function. This has proven quite an intractable problem. The simplest case of a one dimensional model, with nearest neighbour interactions was solved by Bethe [71]. The 2 dimensional square lattice was solved by Onsager [72], allowing for an anisotropic nearest neighbour interaction. This remains an impressive piece of work, and no further systems have been solved analytically. A slightly simpler account of Onsager's proof was given a few years later [73].

The mean field approximation makes the assumption that the state of a system of many points may be approximated by replacing all the values at

those points with a single value that is equal to the average of all the points. The effect of this is to reduce a system that depends on N variables to a system that depends on only one. This gain in simplicity is offset by the loss in accuracy of the model - notably, by enforcing a single value across the system, it prevents the existence of fluctuations.

Within the Ising model, this replaces the individual spins with the expectation value, and overestimates the temperature of any order / disorder transition. In cases where there are multiple symmetry non-identical sites, the spin across all identical sites is replaced by a single average value, resulting in one value per non-identical site.

Mean field theory uses approximate descriptions of systems, and leaves the form of any operator essentially unchanged. The actual evaluation of these operators become significantly simpler, however.

The definition of the expectation value of some parameter, A, from statistical mechanics, is:

$$\langle \mathbf{A} \rangle = \frac{\sum_i \mathbf{A}_i e^{-\frac{E_i}{k_B T}}}{\sum_i e^{-\frac{E_i}{k_B T}}} \tag{2.114}$$

where i runs over all possible states, and E_i is the energy of the i'th state. In the case of the mean field approximation, the energy can be replaced with the expectation value of the Hamiltonian giving:

$$\langle \mathbf{S} \rangle = \frac{\sum_i \mathbf{S}_i e^{-\frac{\hat{\mathbf{H}}_{mf}\bar{\mathbf{S}}}{k_B T}}}{\sum_i e^{-\frac{\hat{\mathbf{H}}_{mf}\bar{\mathbf{S}}}{2k_B T}}} \tag{2.115}$$

Here, the term $\bar{\mathbf{S}}$ denotes the mean spin of the system, and $\langle \mathbf{S} \rangle$ is the expectation value of the spin operator. Mean field equates these, and thus this expression gives the mean field in terms of itself. There are two possible values for S_i, +1 and -1. Replacing the first summation explicitly and writing the Ising Hamiltonian as:

$$\hat{\mathbf{H}}_{ising} = -\frac{1}{2J_{se}} \left(-X \sum_{i}^{N_L} \sum_{j}^{nn} \mathbf{S_i S_j} + \sum_{i}^{N_L} \sum_{j}^{nnn} \mathbf{S_i S_j} \right) \tag{2.116}$$

where $X = J_d/J_{se}$, and $\Delta N_{(nn)}$ $\Delta N_{(nnn)}$ are as before, gives

$$\langle \mathbf{S} \rangle = -\frac{\sum_{i}^{N_L} \mathbf{S}_i \cdot e^{\frac{\Delta N_{(nn)} \langle \mathbf{S} \rangle \sum_{i}^{N_L} \mathbf{S_i} - X \langle \mathbf{S} \rangle \sum_{i}^{N_L} \mathbf{S_i}}{2k_B T J_{se}}}}{\sum_{i}^{N_L} e^{\frac{\Delta N_{(nn)} \langle \mathbf{S} \rangle \sum_{i}^{N_L} \mathbf{S_i} - X \langle \mathbf{S} \rangle \sum_{i}^{N_L} \mathbf{S_i}}{2k_B T J_{se}}}} \tag{2.117}$$

$$\langle \mathbf{S} \rangle = -\frac{e^{\frac{\Delta N_{(nn)} (+1) \langle \mathbf{S} \rangle - X \Delta N_{(nnn)} (+1) \langle \mathbf{S} \rangle}{2k_B T J_{se}}} - e^{\frac{\Delta N_{(nn)} (-1) \langle \mathbf{S} \rangle - X \Delta N_{(nnn)} (-1) \langle \mathbf{S} \rangle}{2k_B T J_{se}}}}{e^{\frac{\Delta N_{(nn)} (+1) \langle \mathbf{S} \rangle - X \Delta N_{(nnn)} (+1) \langle \mathbf{S} \rangle}{2k_B T J_{se}}} + e^{\frac{\Delta N_{(nn)} (-1) \langle \mathbf{S} \rangle - X \Delta N_{(nnn)} (-1) \langle \mathbf{S} \rangle}{2k_B T J_{se}}}} \tag{2.118}$$

$$\langle \mathbf{S} \rangle = \tanh \left(\frac{X \Delta N_{(nn)} \langle \mathbf{S} \rangle - \Delta N_{(nnn)} \langle \mathbf{S} \rangle}{2k_B T J_{se}} \right) \tag{2.119}$$

In general, it is not possible to solve this equation analytically. However, at the transition to a paramagnetic phase, the system becomes disordered, so that the expectation value of the spin, $\langle \mathbf{S} \rangle$, tends to zero at the transition

point. Using this, and the result:

$$\lim_{x \to 0} \tanh(x) = x$$

it can be shown that

$$\lim_{T \to \tilde{T}_c, \langle \mathbf{S} \rangle \to 0} \langle \mathbf{S} \rangle = \beta \left(X \Delta N_{(nn)} \langle \mathbf{S} \rangle - \Delta N_{(nnn)} \langle \mathbf{S} \rangle \right) \tag{2.120}$$

where $\beta = \frac{1}{k_B \tilde{T}}$. From this, the transition temperature for any system can be estimated, in the mean field, once the local environments of each atom are known. It is convenient to define a reduced temperature, $\tilde{T}$ as:

$$\tilde{T} = \frac{k_B T}{J_{se}} \tag{2.121}$$

Results phrased in the form of a reduced temperature are independent of any particular system, and may be applied by the simple procedure of finding the ratio of J_d to J_{se}, to find qualitative behaviour, and then scaling with the J_{se}. The same approach is used in the Monte Carlo simulations.

It's now possible to calculate the reduced temperature for the order / disorder transition, for a specified lattice and magnetic order. The named ordering for the rocksalt structure is sumarised in table 2.1. Note that these definitions are based on the local order at each atom.

Real magnetic systems with the rocksalt structure have the AF2 ordering in the bulk ground state. This arises from the nature of the coupling constants J_d and J_{se}. These are empirically applied, and thus can cover more than one fundamental mechanism. The next nearest neighbour interaction

coefficient J_{se} is dominated by super exchange, but the nearest neighbour interaction J_d covers two competing interactions - direct exchange, and Pauli repulsion. The direct exchange will tend to align spin in neighbouring atoms, whilst the Pauli repulsion will tend to separate the two spin states. The net effect of this is that J_d tends to be smaller in magnitude, and may be either parallel or antiparallel, whilst J_{se} is always antiparallel in nature. There are other effects that are included in these aggregate coefficients, but these effects dominate. For this reason, the two coefficients may be replaced by a single ratio, where the sign of the ratio determines the sign of J_d, and J_{se} is defined to be antiparallel. Such a simplification is made in figure 2.4, which shows the meanfield predicted order to disorder transition temperatures, as a function of that ratio.

2.5 Monte Carlo simulation

Monte Carlo methods are a way of carrying out importance sampling on some configuration space. For a system where there are a large number of possible configurations, the Monte Carlo procedure will select those configurations that make the greatest contribution to the ensemble. This allows for a sum over all configurations to be replaced with a sum over a small number of the most important configurations.

These methods operate on the principle of a Markov chain, whereby over a number of iterations, the system tends to the equilibrium configuration. It is useful to consider the concept of a fictitious time, t, which represents how many iterations have occurred. The system is thought to be in equilibrium,

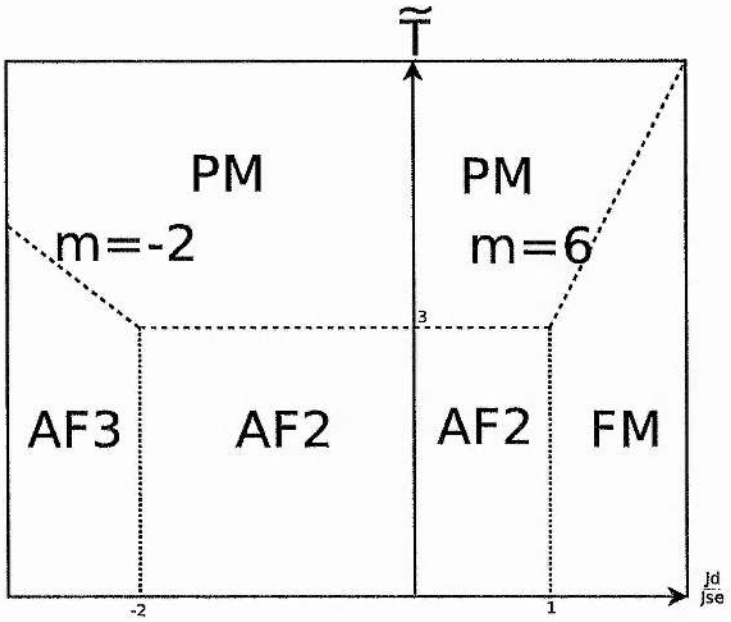

Figure 2.3: Phase diagram for Ising model rocksalt structures, restricted to antiparallel next nearest neighbour interactions. Magnetic states are defined in table 2.1, with PM being the disordered paramagnetic state.

and thus is invariant over real time.

The aim of Monte Carlo simulation is that as t increases, the system tends to the equilibrium state, from some initial state. To do this, some aspect of the system is examined, and possibly altered. It can be seen that, for a system at equilibrium in some microstate A, at some fictitious time t, the probability that it moves to some microstate B, $P(A \rightarrow B)$ must obey the condition

$$P(A \rightarrow B)s(A,t) = P(B \rightarrow A)s(B,t); \forall A, B \qquad (2.122)$$

where s(A, t) is the probability that the system is in microstate A at time t. This is often called the detailed balance condition, and arises because the rate of change of a system at equilibrium is zero, thus the probability of entering any particular microstate is equal to the probability of leaving it. It was shown by Metropolis et al [74] that if an algorithm is well defined for $P(A \rightarrow B)$ for all microstates A and B, and satisfies the condition of detailed balance, then as t tends to infinity, for any particular Markovian chain, the probability of any state A occurring is equal to its equilibrium probability of $e^{-k_b T E_A}/Z$, where Z is the partition function of the system, and E_A is the energy of the microstate.

There are many methods that obey the condition of detailed balance, but the most commonly used is the Metropolis algorithm, equation 2.123. The main limitations on the Metropolis algorithm are that as the temperature grows large, the probability of transition tends to 1, thus meaning that in the high temperature limit the system will not become stable and near a transition point it can take a long time to reach equilibrium. As the work carried out here is only interested in low temperature behaviour, and is not looking for high precision in the vicinity of transition points, neither of these limitations is relevant.

$$\begin{aligned} P(A \rightarrow B) &= e^{\frac{-\Delta E_{AB}}{kT}} \quad ; \Delta E_{AB} > 0 \\ &= 1 \qquad\qquad ; \Delta E_{AB} \leq 0 \end{aligned} \tag{2.123}$$

The principle of ergodicity states that all possible configurations of the system should be obtainable, from any arbitrary starting point. If the simulation is not ergodic, then the results may not be valid. Whilst it may

appear that the Metropolis algorithm is always ergodic, it can depend on the suitability of the random number generator, which is used to decide if a particular change of state should occur, in accordance with the probabilities outlined above.

It can take some time, dependent on the temperature of the system, to reach a state where the initial condition has negligible effect on the state of the system. For this reason, it is common to discard a number of configurations at the start of the process, before collecting statistics on the configurations. The Monte Carlo simulation gives a set of configurations that make the biggest contribution to the partition function. As the fictitious time increases, the configurations that make more contribution are more likely to occur. Thus, for systems where only a few configurations are important, only a short time is required, whilst for a system where many configurations are important, a longer run time is required, as more configurations must be examined. One knock-on effect of this is at a transition point, where the effective correlation length grows large. As this occurs, that represents an increase in the number of configurations that contribute to the real states. Essentially, the number of configurations sampled grows near a transition point, requiring more computation for the the same accuracy. This makes locating a transition point much simpler than describing the systems behaviour at that point - where the correlation length is infinite.

One of the most useful statistics calculated in the simulation is that of the specific heat. As the system is of fixed size, this is the specific heat at constant volume, and is of use in identifying transitions between states. The specific heat at constant volume (Cv) increases in the vicinity of a transition, and

becomes theoretically infinite at the transition point. In practice, numerical accuracy means that a finite sized peak in the Cv is observed. This statistic is calculated from a fluctuation based approach [75], as shown in equation 2.124, where k_B is Boltzmann's constant, T is the temperature, and $\hat{H}$ is the Hamiltonian of the system.

$$k_B T^2 C_v = \left\langle \hat{H}^2 \right\rangle - \left\langle \hat{H} \right\rangle^2 \tag{2.124}$$

For the simulations, the expectation value of the Hamiltonian can be calculated directly for each microstate, and the appropriate summing and averaging gives the Cv.

2.5.1 Random number generator

The random number generator used was the internal procedure in XL Fortran. In order to ensure that the generator was suitable for simulation work, a number of statistical tests were performed. These were taken from Knuth's book [76], and are presented here with only brief details.

The desirable criteria for the random number generator are that the numbers produced are equidistributed between 0 and 1, and that they are independent on successive requests. The requirement of independence cannot be strictly met with any algorithm on a computer, as it is deterministic with finite storage space, thus must eventually repeat. The purpose of the tests, then, is to give some assurance that the values are independent enough, for the purposes desired.

The tests work by collecting statistics, and then applying the chi-squared

test, for discrete categories, or the Kolmogorov-Smirnov test for a continuum of possible values. These tests then give a number, describing the likelihood of an equidistributed random sequence producing that set of values. Both tests rely on the number of observations being large. It is not possible to quantify how large, however, because as the number of observations, n, increases, globally non-random behaviour is more apparent, but locally non-random behaviour is less apparent. Each test should therefore be run with a series of values of n. Passing these tests is a necessary, but not sufficient test of randomness.

The equidistribution test examines the spread of numbers to see if they generated uniformly between 0 and 1. This test was performed by choosing a convenient integer, d, say 100, and multiplying the sequence by this number, and taking the integer part, producing a sequence of integers in the range 0 to $d-1$. The frequency of each number was counted and a chi-squared test with d degrees of freedom, with the probability $\frac{1}{d}$ for each category was applied. This can also be done by applying a Kolmogorov-Smirnov test to the reals produced with the distribution function $F(x) = x$.

In addition to testing that the sequence generates the full spectrum of numbers, a random sequence has no relation between successive pairs of numbers. To test for this, the sequence of real numbers is, again, converted to integers in the same way as above. The frequency of successive pairs of integers are counted, noting that each number can be counted only once. A chi-squared test is then applied to these categories, with d^2 degrees of freedom, and probability of $\frac{1}{d^2}$ of each category. It is apparent that this test, the serial test, can be generalised to 3, 4, and higher sets. As the purpose

of the tests is to ensure that the simulation will be ergodic, it is sufficient to test triples, on the basis that there is one number used per site, and that any short range correlation shorter than three will impact on the overall results.

All tests were reduced to a chi-squared test, where 1000 and 10000 observations on average per category were recorded. Each test was run 100 times at each level of observation. Table 2.5.1 gives the results for 1000 observations, and table 2.5.1 for 10000 observations.

These tables consist of a banding of the results of the chi-squared test, into likely hood bands. These represent the probability of sequence of independent values evenly distributed between 0 and 1 giving rise to the observations noted. For a good generator, the probability of any given chi-squared value should be proportional to the size of the category, although for a truly random number generator, there will be variance from that.

The meaning of the codes in the tests column is given in table 2.5.1.

Test	Categorised Results							
	>99%	99-95%	95-75%	75-50%	50-25%	25-5%	5-1%	<1%
Eq(10)	0	0	16	35	33	16	0	0
Eq(20)	0	1	13	28	37	20	1	0
Eq(30)	0	1	11	30	43	14	1	0
Eq(40)	0	1	10	39	34	16	0	0
Eq(50)	0	0	18	35	26	19	2	0
Eq(100)	0	1	20	29	30	19	1	0
Eq(150)	0	1	12	33	37	15	2	0
Eq(200)	0	3	14	28	38	17	0	0
Pair(10)	0	1	12	25	45	16	1	0
Pair(20)	0	1	19	33	29	18	0	0
Pair(30)	0	1	13	31	31	24	0	0
Pair(40)	0	0	14	36	30	19	1	0
Pair(50)	0	1	13	33	36	14	3	0
Pair(60)	0	1	12	28	37	21	1	0
Pair(70)	0	1	17	30	34	17	1	0
Pair(80)	0	0	8	22	43	21	5	1
Pair(90)	0	0	19	29	33	17	2	0
Pair(100)	0	0	15	26	37	20	2	0
Trip(10)	0	0	16	30	38	12	4	0
Trip(15)	0	2	7	40	27	23	1	0
Trip(20)	0	2	19	35	23	21	0	0
Trip(25)	0	6	18	36	36	4	0	0
Trip(30)	0	0	12	28	31	24	5	0

Table 2.3: Chi-squared results of randomness test for 1000 observations

Test	Categorised Results							
	>99%	99-95%	95-75%	75-50%	50-25%	25-5%	5-1%	<1%
Eq(10)	0	0	21	32	32	15	0	0
Eq(20)	0	1	22	33	27	17	0	0
Eq(30)	0	0	19	34	32	15	0	0
Eq(40)	0	0	17	35	31	16	1	0
Eq(50)	0	1	20	27	30	21	1	0
Eq(100)	0	2	27	31	25	14	1	0
Eq(150)	0	5	24	33	30	8	0	0
Eq(200)	0	3	25	33	36	3	0	0
Pair(10)	0	0	12	30	38	18	2	0
Pair(20)	0	0	14	37	26	19	4	0
Pair(30)	0	0	15	33	36	16	0	0
Pair(40)	0	1	17	28	32	20	2	0
Pair(50)	0	0	14	34	32	20	0	0

Table 2.4: Chi-squared results of randomness test for 10000 observations

Code	Description
Eq(n)	Equidistribution test for n categories
Pair(n)	Serial test, on pairs, for n categories
Trip(n)	Serial test, on triplets, for n categories

Table 2.5: Description of the test codes given in tables

Chapter 3

(111) layers

3.1 Introduction

Experimental results for FeO(111) on Fe [77] found the surface to have ferromagnetic order, at temperatures above the bulk Néel temperature. A number of possible explanations have been given, most considering some surface reconstruction to be responsible. Phase diagrams of $\hat{H}_{Ising}$ projected onto (100) layers of FCC lattice by Mackrodt and Noguera [78] found multicritical behaviour, and a quantitative description of the reduction of the Néel temperature in films found by Alders et al [69].

Where the (100) film ordered with AF2 ordering, as most magnetic top row transition monoxides do, if there are an odd number of layers in the film, the outermost layers have a distinct, and slightly lower, transition temperature from the subsurface layers. Surprisingly, where there are an even number of layers in the film all the layers share a single critical temperature. The position of the phase boundary between AF2 and the ferromagnetic phase

was also predicted to move slightly, although this was quite a small change. The agreement with Alders et al experimental data was good, confirming that the Ising model is a good predictor of the observable change in Néel temperature with film thickness.

In light of these studies, the Ising Hamiltonian projected onto the (111) layers was studied. One aim was to examine the behaviour for any behaviour not seen in the bulk, such as the multicritical behaviour for the (100) layers, and also to provide a foundation for examining the effect of any surface reconstructions on the magnetic order. As a first step towards understanding the behaviour of real films, unreconstructed, stoichiometric films were examined. For the thinest films these may correspond to physically meaningful cases, and serve as an initial approximation for other cases.

In the (111) orientation rocksalt type structures present a polar surface [20], which has the direct consequence that, in general, it must be stabilised to avoid large surface energies. Nevertheless, examining the behaviour of the perfect structure is an instructive first approximation to the real world behaviour of these systems. Additionally, as the dipole moment is dependent on the thickness of a film, it is possible to construct thin, stoichiometric films of the (111) surface.

For NiO (111) surfaces on Au(111) [22] and Ni(111), low energy electron diffraction (LEED) experiments show a p(2x2) reconstruction, where recent [79] grazing incidence x-ray diffraction (GIXD) experiments have confirmed the octopolar reconstruction, with Ni termination of a single crystal, and both terminations observed on a thin film. This was kept in mind with the code developed here, so as to allow maximal code reuse.

3.2 Methods

3.2.1 Mean field implementation

The mean field approximation can be solved analytically for the order -> disorder transition temperature in (111) rocksalt structured systems. It can also be found by a numerical eigenvalue solution, or by successive approximation solution. All three methods were used here. Although the use of the numerical methods is perhaps redundant when the analytic result is available, it allows for checking of the solving routines, looking ahead to using the same routines in situations where no analytic solution is available, such as with a surface reconstruction. In addition, the successive approximation solver gives the order by layer as a function temperature, which is not accessible by the other methods.

To produce an iterative solution, it is first necessary to rewrite equation 2.119 in a recurring form. Using equation 2.121 to simplify and writing in terms of $\tilde{T}$ gives (3.1).

$$\langle \mathbf{S_{n+1}} \rangle = \tanh\left(-\frac{1}{2\tilde{T}}\left(X n_d \langle \mathbf{S_n} \rangle - n_{se} \langle \mathbf{S_n} \rangle\right)\right) \tag{3.1}$$

In practice, (3.1) is insufficient to model a layered system. It has reference to only a single mean spin value, and thus treats all spin carrying locations as identical. Whilst this is the correct model for a bulk system, infinite in three dimensions, it is necessary to consider each layer as a distinct entity to allow for the effect of a surface. This transforms the mean spin into a vector of mean spins, and the interaction coefficients, n_d and n_{se}, become matrices

of coefficients, $\mathbf{N_d}$ and $\mathbf{N_{se}}$ respectively. These matrices are tridiagonal for a set of (111) layers, but are straight forward to convert to a description of the periodic bulk, by application of boundary conditions. The general form of the matrices are shown in (3.2), where setting $c = 0$ gives the layered system, and $c = b$ gives periodic boundary conditions which model the bulk case. Although no new information would be gained by applying a periodic boundary condition, it has value as it allows for the calculation of situation where the results are well known and thus acts as method of checking the calculation routines.

$$\mathbf{N} = \begin{bmatrix} a & b & 0 & & 0 & 0 & c \\ b & a & b & \cdots & 0 & 0 & 0 \\ 0 & b & a & & 0 & 0 & 0 \\ & \vdots & & \ddots & \vdots & & \\ 0 & 0 & 0 & & a & b & 0 \\ 0 & 0 & 0 & \cdots & b & a & b \\ c & 0 & 0 & & 0 & b & a \end{bmatrix} \tag{3.2}$$

The actual values of a and b are determined by the lattice structure, which are calculated separately from the details of the solution, and will be dealt with later. It should be noted that there is no theoretical reason to restrict the interaction matrices to tridiagonal form - there are many geometries that would involve an interaction with an atom two layers removed, such as (100) NiO. It is clear that the two matrices $\mathbf{N_d}$ and $\mathbf{N_{se}}$ can be combined. At the

transition point the mean spin tends to 0, so the hyperbolic tangent function is of no significance (Eq 2.4), giving (3.3) where $\mathbf{N} = \mathbf{N_{se}} - X\mathbf{N_d}$.

$$\langle \mathbf{S} \rangle = \frac{1}{2\tilde{T}} \mathbf{N} \langle \mathbf{S} \rangle \tag{3.3}$$

The iterative solver solves the equation, as written in (3.4).

$$\langle \mathbf{S_{n+1}} \rangle = \tanh\left(\frac{1}{2\tilde{T}} \mathbf{N} \langle \mathbf{S_n} \rangle\right) \tag{3.4}$$

It's clear that (3.3) is a simplification of the above to the transition point. The successive approximation solver evaluates this equation many times, until a solution is found. The general procedure is to raise the reduced temperature a small amount, and then iterate through n steps, until the vector $\bar{\mathbf{S}}_{\mathbf{n+1}} = \bar{\mathbf{S}}_{\mathbf{n}}$. This is then repeated until the stable point where $\bar{\mathbf{S}} = (0, 0, ..., 0)$, at which point the transition temperature has been found. This relies on the increase in temperature being small, so the error in the position of the transition point is, approximately, the temperature interval used. In practice, the eigenvalue solution was calculated first, and the results compared. Any difference would indicate an error in the calculation, typically that the size of the temperature interval used in the successive approximation solver was too coarse, or an incorrect initial state was used.

This method requires an initial set of spins. Choosing a set of spins that did not correspond to a valid ground state resulted in either numerical instability, or a solution that was at odds with the eigenvalue solution. By empirical observation, the code was set to start the successive approximation from a reduced temperature of 0.4. This was mostly to reduce the number of

irrelevant data points, as the total computational time involved was typically under 5 seconds. The other major refinement was to include a damping factor, which was gradually reduced as convergence was approached, which improved numerical stability.

The interaction matrices used by the solver are fairly large, and mostly self similar within small offsets. This is an ideal candidate for construction by computer, so a program was written in C to produce these matrices, for any specified number of layers. The matrices of interaction coefficients are determined by the geometry of the situation. The eigenvalue solver was implemented in Fortran 90, using the Lapack routine "dgeev" to calculate the eigenvalues directly. The Fortran solver routine had no knowledge of any particular geometry, which was all supplied to it by the C code.

In order to take account of the geometry, it is necessary to examine the local interactions at each atom. These were given in Table 2.2 (on page 46), where account was taken of the (111) layer boundary condition. It is evident that the mean field results will depend on the number of layers present in the system.

It is worth noting that, for the successive approximation solver routines, the initial spin matrix is important. When given an inital condition that does not correspond to the ground state, the solver was often numerically unstable, and normally gave incorrect answers (in disagreement with the eigenvalue solutions). Therefore, it should be considered valid only for a correctly specified ground state.

3.3 Mean field results

To calculate the order to disorder transition temperature in mean field, first the interaction matrices are constructed. There are a number of unique mean spins, depending on the thickness of the system. Although, in the case of a bilayer, there is only a single mean spin, it shall be worked through as an anchoring for thicker systems. These equations are expressed in matrix form.

$$FM: \begin{pmatrix} \bar{S}_1 \\ \bar{S}_1 \end{pmatrix} = vtanh\left(\frac{-1}{2\tilde{T}}\left[x\begin{pmatrix} -6 & -3 \\ -3 & -6 \end{pmatrix} - \begin{pmatrix} 0 & -3 \\ -3 & 0 \end{pmatrix}\right] \cdot \begin{pmatrix} \bar{S}_1 \\ \bar{S}_1 \end{pmatrix}\right) \tag{3.5}$$

$$AF2: \begin{pmatrix} \bar{S}_1 \\ \bar{S}_1 \end{pmatrix} = vtanh\left(\frac{-1}{2\tilde{T}}\left[x\begin{pmatrix} -6 & 3 \\ 3 & -6 \end{pmatrix} - \begin{pmatrix} 0 & 3 \\ 3 & 0 \end{pmatrix}\right] \cdot \begin{pmatrix} \bar{S}_1 \\ \bar{S}_1 \end{pmatrix}\right) \tag{3.6}$$

$$AF3: \begin{pmatrix} \bar{S}_1 \\ \bar{S}_1 \end{pmatrix} = vtanh\left(\frac{-1}{2\tilde{T}}\left[x\begin{pmatrix} 2 & 1 \\ 1 & 2 \end{pmatrix} - \begin{pmatrix} 0 & -1 \\ -1 & 0 \end{pmatrix}\right] \cdot \begin{pmatrix} \bar{S}_1 \\ \bar{S}_1 \end{pmatrix}\right) \tag{3.7}$$

The operator *vtanh* operates on a vector to give a vector, and is defined as

$$vtanh\begin{pmatrix} v_1 \\ v_2 \end{pmatrix} = \begin{pmatrix} tanh(u_1) \\ tanh(u_2) \end{pmatrix} \tag{3.8}$$

It is clear to see that that as each element u_i tends to zero, v_i tends to

u_i, the same as the behaviour of the scaler function *tanh*, equation (2.4). Combining the pair of matrices, and then applying the limits at $\tilde{T}_c$ gives

$$FM: \begin{pmatrix} \bar{S}_1 \\ \bar{S}_1 \end{pmatrix} = \frac{-1}{2\tilde{T}_c} \begin{pmatrix} -6x & -3x+3 \\ -3x+3 & -6x \end{pmatrix} \cdot \begin{pmatrix} \bar{S}_1 \\ \bar{S}_1 \end{pmatrix} \tag{3.9}$$

$$AF2: \begin{pmatrix} \bar{S}_1 \\ \bar{S}_1 \end{pmatrix} = \frac{-1}{2\tilde{T}_c} \begin{pmatrix} -6x & 3x-3 \\ -3x-3 & -6x \end{pmatrix} \cdot \begin{pmatrix} \bar{S}_1 \\ \bar{S}_1 \end{pmatrix} \tag{3.10}$$

$$AF3: \begin{pmatrix} \bar{S}_1 \\ \bar{S}_1 \end{pmatrix} = \frac{-1}{2\tilde{T}_c} \begin{pmatrix} 2x & x+1 \\ x+1 & 2x \end{pmatrix} \cdot \begin{pmatrix} \bar{S}_1 \\ \bar{S}_1 \end{pmatrix} \tag{3.11}$$

Solutions to the above are straightforward, as the vector of spins is degenerate. Thus, we find that

$$FM: \tilde{T}_c = 3x + \frac{3x}{2} - \frac{3}{2} = 4.5x - 1.5 \tag{3.12}$$

$$AF2: \tilde{T}_c = 3x - \frac{3x}{2} + \frac{3}{2} = 1.5x + 1.5 \tag{3.13}$$

$$AF3: \tilde{T}_c = -x - \frac{x}{2} + \frac{1}{2} = -1.5x - 0.5 \tag{3.14}$$

Repeating the above procedure for a trilayer system, it is noted that there are now two distinct mean spins - for the outer and inner layers.

State	a	b
FM	-6x	-3x+3
AF2	-6x	3x-3
AF3	2x	x+1

Table 3.1: Coefficients for matrix N (equation 3.2)

$$FM: \begin{pmatrix} \bar{S}_1 \\ \bar{S}_2 \\ \bar{S}_1 \end{pmatrix} = \frac{-1}{2\tilde{T}_c} \begin{pmatrix} -6x & -3x+3 & 0 \\ -3x+3 & -6x & -3x+3 \\ 0 & -3x+3 & -6x \end{pmatrix} \cdot \begin{pmatrix} \bar{S}_1 \\ \bar{S}_2 \\ \bar{S}_1 \end{pmatrix} \quad (3.15)$$

$$AF2: \begin{pmatrix} \bar{S}_1 \\ \bar{S}_2 \\ \bar{S}_1 \end{pmatrix} = \frac{-1}{2\tilde{T}_c} \begin{pmatrix} -6x & 3x-3 & 0 \\ 3x-3 & -6x & 3x-3 \\ 0 & 3x-3 & -6x \end{pmatrix} \cdot \begin{pmatrix} \bar{S}_1 \\ \bar{S}_2 \\ \bar{S}_1 \end{pmatrix} \quad (3.16)$$

$$AF3: \begin{pmatrix} \bar{S}_1 \\ \bar{S}_2 \\ \bar{S}_1 \end{pmatrix} = \frac{-1}{2\tilde{T}_c} \begin{pmatrix} 2x & x+1 & 0 \\ x+1 & 2x & x+1 \\ 0 & x+1 & 2x \end{pmatrix} \cdot \begin{pmatrix} \bar{S}_1 \\ \bar{S}_2 \\ \bar{S}_1 \end{pmatrix} \quad (3.17)$$

It can be seen that there is a pattern in the matrices. This can be exploited, by reference to equation 3.2, where we can assign values to the terms a and b there.

The matrix N is tridiagonal, with a single value on the diagonal, and a single value for the sub- and super-diagonals. This can be solved analytically. For a matrix with some value a on the diagonal, and b above and below the diagonal, the eigenvalues are given by (3.18), for an NxN matrix.

$$E_k = a + 2b\cos\left(\frac{k\pi}{N+1}\right); k = 1, ..., N \tag{3.18}$$

For the bilayer case, the cosine function gives values of { 0.5 , -0.5 }, which gives expressions for $\tilde{T}_c$ of { 4.5x + 1.5, -3x - 1.5 }. Clearly, the latter expression will be negative over the region where FM is favoured, and thus may be ignored here. Similarly, for the other magnetic states of the bilayer, only the first eigenvalue is the correct one. In the case of the trilayer, the cosine function gives values of { $\sqrt{0.5}$, 0, -$\sqrt{0.5}$ }, which give the set of expressions { 5.12x - 2.12, 3x, 0.87x + 2.12 } for the FM state. Again, the first eigenvalue is the desired expression, which can be justified as being the only transition temperature greater than for the bilayer case. The question may be raised, however, what do the other eigenvalues represent, if anything? It is not inconceivable that they might, as with (100) layers, indicate multicritical behaviour.

The numerical solver can produce, by successive approximation, the order parameter as a function of the reduced temperature. This will show multicritical behaviour by the order parameters for different layers reaching zero mean spin at different reduced temperatures. The graph of the order parameter calculated is shown in Figure 3.1 for the trilayer, where it can be seen that there is only one critical temperature which corresponds to the first eigenvalue in the set given above. Thicker systems and other magnetic states agree with this one in predicting only a single critical point, and agreeing with the first eigenvalue.

That the first eigenvalue is the correct one can be seen by examining

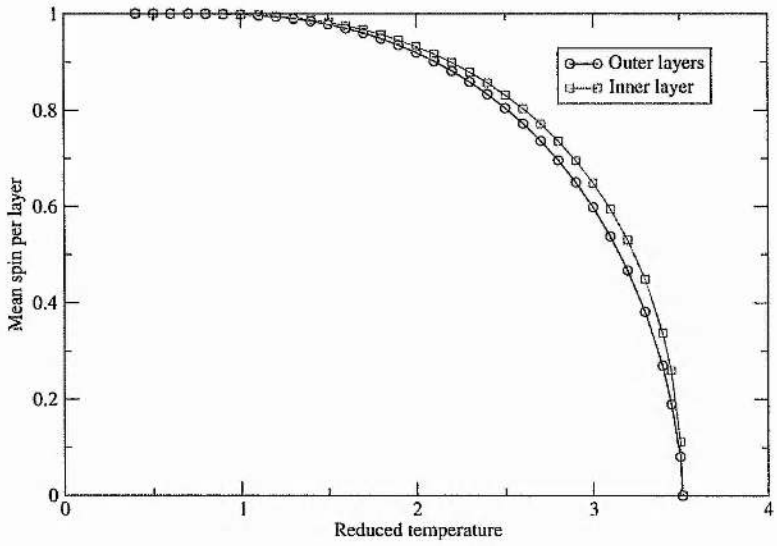

Figure 3.1: Calculated mean spin per layer, for a trilayer system, showing only a single critical temperature at 3.512. This particular graph is for a ferromagnetic system with the ratio X set at 1.1, although the same form was seen throughout all of range of X examined.

the effect as the number of layers tends to infinity. For an infinitely thick system, the form of the transition temperature is such that the equivalent to Equation (3.18) is $a + 2b$. Thus, the cosine function must result in a value of 1. This is the case for the first value of the cosine function only, which tends to 1 as N tends to infinity. Thus, in order to be correct in the limit of large thickness, it must be the first eigenvalue that is correct. Additionally, as no other eigenvalue tends to the same value, this agrees that there is only a single critical point.

Table 3.2 lists the appropriate expressions for the three states, over a range of film thicknesses, and includes the case of the bulk.

Thickness	AF3	AF2	FM
2	-x - 0.5	1.5x + 1.5	4.5x - 1.5
3	-1.41x - 0.71	0.87x + 2.12	5.12x - 2.12
4	-1.62x - 0.80	0.57x + 2.42	5.42x - 2.42
5	-1.73x - 0.86	0.40x + 2.60	5.60x - 2.60
10	-1.92x - 0.96	0.12x + 2.88	5.88x - 2.88
15	-1.96x - 0.98	0.06x + 2.94	5.94x - 2.94
Bulk	-2x - 1	3	6x -3

Table 3.2: Meanfield expressions for various thicknesses of (111) films.

3.3.1 Monte Carlo implementation

For a Monte Carlo implementation it is necessary to establish relationships between the atoms, to allow for the existence of multiple atom fluctuations. Whilst the term atom is not strictly correct when referring to the magnetically active interacting sites, it is used as a convenient shorthand term. The positions and nature of any non-magnetically active atoms (such as oxygen in NiO) are ignored. The effect that they have on the magnetic ordering is limited to mediating super-exchange interactions, which are allowed for explicitly in the building of neighbour lists.

A Fortran code was written so that the set of neighbours of an atom in position (x, y, z) could be expressed as $(x + i, y + j, z + k)$. The axes are not orthogonal, but along the [101], [111] and [-1-1-1] directions. This representation of the neighbours has a number of advantages, notably clarity and independence of the boundary conditions applied to the slab. The set of neighbour interactions is listed in Table 3.3. The boundary conditions of the slab under consideration were applied separately, and were periodic in the x and y directions, and open in the z directions. The periodic conditions were

a simple periodic condition, so that $x + U_x = x$, where U_x is the dimension of the slab in the x direction.

The Monte Carlo code developed for the simulations reported here was based on a previous code [80], written in Fortran 77. The code was compiled with IBM XL Fortran for AIX, on an IBM RS/6000 Model 3CT, which has a POWER 2 processor, and was fitted with 128MB of RAM. The original code was designed to examine rock salt (100) layers of based on a nearest and next-nearest neighbour Ising model. The code was adapted for the (111) layers and translated into Fortran 90 and optimised. For the new code the IBM XL Fortran 90 compiler was used.

The code generates an array, with each point in the array representing an atom. Each point can be assigned a state of +1 or -1. This was adapted from the previous code, which used 0 and 1, so that extension to allow for single non-interacting atoms is possible. It also simplified many of the statistics collected on the lattice. Lists are kept of what lattice points are in the locality of any specified atom. There is one neighbour list for the direct exchange interactions, and another for the super exchange interactions.

For programming simplicity arrays of fixed size were used, resulting in a hard upper limit to the size of system under study. To make the system specific to a particular structure and orientation, portions of the code - namely the calculation of neighbour lists and order parameters - require to be written. All other physical parameters are supplied to the program at runtime.

3.4 Neighbour list preparation

The lists of both direct and super exchange neighbours of each atom are computed at the start, and held in arrays. This allows alternate geometries to be implemented by writing only localised routines, rather than distributed throughout the code.

Direct neighbours	Super neighbours
$(x-1, y \quad , z+1)$	$(x+1, y-1, z+1)$
$(x \quad , y \quad , z+1)$	$(x-1, y-1, z+1)$
$(x \quad , y-1, z+1)$	$(x-1, y+1, z+1)$
$(x+1, y \quad , z)$	
$(x \quad , y+1, z)$	
$(x-1, y+1, z)$	
$(x-1, y \quad , z)$	
$(x \quad , y-1, z)$	
$(x+1, y-1, z)$	
$(x+1, y \quad , z-1)$	$(x-1, y+1, z-1)$
$(x \quad , y \quad , z-1)$	$(x+1, y+1, z-1)$
$(x \quad , y+1, z-1)$	$(x+1, y-1, z-1)$

Table 3.3: Neighbour list definitions for (111) films of the rocksalt structure.

Two conditions can be applied to these coordinate sets. Firstly, if atom A at (x, y, z) has a neighbour B at $(x+i, y+j, z+k)$ then atom B must have a neighbour at $(x-i, y-j, z-k)$. Secondly, the coordinate set may be changed by a rotation of the coordinates, in particular a 3-fold axis of rotation normal to the layers, and must still be self consistent and have the same meaning.

The form of neighbour list calculation presented on page 166 here utilises the function "combine", which packs the three index hexagonal coordinate system, that is well suited to the geometry of the problem, into the pair

of indices used by the code. This gives a very simple form in writing the code, so that it is clear there are no implementation induced errors in the neighbour list calculation.

The combine function (page 168) utilises Fortran's modulo arithmitic operator to apply the periodic boundary condition in the plane, and pack the two planar indices into the single index used for storage. These are straight periodic boundary conditions, as opposed to the screw boundary conditions sometimes used. The boundary conditions perpendicular to the (111) planes were applied explicitly, which allowed a simple conversion to do calculations on a bulk system, which were done as a method of checking the results.

Table 3.3 gives a complete list of the neighbour definitions for the (111) rocksalt structure. It can be observed that these from a self consistent set.

3.5 Transition probabilities preparation

As in other codes [80] an array containing all possible transition probabilities is precomputed, so that the time consuming exponential need be calculated only once for any local situation. These probabilities are held in the array, p, which has two indices. The first index relates to the direct interaction, whilst the second interaction is the super exchange interaction. The indices are the spin at the site under examination, multiplied by the negative of the sum of the spin of all the neighbours, or

$$index_1 = spin\_value(xy, z) \cdot - \sum_{i=1}^{n1(xy,z)} spin\_value\left(n1p(i, xy, z), n1c(i, xy, z)\right) \tag{3.19}$$

where $n1(xy, z)$ is a list of all the neighbours of the atom at the point (xy, z). The lists $n1p$ and $n1c$ give the in plane and layer coordinates respectively, for the i^{th} neighbour to the atom at (xy, z). Similarly, an $index_2$ was calculated for the next nearest neighbours, with appropriate definitions of $n2$, $n2p$ and $n2c$. The reason for this definition is that it simplifies calculations in the thermalisation routine.

The code for calculating the energy array is presented on page 169. It is here that the sign convention is applied to the ratio J_d/J_{se}, and thus the J_d and J_{se} parameters. J_{se} is set to always be positive (antiferromagnetic), and runs throughout the range $0 < J_{se} < \infty$, whilst the sign of J_d is the same as that of the ratio, and both are allowed to vary between $-\infty$ and ∞. This is the most physically meaningful sign convention, and the J_d coefficient includes a number of interactions, including direct exchange and Fermi repulsion, and thus may be of either sign, while the J_{se} represents pure super exchange, thus favouring an antiferromagnetic alignment of spins.

3.6 Monte Carlo routine

This is the main routine of the program which links everything together, and is shown on page 170. It starts by reading in the required parameters. The routine is written so that it can calculate multiple temperatures, using the

final spin state from the previous temperature as the starting configuration. Once all the parameters are read in, the neighbour lists and initial spin state are set up.

The code then loops over all specified temperatures, calculating the p array, and initial order (*AF2lro* and *Ferrolro*). The spin correlation functions (*spcorr1* and *spcorr2*) are used to calculate the energy and specific heat, from the total interactions. The variables $na1$ and $na2$ count the number of direct and super exchange interactions respectively, and are used as an index into the array p, the transition probabilities array. The approach means that less than 1/3 of the execution time is spent in the actual thermalisation routine. The rest of the time is spent calculating the statistics of the spin states, notably the spin correlation functions.

3.7 Order parameter calculation

The calculation of the order parameter for the AF2 and FM states is straightforward, due to the coincidence of the geometry of those states, and the system under examination. Firstly, an "order parameter" p_i is calculated for each layer, being simply the mean spin of that layer. The FM order parameter, P_{FM} is then the normalised sum of these "by layer" parameters, or, for n layers of an l by l system:

$$P_{FM} = \sum_{i=1}^{n} p_i \tag{3.20}$$

For AF2, the order parameter P_{AF2} is the antisymmetric sum of the by

layer values:

$$P_{AF2} = \sum_{i=1}^{n} (-1)^i p_i \tag{3.21}$$

The AF3 order parameter is more complicated. The isomagnetic planes are in a (210) direction, which forms stripes within the (111) layers. It is calculated as:

$$P_{AF3} = \sum_{i=1}^{n} \sum_{j=1}^{l} \sum_{k=0}^{l-1} \sigma(j + l * k, i) * (-1)^{floor(\frac{i+k}{2}+k+i)} \tag{3.22}$$

where the floor function takes the greatest integer that is smaller than its argument.

3.8 Results

The first set of Monte Carlo runs were performed to examine the bulk phase diagram. This behaviour is known, and thus serves as a confirmation of correctness and accuracy of the code. The results agreed with expectations, showing no deviation from previous work. The mean field solver gave results that agreed with the eigenvalue solution for the bulk, irrespective of the number of layers, when the periodic boundary conditions were applied. These matched the analytic results for mean field.

A series of calculations was performed on a set of sample sizes, in order to calibrate the accuracy of the simulation. These were performed on a model of the bulk system, in order to compare with known values. It was found that increasing the size of the repeat unit above around 30 sites on a side

had negligible effect on the results. Accordingly, it was decided to consider a 40x40x40 system as a good model of the bulk. Similarly, for a thin film, the properties of the simulated system converged at around a 30x30 tile size in plane, so a 40x40 tile size was used in all cases.

The first part of any simulation was discarded, to allow the system to reach equilibrium, and it was found that increasing the length of initial part beyond 10^3 cycles did not change the results, within the accuracy of the simulation, for either the bulk or a film. The accuracy of the simulation was estimated by examining the behaviour for a vanishingly small change in either of the real-valued parameters - the temperature and the ratio X. The observed noise in any calculated parameters can then be taken as the uncertainty of the simulation. Clearly, this will vary somewhat, and is expected to be largest near a phase boundary. This was estimated at a range of values of the ratio X around 0.95, and a range of temperatures around the transition point. The calculated specific heat varied by around 3-4% for vanishingly small changes in input, over 10^4 cycles for a thin film. Although not the most accurate set of conditions, this was deemed sufficient for the work, given that the main aim was to establish the qualitative behaviour.

The previous work on (100) layers by Mackrodt and Noguera [78] showed that the positions of phase boundaries predicted by zero temperature energetic analysis agreed with the values from the simulation, and that the multicritical behaviour predicted by the mean field analysis was also seen in simulation - i.e. the mean field was qualitatively correct. This lead to the inital expectation of the three phases behaving similarly to the prediction from mean field, with a lower critical temperature, the depression is greater

near the phase boundaries, but always a smooth function of X.

The results for the (111) layers were quite distinct from expectation. The effect of fluctuations is to depress the critical temperature, more so in the vicinity of a phase boundary, which was observed for values of x of 0.4 and greater. Around the ratio Jd / Jse = 0, a sudden drop was observed in the transition temperature, as measured by the location of the peak in Cv, with the critical temperature being depressed smoothly above that point. This was seen to greatest extent in the bilayer, as can be see in Figure 3.2. These calculations were run with a 40x40 atom dimension in the plane.

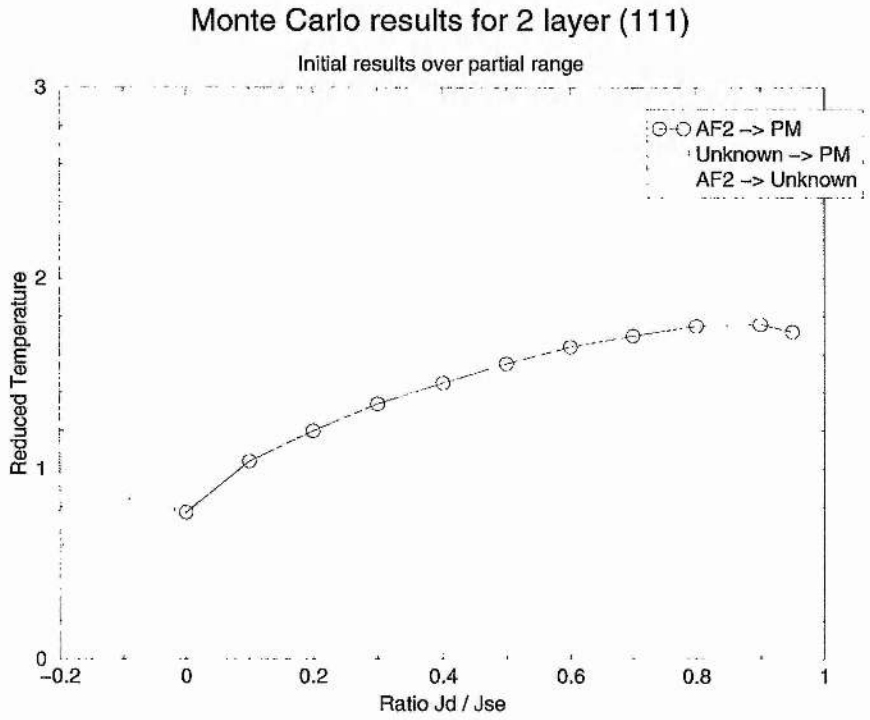

Figure 3.2: Monte Carlo predicted position of AF2 -> disorder transition for a bilayer of (111) rocksalt type MO

The first set of simulations were performed for a value of Xat 0.4. This was chosen semi-arbitrarily, as a value that was distant from predicted phase boundaries, so that the deviation from the mean field was expected to be low. Once the simulated properties were well established for that point, neighbouring values of Xwere examined extending the range towards the AF2:FM phase boundary at $X = 1$ and towards negative X.

The results did not agree with the expectations, and gave the behaviour seen in Figure 3.8 for negative Xvalues, with the pair of Cv peaks, indicating two phase transitions. The higher temperature transition was an order-disorder type, whilst the lower one was between two ordered phases.

Examining the order parameters of the simulated system showed a very sharp transition between ordered phases at the lower temperature. This additional phase was not in agreement with the mean field results and was too sharp to be a physical transition, implying that the initial state given to the simulation was not the correct ground state, and that there was another spin alignment of lower energy.

In order to identify the new, and as yet unidentified phase, a simulation was run, at a negative value of X, at a temperature between the two transitions observed. After reaching equilibrium, the spin state was examined (Figure 3.3), from which it could be seen that it was not an AF3 type order, nor the AF2 order that was expected. Although this only provides a snapshot of a single contribution to the true thermalised system, the simulation was run for long enough, and the temperature was low enough that it gave a single ordered state, and allowed the fully ordered state to be identified empirically, and was named AFX, as it was an unrecognised antiferromagnetic

state. Figure 3.3, where, for clarity, only a 10x10 section of the 40x40 repeat unit is shown. It can be seen that the order consists of "stripes" in the plane of the film.

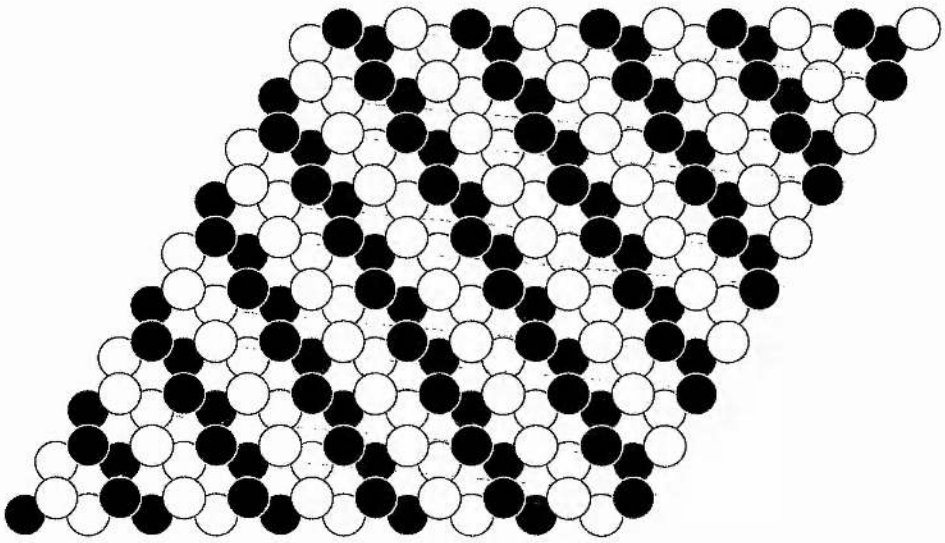

Figure 3.3: Final spin state from a Monte Carlo analysis of 10x10 bilayer at $X = -0.10$. The black and white circles represent spin up and down, and the super exchange mediating atoms are not shown.

In order to ensure that the correct spin alignment had been established code was implemented to calculate an order parameter for this state and then the bilayer calculation was repeated. This order parameter is slightly more complex than the others, however, as there are 6 degenerate states with the observed order. One of the transformations between the two states is a simple change of sign of all the magnetic sites, as with all the other

states, and is straightforward to encompass by allowing the order parameter to range from -1 to +1, depending on which of the two states was observed. The other transformation is a three fold rotation axis normal to the layers, which presents more difficulty. Two of these states have the isomagnetic lines parallel to an in-plane axis, and the other is as depicted in Figure 3.3.

The implemented solution was used to evaluate two different order parameters, depending on whether the isomagnetic stripes within the planes were oriented parallel to the two axes, and then to select the parameter that had the largest absolute value. The major flaw with this approach is that if there are domains present within the system, then the reported order parameter will underepresent the long range order in the system.

The long range order, as reported by the new code, can be seen in Figure 3.4. The transition from the AF2 initial state to the AFX state can be clearly seen as a very sharp transition in the order parameters. The AFX ordering persists up to the disordering, showing the typical curve down to zero, like the mean field predictions for AF2, and unlike the (100) results previously mentioned, which showed a gradual change, with the rate of change peaking at the transition point.

Once the order parameter calculation was shown to be correct, code was implemented to use this order as an initial condition. As the possible orderings are degenerate only one of them was implemented, having the isomagnetic stripes aligned with the x axis. With this set as the ground state there was only one transition observed, from the AFX state to disorder. This showed that the AFX state was the true ground state for the region under examination, and the persistence of the AF2 order from an initial condition

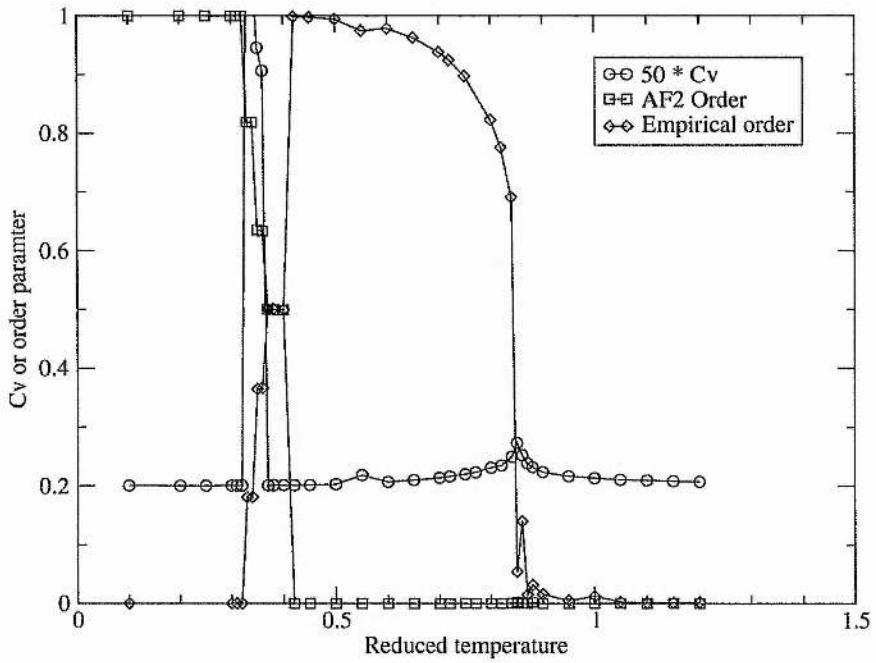

Figure 3.4: Monte Carlo predicted position of order -> disorder transition for a bilayer of (111) rocksalt type MO. The specific heat data has been scaled and shifted to show it on the same scales as the order parameter. The phases transitions between 0.4 and 0.5 can be clearly seen to be quite different from the transition at around 0.8. This graph was run taken from a simulation with an AF2 initial state, and X = -0.10.

for low temperatures was attributed to insufficient energy to change from the excited state of AF2 to the true ground state, i.e. the spins were "frozen" in place.

To establish a mean-field guide for the order -> disorder transition it is necessary to revisit the short range ordering. Careful examination of Figure 3.3 shows that around each atom there will be three nearest neighbour interactions of the same sign, and three of opposed magnetic sign. Continuing this counting, for the ground state gives rise to the value in Table 3.4. The

appropriate values for AF2 from Table 2.2 have been included also. Extending the pattern of spins to a trilayer system allows the "out of plane (above)" entries to be deduced, and they are, unsurprisingly, the same as the "out of plane (below)" values.

	Spin state	AFX	AF_2
Out of plane (above)			
Direct neighbours	Opposed	1	3
	Parallel	2	0
Super neighbours	Opposed	3	3
	Parallel	0	0
In plane			
Direct neighbours	Opposed	4	0
	Parallel	2	6
Out of plane (below)			
Direct neighbours	Opposed	1	3
	Parallel	2	0
Super neighbours	Opposed	3	3
	Parallel	0	0
Total interactions			
Direct neighbours	Opposed	6	6
	Parallel	6	6
Super neighbours	Opposed	6	6
	Parallel	0	0

Table 3.4: AFX local interactions, and comparison to AF2

The assignment of "in plane" and "out of plane" distinctions is an artifact of the projection upon (111) layers. In the case of a bulk system, these two categories are the same, and the description reduces to a set of four numbers. Calculating what these would be for the AFX ordering gives the "total interactions" in Table 3.4, and it can be seen that this is the same as for AF2.

This arises because there are four members of the (111) family of planes,

in FCC, that are identical. When a film of (111) alignment is taken, this partitions these into two sets, one containing a single element (where the alignment of the isomagnetic planes and the crystal surfaces matches, called simply AF2 till now), and the other containing three (the three orders called AFX previously). The case where the film and the isomagnetic planes align will be refered to as AF2 order, as before, and the three AFX orders will be called AF2'. The three AF2' orders can be seen as the three in-plane directions for the isomagnetic stripes in the bilayer, mentioned before.

The position of the phase boundary between AF2 and AF2' can be calculated from the energetics of the interactions mentioned above (Table 3.4). This can be done at zero temperature, as none of the relationships are temperature dependent. The ground state will be the one that has the lowest energy and this be calculated in a straight forward manner. The complication to note is that the total energy per layer is the same between AF2 and AF2', except for the outermost layers. Therefore, the ground state can be determined from the bilayer case, and is the same irrespective of the thickness of the film, and is calculated per atom in a tile.

$$E_{AF2} = E_0 - 3J_d - 3J_{se} \tag{3.23}$$

$$E_{AF2'} = E_0 + 1J_d - 3J_{se} \tag{3.24}$$

It can be clearly seen that the energies for AF2 (3.23) will be favoured (more negative) over AF2' (3.24) whenever J_d is positive, i.e. when it favours parallel spins. Likewise, AF2' is the ground state when J_d is negative, favour-

ing opposed spins, thus the changeover point will be at the point where the ratio $X = 0$. A similar calculation shows that the phase boundary between AF2'and AF3 is at X= -2 for the bilayer, which is the same as the bulk. The dependence on the number of layers is different between AF3 and AF2', thus the full expressions must be derived.

Extending the ground state analysis to many layers results in (3.25),

$$E_{AF2'_n} = E_0 + 1J_d - (3 + 3(n-2))J_{se}; n > 2 \tag{3.25}$$

The limit as Xtends to infinitely large (i.e. the bulk case), is 3. This is the same as the AF2 bulk. Equating this energy expression with the expression for the ground state energy of AF3 gives:

$$E_{AF2'_n} = E_{AF3_n} \tag{3.26}$$

$$1x - (3 + 3(n-2)) = (3 + 2(n-2))x + (1 + 1(n-2)) \tag{3.27}$$

$$x = \frac{4 + 4(n-2)}{-2 - 2(n-2)} = -2 \tag{3.28}$$

This predicts that the phase boundaries for the layered system are in the same places as the bulk, save for the addition of the AF2 / AF2' boundary.

Now that a simpler representation of the local environment (i.e. not the p(2x2) expansion) is available, it is possible to solve the mean field equations analytically. In the language of the expressions used earlier, equation (3.18), the diagonal element, a is $2x$ and the sub- and super-diagonal elements, b are $x + 3$. From these, we can extend Table 3.2 with the appropriate values

Thickness	AF3	AF2'	AF2	FM
2	-1.5x + 0.5	-0.5x + 0.5	1.5x + 1.5	4.5x - 1.5
3	-2.71x + 0.71	-0.29x + 2.12	0.87x + 2.12	5.12x - 2.12
4	-2.81x + 0.80	-0.19x + 2.42	0.57x + 2.42	5.42x - 2.42
5	-2.86x + 0.86	-0.13x + 2.60	0.40x + 2.60	5.60x - 2.60
10	-2.96x + 0.96	-0.04x + 2.88	0.12x + 2.88	5.88x - 2.88
15	-2.98x + 0.98	-0.02x + 2.94	0.06x + 2.94	5.94x - 2.94
Bulk	-3x + 1	3	3	6x -3

Table 3.5: Meanfield expressions for various thicknesses of (111) films, including the AF2'

for the additional state, as is done in Table 3.5.

The Monte Carlo results covering all the different ground states for the bilayer are shown in Figure 3.5. The drop in transition temperature near a phase boundary can be clearly seen and shows up the change of ground state between AF2 and AF2' vividly.

As the number of layers is increased, the phase diagram tends towards that of the bulk, as is expected. This results in the impact of the AF2 / AF2' phase boundary decreasing, as the number of layers increases, as can be seen from Figure 3.5. Monte Carlo simulation predicts that the effect of the phase boundary will be negligible for thickness above 10-12 layers, when compared to the depression of the transition temperature due to the phase boundary inherent in a thin layer.

$X \rightarrow 1$ behaviour

As the ratio x approaches 1 from below, it can be seen that the simulated transition temperatures show an interesting reversal of the usual pattern. The transition temperatures for the thinner layers are at a greater tempera-

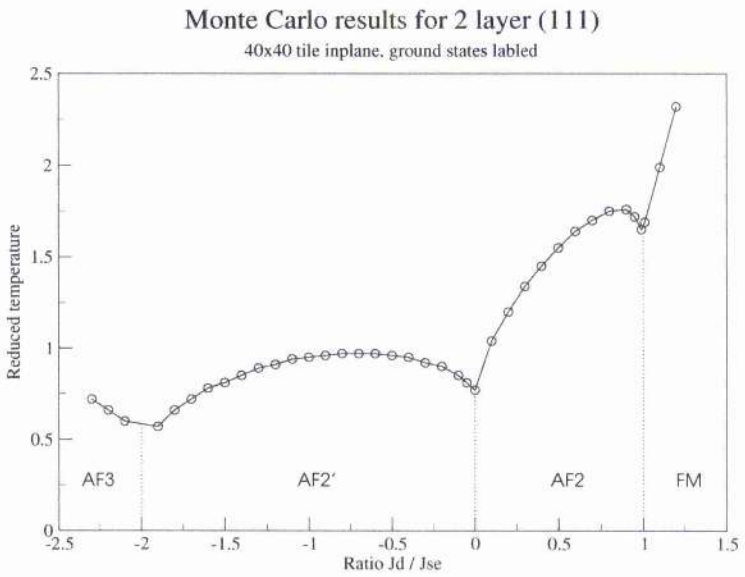

Figure 3.5: Phase diagram for (111) bilayers for a 2 layer system with a 40x40 in-plane tile.

ture than for the thicker layers. Whilst in all cases the trend for the behaviour to tend to the bulk behaviour as the films become thicker, within this region the transition temperatures approach from above, rather than below. The most surprising aspect of this is that the direction it approaches the bulk from changes, dependent on the value of Xwithin a single phase.

As this is not the case with the mean field results, which always approaches the bulk behaviour from below, the reason for this change must be due to the effect of fluctuations. The difference between the true behaviour, of which the Monte Carlo simulation is a good approximation, and the mean

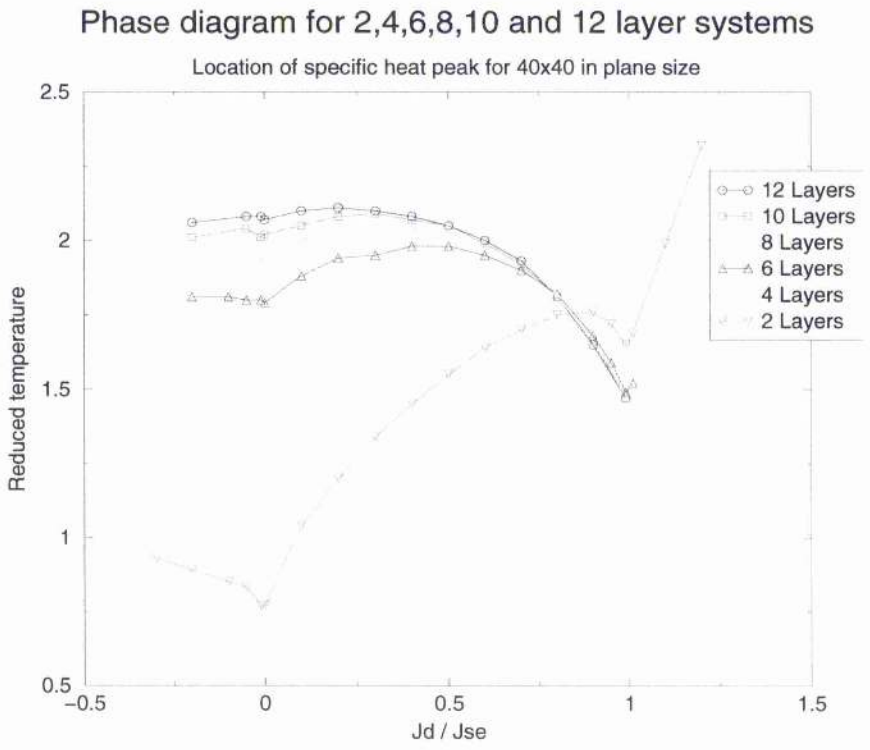

Figure 3.6: Partial phase diagram for (111) layers, for a 2,4,6,8,10 and 12 layer systems with a 40x40 in-plane tile.

field is due to the effect of fluctuations. The difference between the Monte Carlo transition temperature and the mean field prediction is shown in Figure 3.7.

This graph shows a regular pattern, with the effect of fluctuations greater in the vicinity of phase boundaries (at $X = 0$ and $X = 2$). The point where fluctuations have the least impact is not in the middle, but is closer to $X = 0$, and depends to a small degree on the number of layers. The overall effect is the same for the thicknesses depicted, with an increase in the magnitude

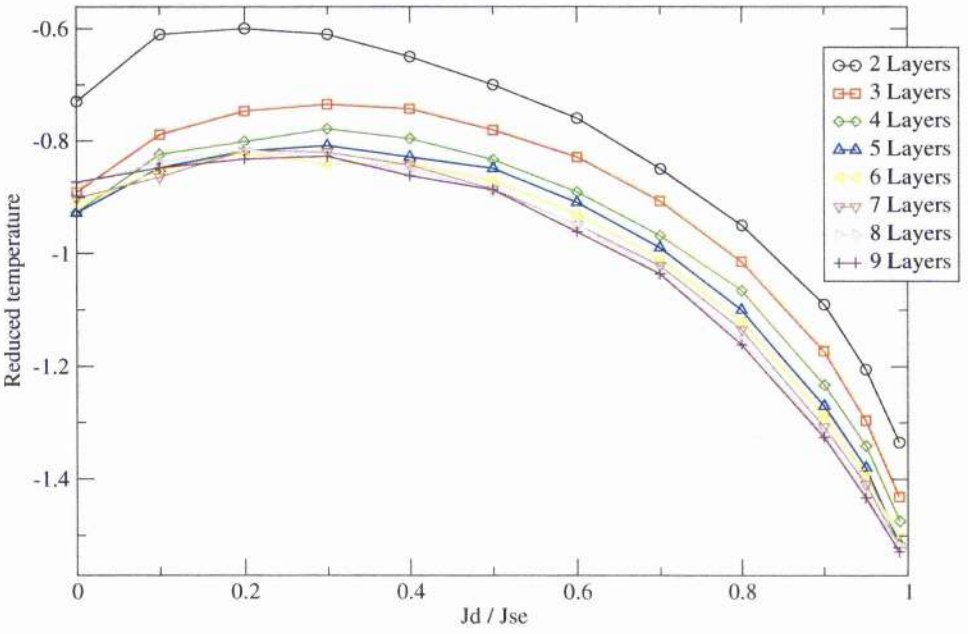

Figure 3.7: Difference in predicted critical temperature between the Monte Carlo and mean field predictions, over a range of X corresponding the AF2 phase. The AF2':AF2 phase boundary is at the extreme left of the x axis, and the AF2:FM phase boundary is at the extreme right. The y axis is the change in transition temperature caused by fluctuations, the lower down the axis, the greater the effect of fluctuations.

of the effect with increasing film thickness. Thus, the origin of the observed change in behaviour is not due to the effect of fluctuations alone.

The thinner films show a strong dependence of transition temperature on X, within mean field, as opposed to the bulk. In the vicinity of the AF2:AF2' phase boundary, the mean field transition temperature is lower than in the vicinity of the AF2:FM phase boundary, for a film. This difference between the two phase boundaries is caused by the large difference between the total number of direct interactions, and the smaller number of next nearest neigh-

bour interactions resulting from the surfaces, and hence is greater for the thinner systems, where the surface effects have a greater contribution to the overall.

Given that the effect of fluctuations is (to a first approximation) dependent only on the film thickness and the ratio X, it can be see that higher transition temperatures for the thinner layers around the AF2:FM phase boundary is due to the interaction between the two effects.

3.9 Conclusion

Monte Carlo analysis shows that the AF2 phase present in bulk rocksalt structured systems splits into two distinct phases, when projected onto (111) films. The phase boundary is at $X = 0$, with depressed Néel temperatures in the vicinity of it in mean field, further reduced by the effect of fluctuations. As the ratio Xin the magnetic first row transition metal oxides of this structure is close to 0, this is of significant interest. This novel observation has no precedent in previous work on (100) films.

Chapter 4

111 layers (Octopolar reconstruction)

4.1 Introduction

The octopolar reconstruction has been proposed as a way that the electronic dipole in (111) ordered systems such as NiO and MgO may be quenched. It is a (2x2) reconstruction, where one surface has 1 in 4 anions removed, and an additional cation, while the opposite side of the film has an additional anion, and 1 in 4 cations removed. This gives a distinction between a metal terminated surface, which ends in a 25% coverage of the metal with a 75% coverage of oxygen beneath it, and an oxygen terminated surface, where the positions are reversed. For the purposes of simulation, these are referred to by the type of termination.

Direct motivation for examining surface reconstructions is found in a paper by Koike and Furukawa [77], who observed that the surface, to a depth of

approximately one monolayer, of (111) FeO was ordered ferromagnetically, at temperatures above the bulk Néel temperature. A p(2x2) reconstruction was observed in the LEED pattern, and it was postulated that the surface order might be due to some effect of the surface reconstruction. There was a well defined relationship between the surface magnetic order and the ferromagnetic Fe substrate.

In any event, in view of the importance of p(2x2) reconstructions, of which the octopolar reconstruction is the most promising, effects of this reconstruction on the magnetism were examined. It is useful to note that the effect of the reconstruction due to oxygen absences can be accounted for implicitly from the neighbour list description after cation removal. This results because the role of oxygen is purely as a super exchange mediator, and that the oxygen ions that were moved would not be participating in super exchange, as they are all on the surface, and not situated between any metal ions. Thus, all the metal ions present are able to partake in a full set of super exchange interactions, depending on the presence of the magnetic ions alone.

With a metal terminated surface, the effect of the reconstruction is to leave no in-plane interactions in the surface layer, whilst retaining the full set of interplane interactions for the remaining magnetic ion. For the oxygen terminated surface, the remaining magnetic ions have 4 in-plane direct interactions, and each has it's full set of interplane interactions.

4.2 Monte Carlo Implementation

A straight forward way to implement the reconstruction is by setting the spin of the removed ions to 0, which results in them being treated as a non-magnetic entity. It is expected that there will be a slight relaxation of the reconstructed surface, which would result in a slight variation in the interaction strengths at the surface. However, this was not expected to change the qualitative behaviour of the system. The implementation of these non-interacting atoms is, strictly speaking, sub-optimal from a computational point of view. However, the huge advantage of this method is that the geometry information need not be changed, other than explicit removal of the appropriate atoms - i.e. no new neighbour lists are required. This allows the neighbour lists used for the non-reconstructed surfaces (listed in table 2.2) to be reused, leading to a significant saving in development time, and removal of a potential source of error.

The correctness of the behaviour of the code was tested by setting an entire layer to non-interacting atoms, and then comparing the results to those of a system one layer thinner, with all atoms present. These showed, as expected, the same results over a range of temperatures and range of X.

Although there is little physical meaning to having one surface reconstructed, and the other surface a perfect surface, it is beneficial to consider the two different reconstructions independently. This allows the effect of each to be studied separately, before looking at the overall effect of the reconstruction. Accordingly, the code used the concept of removing magnetic ions to produce the surfaces, and thus held no concept of balancing mass nor

magnetic moments.

The reconstruction is p(2x2), with one of the four magnetic ions removed for a metal terminated surface, and three of the four magnetic ions removed for the oxygen terminated surface. One side effect of this implementation is that a notionally n layer system, with one surface modified for a metal terminated surface, and the other modified for an oxygen terminated surface contains a number of atoms equal to only that of an n-1 layer system. Throughout this section, the number of layers shall refer to the notional number of layers, before any removals to produce the effect of a reconstruction.

4.2.1 Mean field model

The immediate effect of a surface modification is to break the symmetry of a film - i.e. the "top" and "bottom" layers of a film are no longer identical. From the point of view of mean field analysis, this increases the complexity of the system of equations requiring to be solved. In the language of a matrix eigenvalue, the super- and sub-diagonal elements are no longer identical, meaning that there is no analytic solution available.

The second complicating factor is that the system cannot be described in terms of a single mean spin per layer, but instead must be described by a p(2x2) expansion. This gives the symmetry of the model the same symmetry as the problem domain. The first step was to produce interaction matrices for this expansion, and then show that they produced the correct results for the known situation of unreconstructed films. These were solved using a combination of numerical eigenvalue and successive approximation methods.

The successive approximation method gives a predicted order parameter as a function of temperature, which is required to be able to identify any differing behaviour in the surface layers.

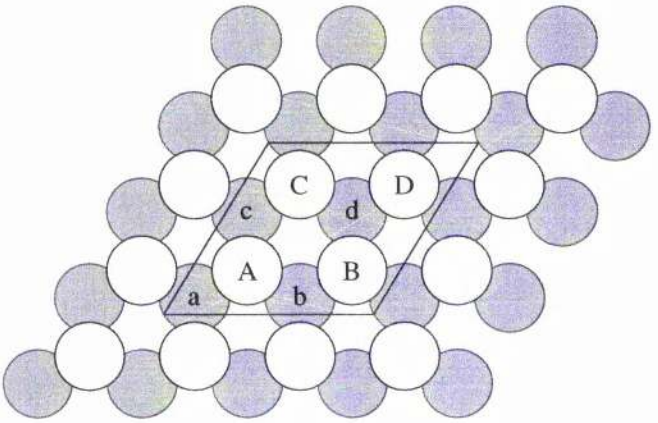

Figure 4.1: Labeling scheme for derivation of intra layer neighbour assignment

The matrix for a p(2x2) expansion of a 2 layer system is presented in equation (4.1), which was derived from the labeling scheme in Figure 4.1. $\mathbf{N_d}$ is the nearest neighbour interaction matrix, and $\mathbf{N_{se}}$ is the next-neared neighbour interaction matrix. The expansion of each single entry in equation (3.2) into a 4x4 block can be seen, where, for example, the first column of the matrix can be thought of as atom A in Figure 4.1, which shows that it has a nearest neighbour interaction with two atoms each of types B, C and D, but no interaction with the atom labeled A (i.e. no self interaction). Similarly, the next four values describe the interactions with atoms a, b, c, and d which are in the layer below. Thus, the top left 4x4 block can be thought of as the interactions within one layer, with the off diagonal 4x4

blocks being the interactions between layers. For larger numbers of layers, the matrix is expanded with additional 4x4 blocks. The C code used to generate the matrices earlier was extended to generate these matrices.

$$\mathbf{N_d} = \begin{pmatrix} 0 & 2 & 2 & 2 & 1 & 1 & 1 & 0 \\ 2 & 0 & 2 & 2 & 1 & 1 & 0 & 1 \\ 2 & 2 & 0 & 2 & 1 & 0 & 1 & 1 \\ 2 & 2 & 2 & 0 & 0 & 1 & 1 & 1 \\ 1 & 1 & 1 & 0 & 2 & 2 & 2 & 2 \\ 1 & 1 & 0 & 1 & 2 & 2 & 0 & 2 \\ 1 & 0 & 1 & 1 & 2 & 0 & 2 & 2 \\ 0 & 1 & 1 & 1 & 0 & 2 & 2 & 0 \end{pmatrix} \tag{4.1}$$

$$\mathbf{N_{se}} = \begin{pmatrix} 0 & 0 & 0 & 0 & 0 & 0 & 0 & 3 \\ 0 & 0 & 0 & 0 & 0 & 0 & 3 & 0 \\ 0 & 0 & 0 & 0 & 0 & 3 & 0 & 0 \\ 0 & 0 & 0 & 0 & 3 & 0 & 0 & 0 \\ 0 & 0 & 0 & 3 & 0 & 0 & 0 & 0 \\ 0 & 0 & 3 & 0 & 0 & 0 & 0 & 0 \\ 0 & 3 & 0 & 0 & 0 & 0 & 0 & 0 \\ 3 & 0 & 0 & 0 & 0 & 0 & 0 & 0 \end{pmatrix} \tag{4.2}$$

A number of test cases were run with the complete matrices, over a range of film thicknesses and values of X. In all cases, agreement with the analytic solutions was obtained. It was necessary to increase the initial damping

factor of the successive approximation solver, compared to the unexpanded matrixes, to prevent numerical instability. This did increase the run times, although they were under 10 seconds.

To model the reconstructed matrices, either the first three or the fourth entry was removed from the matrix. This gives the effect of a metal terminated or an oxygen terminated surface, respectively.

4.3 Phase boundaries

Revisiting the equations for the position of the AF2' / AF2 phase boundary (3.23) and (3.24), it can be shown that this phase boundary, and indeed, none of the phase boundaries, change under this reconstruction. The position of the phase boundaries are determined solely by the ratios of the different interactions present. Any change in the total interactions that does not change this ratio cannot change the position of the phase boundary, at zero temperature.

The positions are derived using the same principles as before. There are two main complications, compared to the unreconstructed layers. Firstly, the calculation is over a 2x2 supercell, where the four atoms are not necessarily in identical environments. Secondly, the symmetry between layers in a film is broken, so that all layers, in principle, need to be considered.

For the middle layers, where there is a complete set of interactions, each site contributes to the total energy an amount equal to the bulk per-site value, which was previously given in equations (2.92), (2.94) and (2.95), and summarised in Table 4.1. Such middle layers do not exist until the system

Layer	AF3	AF2'	AF2	FM
B	$4E_0 + 8J_d + 4J_{se}$	$4E_0 \quad - 12J_{se}$	$4E_0 \quad - 12J_{se}$	$4E_0 - 24J_d + 12J_{se}$
U	$4E_0 + 6J_d + 2J_{se}$	$4E_0 + 2J_d - 6J_{se}$	$4E_0 - 6J_d - 6J_{se}$	$4E_0 - 18J_d + 6J_{se}$
M	$E_0 + 1J_d + 1J_{se}$	$E_0 - 1J_d - 3J_{se}$	$E_0 + 3J_d - 3J_{se}$	$E_0 - 3J_d + 3J_{se}$
O	$3E_0 + 3J_d + 1J_{se}$	$3E_0 + 1J_d - 3J_{se}$	$3E_0 - 3J_d - 3J_{se}$	$3E_0 - 9J_d + 6J_{se}$

Table 4.1: Individual contributions to ground state energies for a 2x2 supercell. A "B layer" is a layer that is not on the surface, and thus has the full set of interactions present in the bulk system. A "U layer" is a stoichiometric unreconstructed surface, whilst "M layer" and "O layer" are the metal and oxygen terminated reconstructed surfaces respectively.

is 3 layers (for a single reconstructed surface) or 4 layers (for both surfaces reconstructed), although this does show that the phase boundaries will tend to the bulk values as the systems get thicker.

For unreconstructed surface layers, the energetic contribution of the atoms on the surface is encapsulated in (2.107), (2.108) and (2.109), and repeated in slightly different form in Table 4.1. Note that a different definition of the constant term E_o is used in this table, where there is one E_0 per atom, rather than a single term for all sites. Although it must cancel, and thus not affect the results, this is a more logical definition when dealing with varying numbers of atoms.

Although not strictly consistent with the previous terms, it is useful to consider the effect of the surface layer of an n layer system, compared to a stoichiometric $n-1$ layer system. For a metal terminated surface this is equal to twice the value of one set of out of plane interactions, whereas for an oxygen terminated surface it is as for a stoichiometric surface, minus two sets of in plane interactions, and twice one set of out of plane interactions. Tables 2.2 and 3.4 give the interactions per atom, from which the expressions

in Table 4.1 are derived. Thus, by way of example, a 3 layer system, with one layer reconstructed is designated as ("U" layer, a "U layer" and an "M" layer) or (a "U" layer, a "B" layer and an "O" layer), depending on the type of reconstruction.

It is clear from the table that the phase boundary between AF2' and AF2 is fixed at $X = 0$, as the J_{se} terms are identical in both cases. This is the most physically important phase boundary, from a physical point of view.

For an n layer system, with a metal terminated reconstruction, there will be ("U", $n-3$ "B" layers, another "U" layer and an "M" layer). The zero temperature energy expressions for this are:

$$E_M(AF3)_n = +(13+8(n-3))J_d + (5+4(n-3))J_{se} \tag{4.3}$$

$$E_M(AF2')_n = + \quad 3J_d - (9+12(n-3))J_{se} \tag{4.4}$$

$$E_M(AF2)_n = - \quad 9J_d - (9+12(n-3))J_{se} \tag{4.5}$$

$$E_M(FM)_n = -(39+24(n-3))J_d + (15+12(n-3))J_{se} \tag{4.6}$$

where the term $(9+4(n-3))E_0$, common to all, has been omitted. Similarly, the n layer, oxygen terminated system is made from a "U", $(n-2)$ "B" and an "O" layer. These are given below, again with the E_0 term omitted.

$$E_O(AF3)_n = +(9 \quad + 8(n-2))J_d + (3 + 4(n-2))J_{se} \tag{4.7}$$

$$E_O(AF2')_n = + \qquad 3J_d - (9 + 12(n-2))J_{se} \tag{4.8}$$

$$E_O(AF2)_n = - \qquad 9J_d - (9 + 12(n-2))J_{se} \tag{4.9}$$

$$E_O(FM)_n = -(36 + 24(n-2))J_d + (27 + 12(n-2))J_{se} \tag{4.10}$$

There are three sets of phase boundaries, one for each type of independent reconstruction, and one for a system with an oxygen terminated surface on one side, and a metal terminated surface on the other (a "fully reconstructed" system). First, the metal terminated systems:

$$E_M(AF3)_n : E_M(AF2')_n -> X = -\frac{8n-17}{4n-7} \tag{4.11}$$

$$E_M(AF2')_n : E_M(AF2)_n -> X = 0 \tag{4.12}$$

$$E_M(AF2)_n : E_M(FM)_n -> X = \frac{8n-4}{8n-1} \tag{4.13}$$

The expression for the AF3:AF2' phase boundary is very close to $-(8n-16)/(4n-8)$ which reduces to the -2 of the unreconstructed system. Similarly, the AF2:FM phase boundary is very close to 1, the unreconstructed value and, in both cases, the deviation from this is greatest at the thinnest layers.

For an oxygen terminated system, again the AF2':AF2 boundary is fixed at $X = 0$.

$$E_O(AF3)_n : E_O(AF2')_n -> X = -2 \tag{4.14}$$

$$E_O(AF2')_n : E_O(AF2)_n -> X = 0 \tag{4.15}$$

$$E_O(AF2)_n : E_O(FM)_n -> X = \frac{8n-7}{8n-4} \tag{4.16}$$

These relationships are represented in Figure 4.3. Note that the value for the AF2:FM phase boundaries are so close that they virtually overlap in the graph. The most striking aspect is the large curve on the metal terminated reconstruction, which predicts a phase boundary at around -1.4 for a reconstructed trilayer, as compared to -2 for an unreconstructed bilayer.

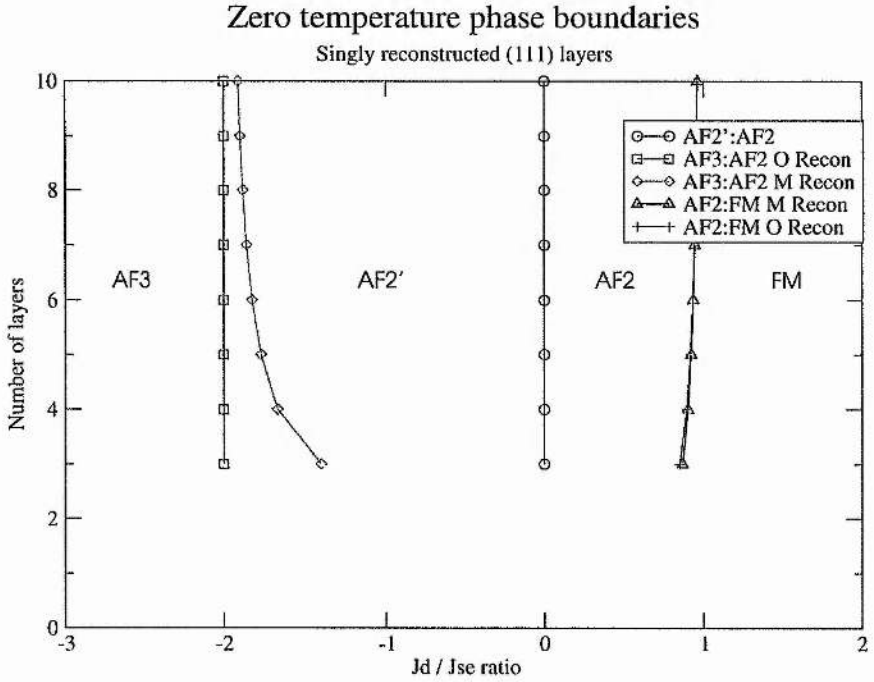

Figure 4.2: Zero temperature predictions of phase boundaries, single reconstructed (111) rocksalt structured layers

4.4 Singly reconstructed surface

The effect of the oxygen terminated surface was studied first, on the grounds that it should to be the closest to the perfect surface. For the simulation, a film was produced, and then one surface modified to give the situation produced in an oxygen terminated surface, by removing one in every four atoms. As with the unreconstructed surfaces, the initial set of simulations were for a value of X of 0.4, with an estimate of the expected transition temperature from the mean field results, and from the Monte Carlo results from the unreconstructed films. Once the behaviour at that ratio of X was established, subsequent calculations expanded the range of X to $-2 < X < 1$.

The Monte Carlo results showed a behaviour of the critical temperature that was qualitatively similar to the unreconstructed layers, but slightly lower in temperature through the range of X, as seen in Figure 4.4. Comparison with Figure 3.6 (page 91) shows that the general shape is the same as the unreconstructed layers, with the reduced temperatures scaled by around 0.9 to 0.95.

The most striking feature of the Monte Carlo results is that, with the exception of the two layer system, the phase boundary between AF3 and AF2' is close to, if not exactly, X = -2, rather than shifted towards X = 0 as the mean field predicted. This gives the general shape of the phase diagram close to that of the unreconstructed system. The simplest explanation for this effect would be that the reconstructed layer disorders rapidly, so that in the vicinity of the transition temperature, it has no net effect on the overall magnetic order, and thus the system behaves as a system with

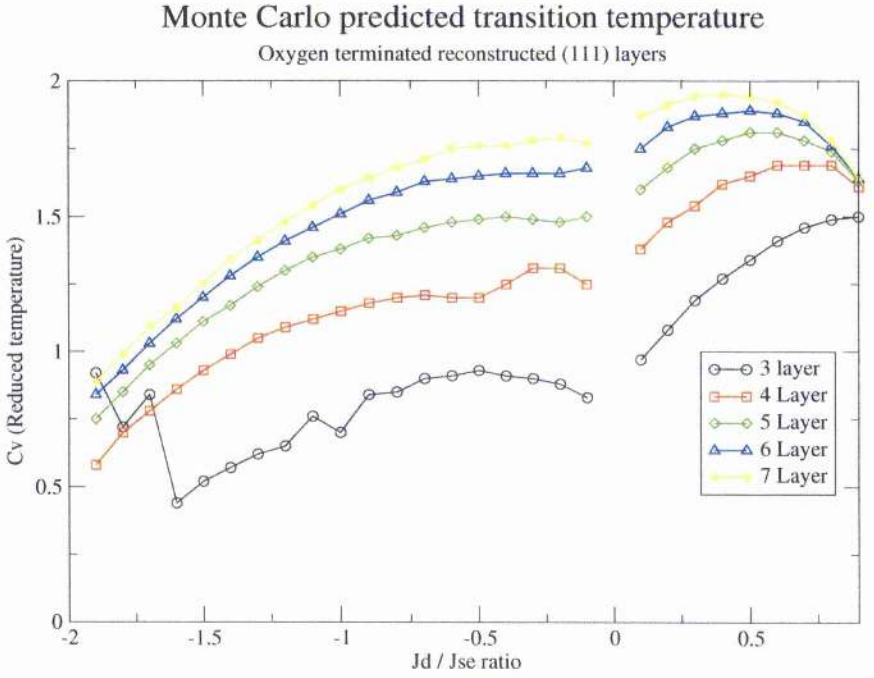

Figure 4.3: Monte Carlo simulation of order/disorder transition temperatures for an oxygen terminated reconstruction on one side of a thin film.

unreconstructed surfaces.

An examination of the order parameter for each layer from the Monte Carlo analysis showed a pattern typified by Figure 4.4. This is taken from a 4 layer system, with the ratio X of $+0.40$, so the ground state was AF2. The order shown for each layer is the absolute value of the mean spin of each layer. This method of calculation will underestimate the order in the reconstructed layer, as it only has a 3/4 occupancy, so the fifth line on the graph is the order for the reconstructed layer scaled by a factor of 1.33, which gives it a range of between 0 and 1.

The order shows some sharp changes at around the transition point. This

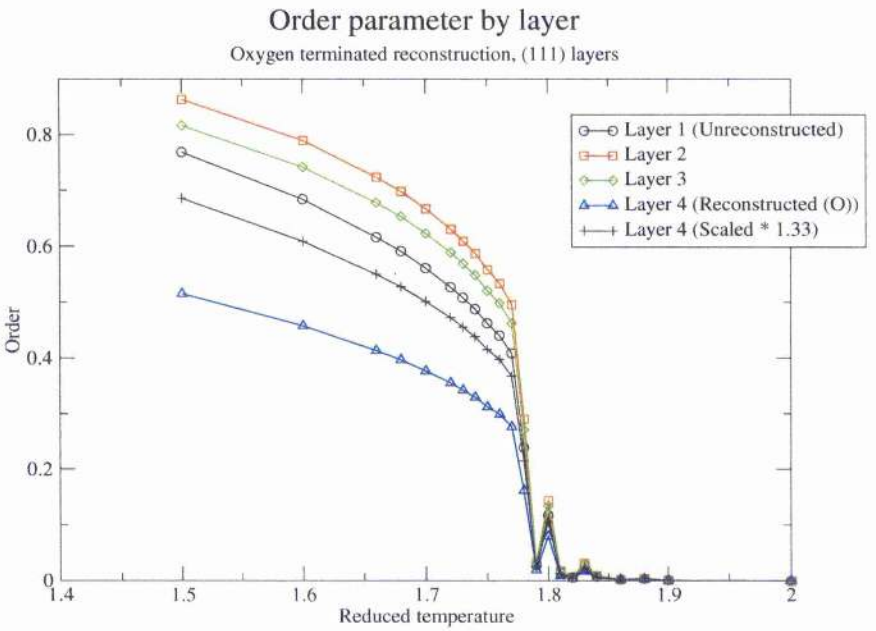

Figure 4.4: Order parameter of each layer in a 4 layer system, Monte Carlo simulations with $X = +0.40$. Layer 4 is the reconstructed layer. The specific heat has a single peak at a reduced temperature of 1.84 for this system.

is due to randomness in the Monte Carlo simulation, which shows particularly at the transition point. As fluctuations cause parts of the system to undergo a spin inversion, this causes the simple sum to tend to zero, even if there are large sections that are ordered. Similar behaviour was observed for the fully reconstructed and bulk cases also.

Even with the reconstructed layer scaled up, it is clear that it disorders faster than any other layer with increasing temperature. Also the layer adjacent to it disorders faster than the equivalent layer next to the unreconstructed surface. Thicker systems show similar behaviour. This supports, but does not prove, the theory that the reconstructed layer disorders, and

thus does not modify the phase boundary.

Given that the symmetry of the reconstructed system is a p(2x2) expansion in-plane, it is a reasonable question to consider if all the four distinct sub-lattice sites carry the same order at each temperature. Clearly, in the case of the reconstructed layer, they do not, if an empty site is assumed to have an implicit order parameter of 0 (the same as a fully disordered site).

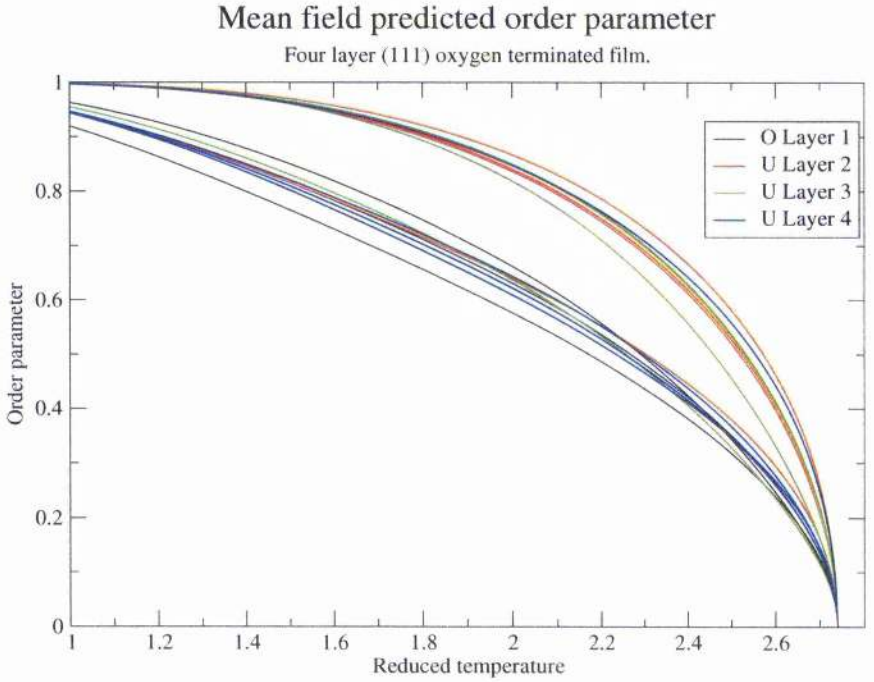

Figure 4.5: Oxygen terminated reconstruction, mean field predicted order parameters by sublattice sites.

Figure 4.4 shows the mean field predictions for a 4 layer system, over each sublattice. Whilst is is difficult to follow individual lines on the graph, it can be clearly seen that the predicted order splits into essentially two groups.

The three sublattice sites for the reconstructed layer and three of the

sites of the other unreconstructed surface are in the lower order group along with one site from each of the other layers. The group with greater order contains the other three sites from the middle layers, and the other site from the unreconstructed surface. This does clearly show that the reconstructed layer disorders faster than the other layers. Other thicknesses show a similar division of sites between groups, the number of groups equal to the number of different orders in an unreconstructed system.

The behaviour of the metal terminated surface was similar. The reduction in the order-disorder temperature was more pronounced than for the oxygen terminated surface, which is understandable given that more magnetic ions have been removed.

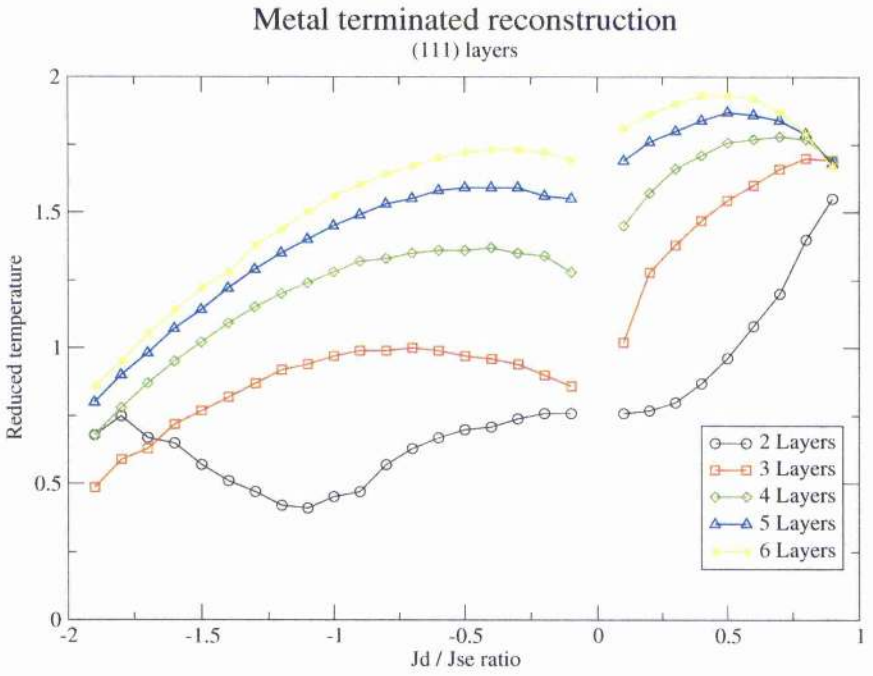

Figure 4.6: Monte Carlo simulation of order/disorder transition temperatures for a metal terminated reconstruction on one side of a thin film.

It is clear that there is a phase boundary for the 2 layer system, at around X = -1, whereas such a transition was at around X = -1.55 for an oxygen terminated system. Examination of the order parameters of the layers shows that the outer layer (which consists of only 25% of a full layer,) disorders rapidly, leaving the remaining layers to behave almost the same as an unreconstructed system one layer thinner. This explains the odd curves for the "2 layer" system, which actually behaves more as a monolayer. In Figure 4.7, the order parameter by layer is shown for a 4 layer system, where, as with the oxygen terminated reconstruction, the additional line is for the reconstructed surface, scaled so that the order is between 0 and 1.

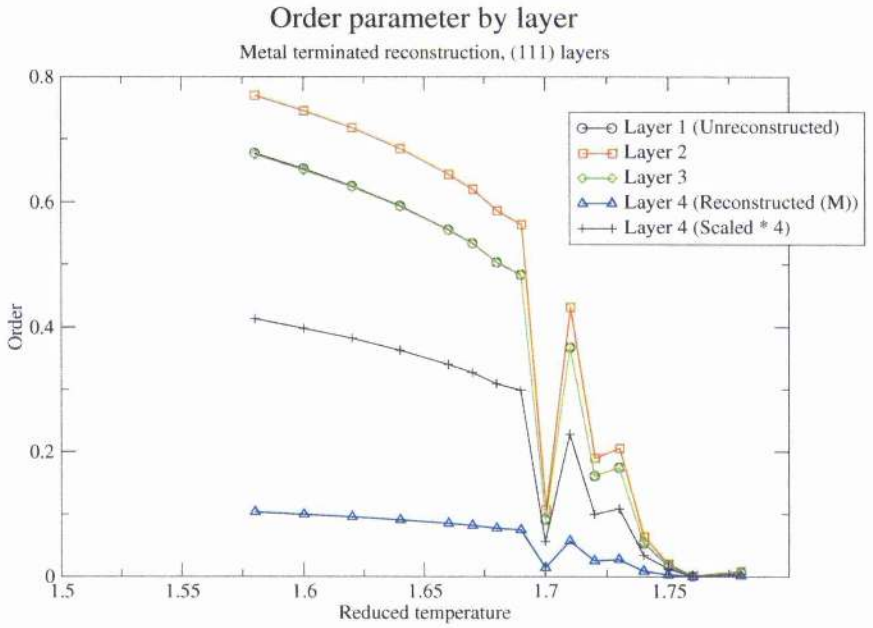

Figure 4.7: Order parameter of each layer in a 4 layer system, Monte Carlo simulations with X = +0.40. Layer 4 is the reconstructed layer. The specific heat has a single peak at a reduced temperature of 1.78 for this system.

This graph also shows some noticeable variation in the order parameter

near the transition point. Indeed, at some points the signs of the order are all inverted, although this cannot be seen here, where only the absolute value of the mean spins is shown. The order for layers 1 and 3 (the unreconstructed surface, and the layer adjacent to the reconstructed layer practically overlap, which is a very clear indication that the order of the system is much closer to the three layer system, rather than the four layer system. This general pattern is the same as predicted by mean field theory, and similar to the case for other ratios of X and thicknesses.

It is also clear that the AF3:AF2' phase boundary is not noticeably different from -2 for the metal terminated system. The rapid disordering of the terminal layer means that the zero temperature phase diagram does not apply around the order - disorder temperature. Similarly, the AF2:FM phase boundary appears not to have moved from $X = 1$, for either of the reconstructions. This is consistent with the rapid disordering of the reconstructed layer noted above. Once the layer is principally disordered at a temperature below the Néel point, it provides no net contribution to the stability of the magnetic phase, and thus has no effect on the position of the phase boundary, which behaves as for the unreconstructed system.

4.5 Fully reconstructed film

The fully reconstructed film was generated by placing an oxygen terminated surface on one side, and a metal terminated surface on the other, and the results of these simulations are shown in 4.5. Again, no quantitative differences in behaviour from the unreconstructed system were observed, although

the nominal 2 layer system was not simulated, on the grounds that it would, on the basis of the singly reconstructed films, behave very much like a monolayer.

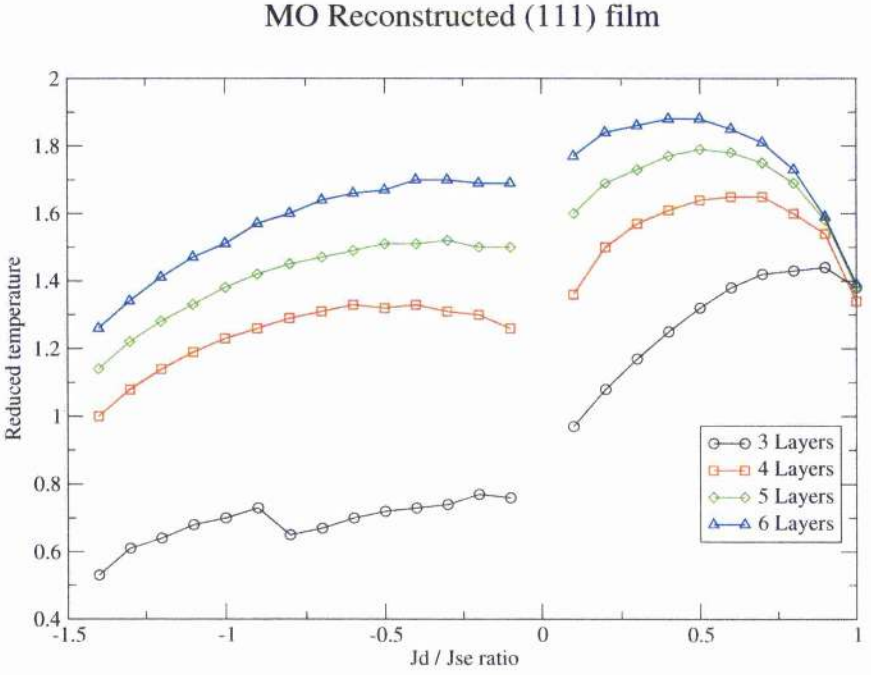

Figure 4.8: Monte Carlo simulation of order/disorder transition temperatures for a metal terminated reconstruction on one side of a thin film, and oxygen terminated reconstruction on the other. No nominal 2 layer system was simulated.

The critical temperature was lower again than for the unreconstructed film, and a representative comparison of the various reconstructed surfaces and unreconstructed surfaces is presented in Figure 4.9. The 3 layer system behaves as a film, and not as a monolayer, which was not entirely expected. If the reconstruction makes a surface layer behave qualitatively, but not quantitatively, as if it was not present, then if might be expected that the

tri layer system behaves as a monolayer. However, it is apparent that this is not a complete explanation. It is more correct to consider the layer as disordered, rather than not present. Both of these situations have the same implication at zero temperature, where the mean spin is zero, but at real temperatures fluctuations extend into these effectively disordered layers, and thus influence the behaviour of the system.

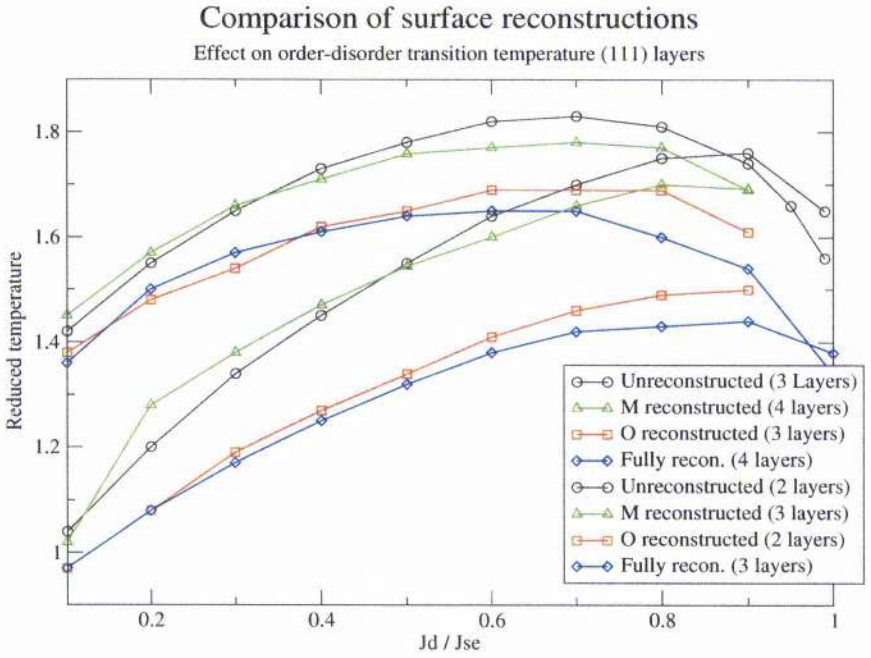

Figure 4.9: Comparison of order-disorder transition temperatures over the AF2 phase of the effect of different surface reconstruction, over a range of similar number of magnetic atoms. "M surface" indicates a single metal terminated reconstructed layer, likewise "O" indicates oxygen terminated, and "U" an unreconstructed layer, with "MO" signifying a fully reconstructed film.

It is very clear that for a metal terminated reconstruction, the transition temperature behaves almost exactly as the unreconstructed film one layer

thinner, with just a small change in the shape of the curves. The nature of the effect of a single oxygen terminated surface is more subtle, and places the overall transition temperature on average about halfway between a system with the same number of layers, and a system one layer thinner, although the shape of the curve is changed. The fully reconstructed film behaves almost exactly like the oxygen terminated, singly reconstructed film, which implies that the three metal ions remove to produce the metal terminated surface have little influence on the overall behaviour of the system.

4.6 Conclusion

The p(2x2) octopolar reconstruction does not qualitatively affect the behaviour of the (111) rocksalt layers, which show the same four phases as the unreconstructed layers, with the phase boundaries at the same values of X. The predicted Néel temperatures from simulation show that the reconstructed layers depress the transition temperature to a greater extent than can be accounted for by lower mass, which implies that surface roughness may play a role in determining the exact transition temperature. The magnitude of this effect appears to be similar in magnitude to that of a monolayer of atoms. Little difference was observed between a singly reconstructed oxygen terminated surface and a fully reconstructed system, whilst the singly reconstructed metal terminated surface showed some distinct qualities.

At no point was any multicritical behaviour, or recurrence of order above an order-disorder transition temperature observed. Thus, in relation to the observations of Koike et al, it can be concluded that the octopolar recon-

struction is not responsible for the surface ferromagnetism observed.

Chapter 5

Magnetic ordering in the corundum structure

5.1 Introduction

The corundum structure is, like the rock salt structure explored previously, also a binary compound, and is exhibited by metal oxides. Unlike the rock salt structure the two components are present in differing quantities, and it is of significantly lower symmetry. The name "corundum" comes from the mineral corundum, being aluminium oxide (Al_2O_3). From a magnetic point of view, however, the more interesting members of the family are the minerals hematite (α-Fe_2O_3) and eskolaite (Cr_2O_3). Other compounds known to crystalise with the same structure are V_2O_3, the mineral karelianite, and the ilmenite group which consist of compounds with the general structure ABO_3, such as ilmenite itself, FeTiO3.

The aim of this work is to determine if the Ising model is a good descrip-

tion of the magnetic behaviour of systems in the corundum structure. The starting point is to see if it can give a good description of the behaviour of the bulk systems. Most of the interest in magnetic systems with this structure is focused on Fe_2O_3, which shows antiferromagnetic behaviour up to high temperatures and is cheap, thus the work will focus on it and Cr_2O_3 to a lesser extent and not consider the ilmenite group explicitly. The applications of antiferromagnetics tend to be as thin films, in layered systems, so the next step after the bulk is to examine a thin film.

5.2 Physical structure

Figure 5.1: Corundum structure, looking along the [1000] direction with the [0001] direction (the long "c" axis) vertical, showing the layered nature of the (0001) planes, and the two metal ion (the smaller spheres) sub-lattices. For the ilmenite group, each of the cation sublattices is filled by a different cation.

α-Fe_2O_3, is the most common of the iron oxides. It has the rhombohedral

corundum structure [81] shown in Figure 5.2, and is antiferromagnetic below its Néel temperature of 955K with the "c" lattice parameter being 13.74 $\AA$, and the "a" length being 5.16 $\AA$. Cr_2O_3 has a slightly smaller unit cell, with an "a" parameter of 5.05 $\AA$ and the "c" parameter at 13.73 $\AA$. Its Néel temperature is significantly lower, at 307K.

It is useful to consider the schematic projection shown in Figure 5.2, from which it can be seen that the (0001) repeat units in Fe_2O_3, or indeed, any material with the corundum structure, are neutral and hence electrostatically stable. A 'monolayer' is a unit of thickness of a sheet, and is defined here as being one stoichiometric repeat unit in height, along the [0001] direction. Such a monolayer is indicated in Figure 5.2.

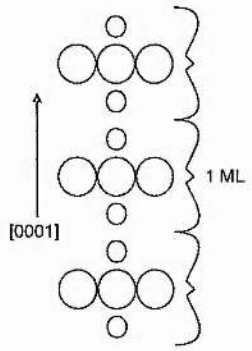

Figure 5.2: Corundum structure, schematic projection of the (0001) layers

It is clear that each monolayer has no net electric dipole, which allows for unreconstructed surfaces to be prepared [82]. Like the (111) planes in FCC lattices such as NiO, these repeat units have hexagonal symmetry, and contain magnetically active atoms in Fe_2O_3, and Cr_2O_3. As a prelude to theoretical work on the magnetic structure of these films, it is useful to have some idea of the strength of magnetic interactions, and to know if they change

significantly at a surface. In particular, in order to relate any theoretical work to a physical system, the strengths of individual couplings for that system would need to be known. Drawing from the known range of interaction strengths for the antiferromagnetic rocksalt structured first row transition metal oxides, it is reasonable to expect that the physically meaningful (in the sense of representing a real magnetic system) interaction strengths will only occupy a part of the space of possible interactions. It is this section of the space formed by the various interaction coefficients that this work will focus on.

Theoretical studies on Al_2O_3, considering factors such as electrostatic considerations [83] and surface energies [84], along with electronic structure calculations all predict that the (0001) surface terminates with a single plane of Al atoms, as shown in the schematic Figure 5.2. Large relaxations are predicted for this surface, from early pair potential methods [85], through to density functional theory [86, 87] and UHF [88] calculations. Grazing incidence X-ray scattering experiments [89], in addition to showing that the surface doesn't reconstruct, have confirmed the presence of a large surface dilation, at -51%, which compares well with the UHF prediction of -40%. The planes of atoms adjacent to the surface also relax a little, although not as dramatically as the outermost layer, +16%, -29% and +20% dilation for the nest layers, from experiment.

Fe_2O_3 and Cr_2O_3 are less studied than Al_2O_3, but there are a number of studies that make predictions consistent with the Al_2O_3 behaviour. UHF film calculations on Cr_2O_3 [90] predict a -50% dilation of the final layer, slightly less than shell model predictions [91] which predicted -59%, with

Magnetic orders			
↑ ↑ ↑ ↑	↑ ↓ ↑ ↓	↑ ↓ ↓ ↑	↑ ↑ ↓ ↓
FM	A_I	A_{II}	A_{III}
$R\hat{3}c$	$R3c$	$R\hat{3}$	$R32$

Table 5.1: Four spin states for corundum structures and the magnetic space group, where the spins are defined by their orientation along the c axis.

LEED measurements predicting -38% [92]. Molecular dynamics calculations [92] predicted a large dilation, of -58%. A recent study on hematite [93] using several different DFT schemas found a surface dilation around -50-60%.

Unsupported films below around 2 ML [94] cannot really be said to have the corundum structure, and so calculations on them have little physical meaning, but may be useful in establishing trends. Films of Fe_2O_3 supported on Al_2O_3 have been made, and are stable down to 1 ML.

5.3 Magnetic structure

There are four distinct orders that involve isomagnetic planes parallel to the basal plane over a 2 monolayer supercell, and thus can be described by considering the relative orientations of the spins of the layers with respect to the c axis. These are the four lowest index magnetic orders, and are described in Table 5.1, with reference to the stacking of monolayers in the hexagonal unit cell.

The ground magnetic state for Fe_2O_3 is the A_{II} state, with the ground magnetic state for Cr_2O_3 being the A_I state.

There is a Morin transition at 250K [95, 96, 97] in hematite, where the spins on the two sublattices cant, leaving the system with a weak ferromagnetic like behaviour. The Morin transitions occurs between the low temperature state with co-linear spins, and the higher temperature state where the spins are not co-linear. Other than the co-linearity, however, the magnetic ordering remains essentially the same across the transition, unlike the order-disorder transition at the Néel temperature. Its origin is in the absolute direction of the spin moments, something which is only accesible from calculations that are relativistic, or at a minimum include spin-orbit coupling. Calculations that take this into account are more computationally expensive and methods that use co-linear spins are sufficient for the majority of purposes which is why non-co-linear spin calculations are significantly more common. Within this thesis, the quantum mechanical calculations utilise co-linear spins only. In addition to the difficulties in modeling this by electronic structure methods, such a transition cannot be modeled by the Ising model, where the spins are inherently co-linear, and would need a Heisenberg description. This should be kept in mind when applying any results to a real system, but it is not expected to affect the qualitative behaviour significantly.

Previous theoretical work on Fe_2O_3 and Cr_2O_3 has focused on the bulk behaviour. Catti et al [33] calculated the energies of the ferromagnetic and the physically observed antiferromagnetic order, and showed that UHF calculations predicted the antiferromagnetic structure to be lower in energy. Later, Catti et al [34] calculated the UHF structure of Cr_2O_3 for the 4 lowest order magnetic orders, and correctly identified the ground state for Cr_2O_3.

As a rough guide to the accuracy of the UHF calculations, comparison

may be made between UHF calculations [98] of s electron density at the iron sites and deductions from Mössbauer spectroscopy [99, 100, 101]. The values calculated by UHF agree, within experimental error to the earlier measurements, and are within 10-12% of the later, more accurate, measurement. Whilst Mössbauer spectroscopy and the magnetic moment of the materials are quite different, both rely on subtle aspects of electronic structure, and thus give a guideline for estimating the error in the magnetic calculations. Additionally, Yang et al [101] examined the change in hyperfine interactions as a function of the distance from a surface, and found that they reached the bulk value at 18±3 $\AA$, which is around 2.6 monolayers.

The most recent theoretical study of Fe_2O_3 [102] involved both GGA and a DFT+U calculations. The magnetic order was defined in terms of the primitive (rhombohedral) cell, rather than the hexagonal cell, and find different energetic stabilities from the UHF calculations. The A_{II} phase is the most stable in both, but the GGA, along with the LDSA calculations by Sandratskii et al [103], find that the phases are ordered $A_{II} < A_I < A_{III} < FM$, and that the energy differences between states are around 10 times that of the UHF energies.

5.4 Ising Spin Hamiltonian

The first step in applying the Ising Hamiltonian to a system with the corundum structure is to identify the possible interactions. Compared with the rocksalt structure, this is complicated by the two cation sublattices in the structure. In turn, this gives rise to two nearest neighbour interactions, and

two next-nearest neighbour interactions.

Using similar nomenclature to that use for the FCC lattice, the nearest neighbour coupling constants will be labeled J_d and J_d', and the next nearest neighbour coupling constants shall be labeled J_{se} and J_{se}'. The appropriate Ising Hamiltonian for this system is

$$H_{Ising} = -\frac{1}{2}J_d \sum_{i}^{N_L} \sum_{j}^{nn} \sigma_i\sigma_j - \frac{1}{2}J'_d \sum_{i}^{N_L} \sum_{j}^{nn'} \sigma_i\sigma_j + \frac{1}{2}J_{se} \sum_{i}^{N_L} \sum_{j}^{nnn} \sigma_i\sigma_j + \frac{1}{2}J'_{se} \sum_{i}^{N_L} \sum_{j}^{nnn'} \sigma_i\sigma_j \tag{5.1}$$

were nn is the set of neighbours appropriate for the J_d, nn' is the set for J_d' and so on. As the numbers of spin opposed and parallel relationships are constants, as with the rocksalt structured systems, the ground state Hamiltonian can be expressed in terms of constants of the form $NN(\uparrow\uparrow)$, the number of nearest neighbours (for J_d) that are aligned parallel, and so on. This gives rise to equation (5.2).

$$\begin{aligned} H_{Ising} = \; & -\tfrac{1}{2}J_d\left(NN(\uparrow\uparrow) - NN(\uparrow\downarrow)\right) - \tfrac{1}{2}J'_d\left(NN'(\uparrow\uparrow) - NN'(\uparrow\downarrow)\right) \\ & -\tfrac{1}{2}J_{se}\left(NNN(\uparrow\uparrow) - NNN(\uparrow\downarrow)\right) - \tfrac{1}{2}J'_{se}\left(NNN'(\uparrow\uparrow) - NNN'(\uparrow\downarrow)\right) \end{aligned} \tag{5.2}$$

This description is, so far, totally general over any structure with two (or less) nearest neighbour and two (or less) next nearest neighbour interactions. To apply this to the corundum structure the numbers of each type of interaction are required. At this stage, each of the interactions is labeled. Figure 5.3 gives this assignment, with reference to Fe_2O_3. From this, it can be seen

Coupling distances (Å)	
J_d	2.89522
J_d'	2.96877
J_{se}	3.30697
J_{se}'	3.70120

Table 5.2: Lengths of coupling distances: $|Jd| > |J'd|$ and $|Jse| > |J'se|$

that there is a total interaction of 1 J_d, 3 J_d', 3 $J_{se}$and 6 J_{se}' per interacting atom, in the bulk.

Interaction no. and type	Structure <0001> ↑	Position (relative)	Interatomic distance
	Fe(↓)	3.97847	3.97847
	OOO		
3 J_{se}'	Fe(↓)	2.29118	3.70120
3 J_{se}	Fe(↑)	1.68722	3.36097
	OOO		
	Fe(↑)	0.0	
3 J_d'	Fe(↓)	-0.60396	2.96887
	OOO		
3 J_{se}'	Fe(↓)	-2.29118	3.70120
1 J_d	Fe(↑)	-2.89522	2.89522
	OOO		
	Fe(↑)	-4.58244	

Figure 5.3: J_d, J_d', J_{se}, J_{se}' with respect to Fe(↑) at origin for A_{II}

It is useful to separate out the distances over which these interactions take place, not least because these vary slightly between different species with this structure. The distances these operate over are shown in Table 5.2, for Fe_2O_3.

The number and type of each interaction is independent of the cation species, and is a property of the structure. The total interactions, and their ground state number for each of the four low index orders are shown in Table

	Spin state	FM	A_I	A_{II}	A_{III}
$J_d$interactions	Opposed	0	1	1	0
	Parallel	1	0	0	1
J_d' interactions	Opposed	0	3	0	3
	Parallel	3	0	3	0
J_{se}interactions	Opposed	0	3	3	0
	Parallel	3	0	0	3
J_{se}' interactions	Opposed	0	0	6	6
	Parallel	6	6	0	0

Table 5.3: Local magnetic environments of atoms for various magnetic orders in the corundum structure

5.3.

With these definitions, the zero temperature expressions for the energy of each state can be derived. As the quantum mechanical calculations are performed at zero temperature, these are the same expressions used to perform the mapping for the Ising model.

$$\begin{aligned} E(FM) &= E_0 - \tfrac{1}{2}J_d - \tfrac{3}{2}J'_d + \tfrac{3}{2}J_{se} + 3J'_{se} \\ E(A_I) &= E_0 + \tfrac{1}{2}J_d + \tfrac{3}{2}J'_d - \tfrac{3}{2}J_{se} + 3J'_{se} \\ E(A_{II}) &= E_0 + \tfrac{1}{2}J_d - \tfrac{3}{2}J'_d - \tfrac{3}{2}J_{se} - 3J'_{se} \\ E(A_{III}) &= E_0 - \tfrac{1}{2}J_d + \tfrac{3}{2}J'_d + \tfrac{3}{2}J_{se} - 3J'_{se} \end{aligned} \tag{5.3}$$

In addition, these same equations can be used to produce phase diagrams for magnetic materials in the corundum structure. As written, it is a four dimensional object. However that can be reduced to three, without loss of generality, by considering three parameters as ratios of the fourth, analogous to the introduction of the ratio J_d/J_{se} for the rocksalt structure. Here, it results in a slightly more complex situation, and there are three ratios to be considered, not just one. Given that all known examples of magnetic

oxides with this structure are antiferromagnetic in character, it is assumed that J_{se} will always play a dominant role in the magnetic ordering, and so it was chosen to be the divisor. However, as the interaction lengths and the nature of the atoms at the end points are similar, it is reasonable to expect that the ratios Y (J_d' /J_d) and Z (J_{se}'/J_{se}) will both be close to 1. If this assumption holds, then a good approximation to the actual phase diagrams for the systems of interest can be obtained by examining only a small range of the possible phase space. In these diagrams, it is further assumed that J_{se} will always favour antiferromagnetic alignment, further reducing the dimensionality of the phase space, and a negative value of the ratio X indicates a change of sign of J_d.

Within this ratio based description, the ground state Ising Hamiltonian changes from

$$E = E_0 + aJ_d + bJ'_d + cJ_{se} + dJ'_{se} \tag{5.4}$$

to

$$E = \frac{E_0}{J_{se}} + aX + bX \cdot Y + c + dZ \tag{5.5}$$

Figures 5.4 and 5.5 show, in schematic form, the ground state for a range of values of the three parameters. The expected range of physically observed systems is a strip across the middle of the two diagrams, which taken together give a usable description of the phases.

From the diagrams, it can be seen that Cr_2O_3, having A_I magnetic ground state, must fit in the cube where $X < 0$, $Y < 0$ and $Z >$ around 0, which

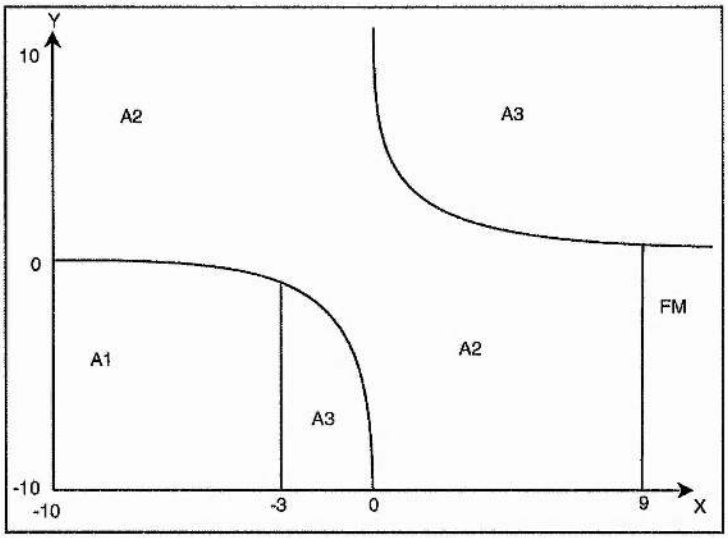

Figure 5.4: $-10 < Y < 10, -10 < X < 10, Z = 1$; zero temperature ground phase for corundum structure, where J_{se}= J_{se}'.

means that J_d is negative and of a different sign to J_d'. The space where A_{II} is the ground state (such as for Fe_2O_3) is less restricted, and includes the space where all the ratios have small values.

5.5 UHF Calculations

Two distinct sets of calculations were performed. In the first instance the bulk energies were recalculated to give a base for analysis of magnetic interactions, and then film calculations were carried out to see if the Ising mapping could be reasonably applied to the reduced dimensionality situation. The major limitation with film calculations is the computational load for such a system. To perform the relaxation for each film is prohibitive, given that the thickest films studied were at the limits of computability and computer time

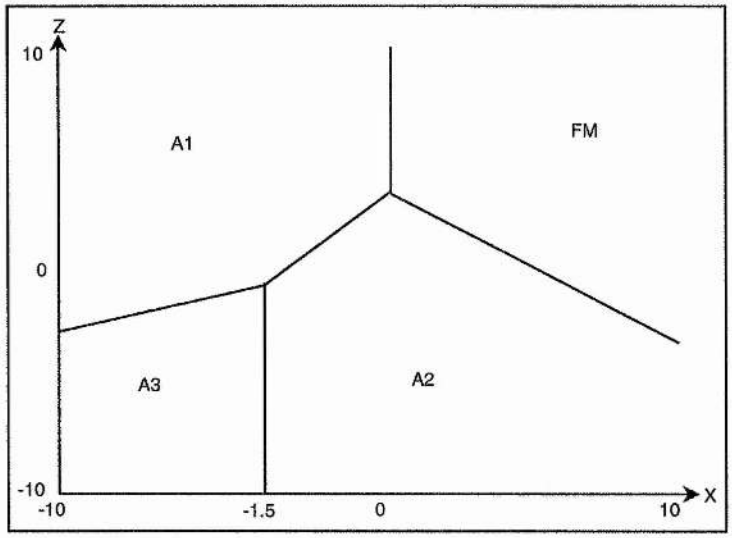

Figure 5.5: $-10 < Z < 10, -10 < X < 10, Y = 1$; zero temperature ground phase for corundum structure, where $J_d = J_d$'.

available. The films studied were treated as a slice of the bulk structure, with no relaxation. This neglect of the surface relaxation is a weakness of the current work.

The calculations were performed on two main platforms. Smaller calculations were performed on Sun Blade 100 systems, with Crystal 98 software. The larger calculations (being 4 monolayers and above) were performed on the Turing supercomputer, based at Manchester Computing Centre, a Cray T3E-1200, using Crystal MPP. The two software packages are essentially the same code, but optimised for either serial or parallel platforms repectivly.

Unrestricted Hartree-Fock (UHF) calculations were performed. The Crystal package [104] uses a local basis set, composed of Gaussian functions. The basis set used is taken from Catti et al [33] and is shown in Table 5.4. This is an all electron basis set. The cut off tolerances for the evaluation of the

Columb and exchange integral series is controlled by a set of 5 numbers, which here were set to 10^{-7} except for the fifth parameter which was set to 10^{-14}. The reciprocal space shrinking factor used was 8. These computational conditions were also used for the film calculations.

The magnetic interaction coefficients are obtained from a mapping from the UHF onto the Ising model. Expressions for the energies of the different magnetic states are constructed in each Hamiltonian, which were numerical values for the UHF calculations, and a combination of a constant (E_0) and the appropriate magnetic interactions coefficients in the Ising model. Such a mapping requires a number of energy values equal (or greater) than the number of terms in the Ising model, which is 5 for this structure.

The results for the bulk system are given in Table 5.5. These differ slightly from the energies given by Catti and Sandrome [35], which can be attributed to the change in computational conditions. This work used more stringent tolerances, as is the modern standard.

These calculations find the lowest energy magnetic state to be the A_{II} state, in agreement with experiment and other theoretical methods. However, the order of stability found, summarised in Table 5.6, is different from that found by the DFT calculations of Rollman [102] (GGA) and Sandratskii et al [103] (LSDA). This indicates vividly that the two calculation schemes would disagree in a qualitative fashion on the values of the coupling constants in an Ising model. In the absence of experimental data to compare with, it is not possible to say definitively which is correct. However, comparison with other crystal systems, particularly with FCC lattices suggests that UHF is liable to give Ising model coefficients closer to physical values.

Shell type	Iron basis			Oxygen basis		
	Exponents	s coefficients	p, d coefficients	Exponents	s coefficients	p, d coefficients
$1s$	3.154[+5]	2.270[-4]		8.020[+3]	1.080[-3]	
	4.569[+4]	1.900[-3]		1.338[+3]	8.040[-3]	
	9.677[+3]	1.110[-2]		2.554[+2]	5.324[-2]	
	2.521[+3]	5.010[-2]		6.922[+1]	1.681[-1]	
	7.597[+2]	1.705[-1]		2.390[+1]	3.581[-1]	
	2.630[+2]	4.033[-1]		9.564	3.855[-1]	
	4.297[+1]	1.434[-1]		3.851	1.468[-1]	
				1.212	7.280[-2]	
$2sp$	7.983[+2]	-5.200[-3]	8.500[-3]	4.943[+1]	-8.830[-3]	9.590[-3]
	1.912[+2]	-6.800[-2]	6.080[-2]	1.047[+1]	-9.150[-2]	6.960[-2]
	6.369[+1]	-1.314[-1]	2.114[-1]	3.235	-4.020[-2]	2.065[-1]
	1.073[+1]	6.433[-1]	3.980[-1]	1.217	3.790[-1]	3.470[-1]
	3.764	2.825[-1]	2.251[-1]			
$3sp$	4.814[+1]	1.220[-2]	-2.150[-2]	0.479	1.0	1.0
	1.746[+1]	-2.278[-1]	-8.500[-2]			
	6.997	-8.801[-1]	2.010[-1]			
	3.079	9.755[-1]	1.302			
$4sp$	1.314	1.0	1.0	0.200	1.0	1.0
$5sp$	5.532[-1]	1.0	1.0			
$3d$	3.048[+1]		5.830[-2]	0.570		1.0
	8.692		2.591[-1]			
	3.101		5.162[-1]			
	1.171		5.656[-1]			
$4d$	4.298		1.000			

Table 5.4: Gaussian basis set for the Fe_2O_3 UHF calculations. The $a[\pm b]$ notation should be read as $a * 10^{\pm b}$.

Magnetic state	Energy (Ha)	Relative energy (meV)
FM	-2749.773000	0.0
A_I	-2749.771307	+46.1
A_{II}	-2749.774820	-49.6
A_{III}	-2749.772363	+17.4

Table 5.5: Energies of the magnetic states for bulk Fe_2O_3.

Calculation type	Stability			
	Most			Least
UHF	A_{II}	FM	A_{III}	A_I
DFT	A_{II}	A_I	A_{III}	FM

Table 5.6: Comparison of energetic ordering of magnetic states of Fe_2O_3 for different calculation methods. The energy differences for DFT calculations vary by the Hamiltonian used, but tend to be around 10 times larger than for UHF methods

The other set of UHF calculations performed were on films of Fe_2O_3. Some results were obtained for films of Cr_2O_3, but it was not possible to obtain a complete set of results due to numerical instability, thus the film results focused on Fe_2O_3. The computational conditions for these calculations were exactly the same as for the bulk calculations above. The total energies for the range of film thicknesses from 2ML to 7ML are presented in Table 5.7.

As is reasonably expected, the energy per monolayer tends asymptotically to the bulk values from above. It can be seen that the differences in energy between magnetic states is around 0.01 to 0.02 Ha, with some variation as a function of film thickness. This variation is clear in Figure 5.6, where the difference between the states has been plotted.

The most striking aspect of Figure 5.6 is that the difference between the A_{II} and FM states is independent of film thickness, whilst the A_I and A_{III}

Thickness (ML)	Magnetic state	Energy (Ha)
2	FM	-2749.568308015
2	A_I	-2749.568074512
2	A_{II}	-2749.569282665
2	A_{III}	-2749.568034340
3	FM	-2749.634988679
3	A_I	-2749.634162170
3	A_{II}	-2749.635936775
3	A_{III}	-2749.634513368
4	FM	-2749.669481712
4	A_I	-2749.668390922
4	A_{II}	-2749.670461090
4	A_{III}	-2749.668921125
5	FM	-2749.690171978
5	A_I	-2749.688922936
5	A_{II}	-2749.691170758
5	A_{III}	-2749.689560368
6	FM	-2749.703965368
6	A_I	-2749.702610710
6	A_{II}	-2749.704977038
6	A_{III}	-2749.703319597
7	FM	-2749.713817630
7	A_I	-2749.712387607
7	A_{II}	-2749.714838470
7	A_{III}	-2749.713147623

Table 5.7: UHF calculated energies for slab calculations on various thicknesses of Fe_2O_3. The energies are specified per monolayer.

states increase asymptotically towards the bulk values. The relative energies for A_I and A_{III} in the two monolayer film case are reversed, although by only a very small difference in energy. These effects on the A_I and A_{III} states show a very clear effect of the surfaces on the magnetic states, over and above the impact of the surface on the electronic energy.

As the aim of the calculations was to obtain some description of the magnetic interactions for arbitrary thicknesses, it was attempted to find a

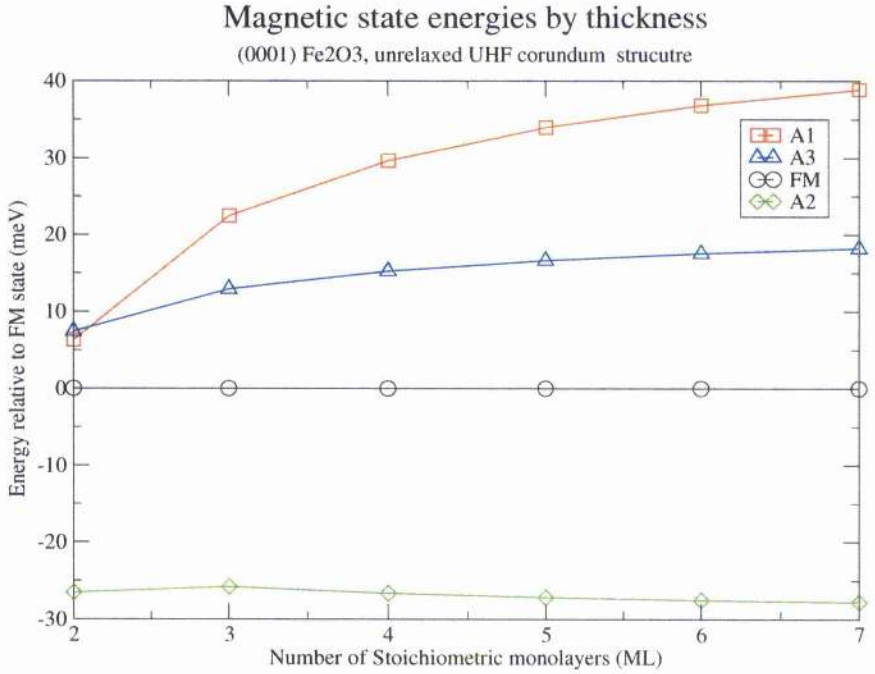

Figure 5.6: Differences in magnetic state energies relative to FM as a function of film thickness.

functional fit to the data. This would give some insight into what the effect of adding further layers might be on the parameters to the Ising model. All the fits were performed separately on each magnetic state, and the energy per monolayer was fitted to the number of monolayers. To help prevent numerical swamping by the large electronic energy, prior to fitting a constant of 2497 was added to the energies, which moved the range of interest much closer to the origin.

A few fits were tried to the total energy. A polynomial fit of the third degree gave a chi-squared of around $8.6 * 10^{-6}$, while an exponential fit with a constant term, for a total of three parameters gave a chi-squared of around

$1,2 * 10^{-5}$. The optimum fit obtained was a two parameter fit, defined by (5.6), where a,b are the two parameters, n is the number of monolayers in the film, and E_n is the energy for a film of n layers. This formula was developed based on the assumption that there are two distinct electronic energies present, one for the surfaces of the slab a, and one for the rest of the slab b (the 'core'). This gives a very good fit to the data, which is detailed in Table 5.8. This fit was performed, discounting the values for the 2 monolayer case, on the grounds that the model implied that the core aught to be present. Repeating the other fits without using the data for 2 monolayers resulted in a slight improvement to the chi-squared values, of around a factor of 10.

$$E_n = \frac{2a}{n} + b\left(1 - \frac{2}{n}\right) \tag{5.6}$$

State	a	b	chi-squared	correlation coefficient
FM	-0.566016	-0.772941	2.07292e-11	1.00000
A_I	-0.565717	-0.771057	1.90432e-11	1.00000
A_{II}	-0.566900	-0.774016	1.68346e-11	1.00000
A_{III}	-0.565711	-0.772125	2.01663e-11	1.00000

Table 5.8: Fitted parameters for the magnetic state of Fe_2O_3, fit as defined in (5.6). This gives the energy per monolayer, for each magnetic state, and was fitted to data over the range 3 to 7 monolayers

Using this fit data to extrapolate to 8 monolayers allows for a basic check. 8 monolayer data was not used to condition the fit, so comparison to the calculated value is a valid test of the fitness of the model. Only one state was able to be calculated in this thickness, being the ferromagnetic state with an energy per monolayer of -2749.721206 Hartrees. The model calculates a value of -0.721209, which is in very good agreement with the calculated value.

This supports the model of two different electronic configurations, one for the surface monolayers and the other for the internal layers.

Another test on the validity of the model is to compare the fitted value of electronic energy to the bulk energy. Comparing the b coefficient in the table above with the values calculated, shown in Table 5.9, shows that they agree to within 22 meV at the worst case (for the A_{II} state), within 7 meV the next worst. For all states, the predicted energies were slightly too high.

State	Predicted (Ha)	Calculated (Ha)	Difference (meV)
FM	-2497.772941	-2497.773000	4.33
A_I	-2497.771057	-2497.771307	6.80
A_{II}	-2497.774016	-2497.774820	21.9
A_{III}	-2497.772125	-2497.772363	3.76

Table 5.9: Comparison of calculated and predictions from film data bulk energies for Fe_2O_3, from UHF calculations.

5.6 Magnetic coefficient results

In order to extract the five parameters (both J_d's, both J_{se}'s and the E_0), at least five equations would be required. This is not available, which means that some approximation must be made. Given that the interaction distances of J_d and J_d' are similar, the most reasonable first approximation to make is to assume that $J_d = J_d$', where the δ r = 0.07365 Å. This results in the simpler Hamiltonian

$$H_{Ising} = -\frac{1}{2}J_d \sum_i^{N_L} \sum_j^{nn} \sigma_i \sigma_j - \frac{1}{2}J_{se} \sum_i^{N_L} \sum_j^{nnn} \sigma_i \sigma_j - \frac{1}{2}J'_{se} \sum_i^{N_L} \sum_j^{nnn'} \sigma_i \sigma_j \quad (5.7)$$

Note that this assumption would not be valid for systems in the ilmenite group, as J_d is between cations on the same sublattice, and J_d' is between cations on differing sublattices. For hematite and similar systems, however, it is the simplest assumption that allows for coupling constants to be extracted from the four low index magnetic orders. The values of the coupling constants extracted from electronic structure calculations are given in Table 5.10, along with the values calculated from other sets of electronic structure calculations.

Parameter	This work (UHF)	Catti and Sandrome (UHF)	Rollman et al (GGA)	Sandratskii et al (LDSA)
J_d	18.82	18.00	15.6	-31.7
J_{se}	9.73	10.00	138.9	157.1
J_{se}'	6.52	6.83	62.5	79.2
X	1.934	1.80	0.11	0.20
Z	0.67	0.68	0.54	0.50

Table 5.10: J_d, J_{se} and J_{se}' for Fe_2O_3 from different electronic structure methods. J_d is the amalgamation of both direct interaction coefficients. X and Z refers to the ratios J_d/J_{se} and J_{se}'/J_{se}, with the Y ratio used earlier defined to be 1.

The two UHF calculations agree on the parameters to around 4% (between 3.5 and 4.7%), whilst it can be seen that the DFT calculations give quite different values of coupling constants. The sets of ratios of coupling constants given for all calculation schemes predict an A_{II} ground state.

Catti and Sandrome's paper on the corundum structure sesquioxides covers the first row magnetic insulators. These results can be analysed in the same manner to Fe_2O_3, to give trends across the periodic table. Mn_2O_3 has a different structure, based on the corundum structure, but with Jahn-Teller distortion [105], and thus was not modeled by Catti and Sandrome. Only three of the four energies calculated for Ti_2O_3 were reported, which prevents

Species Magnetic order	V_2O_3 A_{II}	Cr_2O_3 A_I	Fe_2O_3 A_{II}	Co_2O_3 A_{II}	Ni_2O_3 FM
J_d	-4.54	-9.83	18.82	110.67	21.00
J_{se}	-5.14	-0.11	9.73	133.22	-8.33
J_{se}'	-0.90	-1.75	6.52	51.83	3.50
X	0.88 (*)	88.5 (*)	1.934	0.83	-0.88 (*)
Z	0.18 (*)	15.8 (*)	0.67	0.39	-0.17 (*)

Table 5.11: Ising model interaction coefficients for magnetic insulator first row transition metal corundum structure sesquioxides. Note that the ratios for V_2O_3, Cr_2O_3 and Ni_2O_3 (marked with an asterix), are generated with a negative J_{se}, which is against one of the assumptions made previously, and thus the phase diagrams given above are invalid for these systems.

its inclusion here. The systems Co_2O_3 and Ni_2O_3 are theoretical models of systems that have not been reliably reported in the literature whose inclusion is principally to extend any observed trends in behaviour. Whilst Catti and Sandrome predict that the A_{II} magnetic order is the most stable of the three antiferromagnetic orders studied for Ni_2O_3, the energies they give show that the ferromagnetic state is more stable than all the antiferromagnetic states.

There are no clear trends in these coupling constants. The general pattern is that the ratio Z is around a quarter to a third the ratio X. With the exception of chromium sesquioxide, which is known to have a different magnetic ground state, the values of these ratios are small, although hematite has ratios twice the others in magnitude (excluding the chromium case again). The signs of the coefficients are not consistent, nor show a trend. The ferromagnetic character of Ni_2O_3 shows in the negative J_{se} and the positive J_d.

Returning to Fe_2O_3, it is possible to calculate these interaction coefficients for each set of film thicknesses for which UHF energies were obtained

above. These results are presented in Figure 5.7. The graph shows the effect of assuming that the there is only a single nearest neighbour interaction coefficient, and show the resulting interaction coefficients over a range of layer thicknesses.

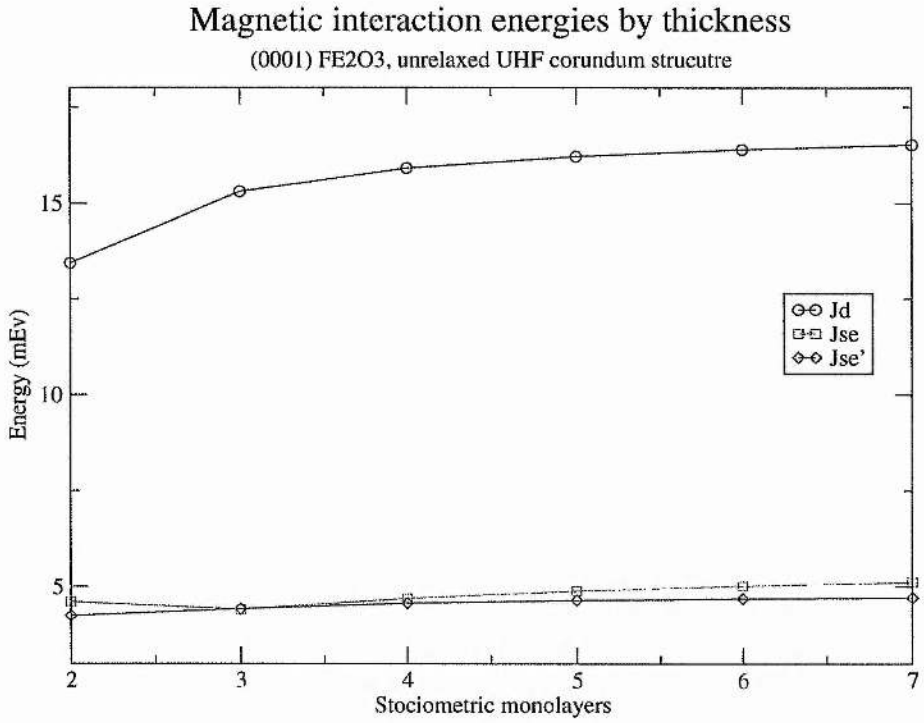

Figure 5.7: Magnetic interaction coefficients for a range of thickness, under single nearest neighbour assumption.

It is possible to calculate a single set of interactions coefficients, using calculated values across several film thicknesses. This relies on the assumption of a single value of energy for the surface monolayers, and a second value for the core monolayers. The success of the fit described by Equation (5.6) suggests that this may yield a good approximation to the actual behaviour. Such a model implies the existence of three sets of interaction coefficients,

being within the surface layers, within the core layers, and between the surface and the core layers. As each set has four coefficients, two J_d and two J_{se}, this requires 13 different equations to be generated (one for each coefficient, and one for the constant). Excluding the results for two monolayers, on the basis that they include surface layer to surface layer interactions, and thus are a special case, that leaves 21 calculated energies, which is much more than the minimum required.

In practice, there are fewer than 13 distinct interaction types. This becomes clear when the interaction matrices, such as (5.8) which shows the matrices for a 4 monolayer film, are examined. These matrices use an expansion by a factor of 2, to show the two metal atoms in each layer separately. In addition, the value of 0 has been replaced with a full stop as a guide to the eye. These matrices are labeled in a similar fashion to the scheme used for FCC lattices, where the matrix $\mathbf{N_d}$ covers the first nearest neighbour interactions, which have the coupling coefficient J_d, $\mathbf{N'_d}$ is the other nearest neighbour interaction, and so on.

$$\mathbf{N_d} = \begin{pmatrix} . & . & . & . & . & . & . & . \\ . & . & . & . & 1 & . & . & . \\ . & . & . & . & . & . & . & . \\ . & . & . & . & . & . & 1 & . \\ . & 1 & . & . & . & . & . & . \\ . & . & . & . & . & . & . & . \\ . & . & . & 1 & . & . & . & . \\ . & . & . & . & . & . & . & . \end{pmatrix} \tag{5.8}$$

There will be no J_d interaction from a surface layer, to another surface layer, except in the case of three monolayers. It is therefore likely that this surface - surface interaction can be neglected.

$$\mathbf{N'_d} = \begin{pmatrix} . & . & . & . & . & . & . & . \\ . & . & 3 & . & . & . & . & . \\ . & 3 & . & . & . & . & . & . \\ . & . & . & . & 3 & . & . & . \\ . & . & . & 3 & . & . & . & . \\ . & . & . & . & . & . & 3 & . \\ . & . & . & . & . & 3 & . & . \\ . & . & . & . & . & . & . & . \end{pmatrix} \tag{5.9}$$

It can be seen that there is no interaction within the same layer for J'_d. This means that, as the two monolayer case is being neglected, there will be no J'_d interaction from a surface layer to a surface layer. There will be a core layer - core layer interaction for the thicker systems.

$$\mathbf{N_{se}} = \begin{pmatrix} . & 3 & . & . & . & . & . & . \\ 3 & . & . & . & . & . & . & . \\ . & . & . & 3 & . & . & . & . \\ . & . & 3 & . & . & . & . & . \\ . & . & . & . & . & 3 & . & . \\ . & . & . & . & 3 & . & . & . \\ . & . & . & . & . & . & . & 3 \\ . & . & . & . & . & . & 3 & . \end{pmatrix} \tag{5.10}$$

The J_{se} interaction does not cross a monolayer boundary, therefore there cannot be a surface - core interaction of this type.

$$\mathbf{N_{se'}} = \begin{pmatrix} . & . & 3 & . & . & . & . & . \\ . & . & . & 3 & . & . & . & . \\ 3 & . & . & . & 3 & . & . & . \\ . & 3 & . & . & . & 3 & . & . \\ . & . & 3 & . & . & . & 3 & . \\ . & . & . & 3 & . & . & . & 3 \\ . & . & . & . & 3 & . & . & . \\ . & . & . & . & . & 3 & . & . \end{pmatrix} \tag{5.11}$$

There is no interaction within a monolayer for J'_{se}, thus, as with J_d, there cannot be a surface to surface interaction of this type. Thus in total there are only 8 or 9 different types of interactions within this model, the ninth being the surface layer to surface layer J_d for a three monolayer system. The label "SS" will be used to identify the surface layer to surface layer interactions, and likewise "SC" for surface layer to core layer and "CC" for the core layer to core layer interactions.

These coefficients are still too many to get analytic solutions for all of them. The obvious approach is to make some approximations, to reduce the total number of distinct coefficients. Once the approximation is made that the SS J_d, SC J_d and SC J'_d are the same, the problem reduces to 7 coefficients, and two constants - electronic energy for each of the core and surface layers. This set of equations can be generated in about $61 * 10^{12}$ different ways, depending on which of the possible UHF results are used

in each construction. A number of these were constructed, and solutions sought. Not all combinations result in a solution, with around 40% of the possible solutions sets being singular, but a great number did. The mean and standard deviation of these is shown in table 5.12.

Due to the different units used for the electronic energies, the standard deviations have been scaled by differing quantities. The interaction coefficients were scaled up by a factor of 10^3 whilst the energies, specified in Hartrees, were scaled up by a factor of 10^6. This makes them almost comparable, with the electronic energies a factor of 27 greater.

It is somewhat unexpected that the CC J_d shows the largest deviation, and that the CC J_{se} and SS J_{se} show relatively large values also. These figures can be taken as an estimate of the degree to which the model does not fit the data - the larger the standard deviation, the less well the model fits the data. The converse is not necessarily true, however - it cannot be claimed from the low deviation of S J_d' that the three parameters it represents are identical. All that can be said is that the change in the three parameters is closely linked, and that they all change by similar proportions across the data points available.

The general magnitude of these calculated coupling constants agrees with the values from the bulk system, but there are differences in the details. Firstly, this approach has enabled calculation of all four of the coupling constants. Interestingly, the difference between J_d and J_d' is roughly equal, in percentage terms, to the difference between J_{se} and J_{sc}' - something that was not suggested by the physical structure. The approximation for the bulk model that the two nearest neighbour coefficients were equal appears to

E_{core}	$E_{surface}$	SS J_{se}	S J'_d	SC J'_{se}	CC J_d	CC J'_d	CC J_{se}	CC J'_{se}
Mean over 106428379 solutions								
-2749.7725267	-2479.5661012	4.0296	-15.3032	4.4172	-15.3080	-17.0917	5.1468	4.8584
Standard deviation over the 106428379 solutions								
0.33234	0.5777	130.8847	1.8984	0.9482	392.8021	1.4871	130.8925	0.7412

Table 5.12: Average interaction coefficients for solutions to the large set of equations for the Fe_2O_3 film UHF results. Note that the term "S J'_d" is the approximate to cover the aggregate SS J_d, SC J_d and SC J'_d. The two energies are in Hartrees, whilst the coefficients are specified in meV. The standard deviations are scaled up by a factor of 1000, except for the electronic energies, where they are scaled up by a factor of 1000000

have increased all the coefficients, and made the difference between the two next-nearest neighbour coefficients greater.

The coefficients found for the CC section are, in principle, the same as those for the bulk. Thus a set of ratios may be taken from these, and used as an indicator of the bulk behaviour. These coefficients wound give an X ratio of 2.974, a Y ratio of 0.896 and a Z ratio of 1.059.

5.7 Mean Field results

The mean field critical temperatures for the various phases can now be evaluated, using the values above, and the interactions in Table 5.3. In order to allow for a range of values for the coefficients, the mean field calculations were performed in terms of the pair of ratios used for the extractions above. The different parameters appearing in these expressions come from two places. The number of each interaction comes from the structure, and are the same as in the matrices shown above. The sign of term is determined by the mean spin of the two spins in the ground state of the specified magnetic order. Thus, for the ferromagnetic case, all the spins are aligned, and all the spin products are positive.

This is slightly more complex than the FCC case studied earlier, due to the pair of interactions of each type, and also because both of the nearest neighbour interactions are collapsed into one at this stage.

For a bulk system then, the ferromagnetic state is described by:

$$FM : \langle \mathbf{S} \rangle = \coth\left[-\beta\left(-4J_d + 3J_{se} + 6J'_{se}\langle \mathbf{S} \rangle\right)\right] \tag{5.12}$$

$$\langle \mathbf{S} \rangle = \coth \left[-\frac{\tilde{T}_c}{2} \left(4X - 3 + 6Z \langle \mathbf{S} \rangle \right) \right] \tag{5.13}$$

$$\tilde{T}_c = \frac{1}{2} \left(4X - 6Z - 3 \right) \tag{5.14}$$

where Z is defined as $Z = \frac{J'_{se}}{J_{se}}$, and X is defined as $X = \frac{J_d}{J_{se}}$, as before. Repeating the same algebra for the other structures gives the following set of expressions:

$$A_I : \langle \mathbf{S} \rangle = \coth \left[-\beta \left(+4J_d - 3J_{se} + 6J'_{se} \langle \mathbf{S} \rangle \right) \right] \tag{5.15}$$

$$\tilde{T}_c = \frac{1}{2} \left(-4X + 6Z - 3 \right) \tag{5.16}$$

$$A_{II} : \langle \mathbf{S} \rangle = \coth \left[-\beta \left(-2J_d - 3J_{se} - 6J'_{se} \langle \mathbf{S} \rangle \right) \right] \tag{5.17}$$

$$\tilde{T}_c = \frac{1}{2} \left(2X + 6Z + 3 \right) \tag{5.18}$$

$$A_{III} : \langle \mathbf{S} \rangle = \coth \left[-\beta \left(+2J_d + 3J_{se} - 6J'_{se} \langle \mathbf{S} \rangle \right) \right] \tag{5.19}$$

$$\tilde{T}_c = \frac{1}{2} \left(-2X + 6Z - 3 \right) \tag{5.20}$$

The experimentally found ground state is A_{II}, and thus it is possible to compare the mean field value for this state with the experimental evidence.

Parameter	This work (UHF)	Catti and Sandrome (UHF)	Rollman et al (GGA)	Sandratskii et al (LDSA)
X	1.934	1.80	0.11	0.20
Z	0.67	0.68	0.54	0.50
J_{se}	9.73	10.00	138.9	157.1
$\tilde{T}_c$	5.444	5.35	3.17	3.2
T_c (K)	1372	1385	11404	13020
$\frac{3}{4}T_c$(K)	1029	1039	8553	9765

Table 5.13: Mean field predicted transition temperatures for bulk α-Fe_2O_3.

Table 5.13 gives the ratios X and Z again, and the mean field predicted critical temperature. This can be compared with an experimental value for the bulk system of 953 K [106].

Mean field always predicts the transition temperature to be greater than it actually is, because mean field theory ignores the effect of fluctuations. However, it is possible to establish a rule of thumb, relating the mean field value to the true value in an appropriate manner. From mean field values for a number of nearest neighbour Ising models [107, Ch. 33] it seems reasonable to estimate that the true transition temperature is around $\frac{3}{4}$ the mean field predicted value. These calculated values from UHF data compare well with the experimental bulk Néel temperature, whereas, as with other crystal system, the DFT calculations are substantially removed from the experimental point.

From the coupling coefficients for the first row transition metals derived previously, mean field predictions can be made. These are summarised in Table 5.14. The effect of the negative J_{se} can be clearly seen in the prediction of a negative reduced temperature. However, this is an effect of taking ratios - the "true" sign of the temperature is the sign of the product of the

Species	V_2O_3	Cr_2O_3	Fe_2O_3	Co_2O_3	Ni_2O_3
Magnetic order	A_{III}	A_I	A_{II}	A_{II}	FM
X	0.88	88.5	1.934	0.83	-0.88
Z	0.18	15.8	0.67	0.39	-0.17
J_{se}	-5.14	-0.11	9.73	133.22	-8.33
$\tilde{T}_c$	-2.38	-178.5	5.44	3.50	-2.75
T_c (K)	316	508	1372	12076	593
$\frac{3}{4}T_c$(K)	237	380	1029	9057	444

Table 5.14: Mean field predictions of transition temperatures for first row transition metal corundum structured sesquioxides. The negative reduced temperatures for chromium and vanadium sesquioxide is a mathematical artifact, as can be seen by the real temperatures predicted.

reduced temperature and the J_{se}. In the cases where J_{se} is always positive, as was assumed earlier, these terms are all positive, which matches with expectations.

The Néel temperature predicted for vanadium sesquioxide is about half of the observed value, being 600 K. It should be noted, however, that vanadium sesquioxide is metallic in character, not insulating as the UHF treatment predicts, making it difficult to draw strong conclusions from this. The value for Cr_2O_3 is very close to the observed 350 K. As mentioned before Co_2O_3 and Ni_2O_3 have not been observed, so there is no measurement with which to compare the prediction. However, in terms of the general behaviour of the magnetic insulators, the value for Co_2O_3 is unbelievably high, being higher than the highest known melting point of any oxide (thorium oxide, at 3600 K), or indeed, any binary compound (hafnium carbide, at 4000K). The predicted Curie temperature for nickel sesquioxide is much more believable.

For the set of interaction coefficients generated from the layered system, it is slightly more complex. For the A_{II} state, the bulk system with all

coefficients gives:

$$A_{II} : \langle \mathbf{S} \rangle = \coth \left[-\beta \left(-3J_d + J'_d - 3J_{se} - 6J'_{se} \langle \mathbf{S} \rangle \right) \right] \tag{5.21}$$

$$\tilde{T}_c = \frac{1}{2} \left(3X - 1YX + 6Z + 3 \right) \tag{5.22}$$

Inserting the values found for the core interactions from the layered systems, finds a bulk reduced critical temperature of 15.56, corresponding in this case to a critical temperature in the mean field of 2073 K, 3/4 of which is 1555 K, significantly higher than the temperature predicted by the three parameter bulk model.

A mean field model can be generated for a layered system. It is reasonable to look for the critical temperature as a function of the number of monolayers. This can be well represented by a matrix containing all the interactions for the system, mathematically equivalent to a system of equations, with one equation per spin. Unlike the FCC (111) layers studied earlier, there is no closed form for the eigenvalues of the matrix, so these matrices were solved by use of the numerical solver previously described.

With so many parameters, it is of little benefit to define a reduced temperature, so the mean field equations were solved to give a value in meV, which was then converted to Kelvin immediately. These are listed in Table 5.15. In the case of the FCC (111) layers, the reduction in film thickness resulted in the mean field predicted temperature reducing, and the difference between the Monte Carlo simulation and the mean field prediction also reduced. Reduction of the dimensionality of Monte Carlo [107] in general

Number of monolayers	3	4	5	6	7	8	9	10
Critical temperature	855	945	986	1277	1311	1333	1346	1354
3/4 T_c	641	709	740	958	983	1000	1009	1015

Table 5.15: Mean field predicted critical temperatures for non-reconstructed (0001) monolayers of corundum structures Fe_2O_3. The bulk value for this set of coefficients is a mean field critical temperature of 2073 K.

supports this trend, so that it is reasonable to consider that the 3/4 estimate is likely to under estimate the critical temperature for the thinnest films. Without detailed Monte Carlo simulations, however, it is not possible to quantify this.

The general trend seen with the mean field predictions is similar to that seen in the FCC lattice, with the thinner layers having a reduced critical temperature. No numerical instability was observed with the successive approximation solver, which would indicate that the initial condition did not match the true ground state, or similar incorrect magnetic state forced upon the system. The mean spin, which is shown in Figure 5.7 for a 6 monolayer system, shows no sign of multicritical behaviour, or any other deviation from a smooth set of curves.

5.8 Conclusion

The combination of UHF electronic structure calculations mapped onto an Ising model predicts bulk transition temperatures for Fe_2O_3 and Cr_2O_3 that are close to the experimentally determined values. This method works less well for bulk V_2O_3, and no general trends were observed across the first row transition metal oxides examined.

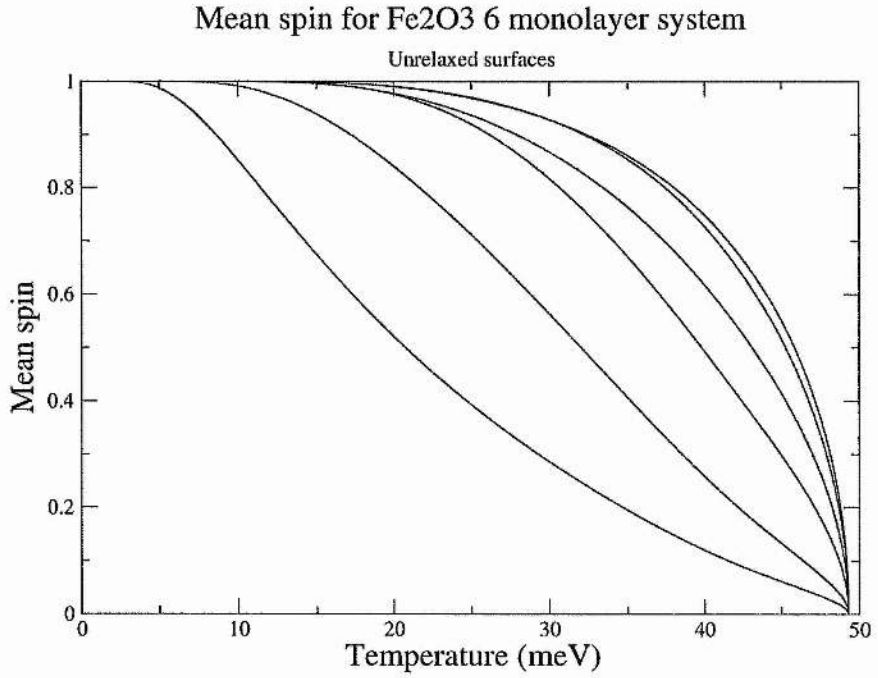

Figure 5.8: Mean spin for a 6 monolayer corundum structured Fe_2O_3. The 6 distinct spins can be clearly seen, with the outer layers in the bottom left, and the inner layers towards the top right.

Fitting of an Ising model to electronic structure data for an unreconstructed film of Fe_2O_3 gave a set of coupling constants, including a set for all four bulk values. Although these were distinct from those obtained from bulk calculations, they do show that the difference in the pair of nearest neighbour interactions and in the pair of next-nearest neighbour interactions is roughly equal in percentage terms. This suggests that for the approximation of a pair of interaction coefficients to be equal is not necessarily better applied to the nearest neighbour interactions, even although they operate over significantly closer distances, compared to the next nearest neighbour interactions.

The mean field predictions for an unreconstructed film show a reduction

in the critical temperature for thinner films, but do not suggest any other change in qualitative behaviour between bulk and the film, for this species.

Chapter 6

Conclusion

Monte Carlo simulations and mean field analysis of thin films of rock salt structured materials with (111) surfaces predict a significant, and hitherto unreported change in the magnetic behaviour in the region where the next nearest neighbour interaction coefficient favours antiparallel alignment, and is much greater in magnitude than the nearest neighbour interaction. This is exactly the situation seen in first row transition metal monoxides that adopt this structure.

There is some debate over the exact values of these interaction coefficients in compounds, with the most studied being the paradigm material of nickel oxide, where the values are known to within around 10 to 15 %. However, it is clear that their behaviour is dominated by the effect of the next nearest neighbour interactions, and that the nearest neighbour interactions favour parallel alignment more strongly as the atomic number increases. The best estimate for MnO predicts that the nearest neighbour interactions favour antiparallel alignment, and in NiO these favour parallel alignment. In the

bulk system, these small interactions are swamped by the much stronger next nearest neighbour interaction, and they have the same qualitative behaviour.

The breaking of the symmetry of the system in a thin film has a striking effect. There is a new phase boundary, not present in the bulk, which separates the case where the isomagnetic planes are aligned parallel with the physical boundaries when the nearest neighbour interactions favour parallel alignment, and the case where the isomagnetic planes are aligned at an angle to the physical surfaces, where the nearest neighbour interactions favour antiparallel alignment. Clearly, this phase boundary is right in the middle of the region of physical interest, and will thus dominate the behaviour of thin films of these oxides.

The most obvious effect of this phase boundary is to depress the Néel temperatures significantly, far below the effect that might have been predicted in the absence of this phase transition. Previous work on films of this structure with a (100) oriented surface predicted a depression of the critical temperature that agreed very well with experimental evidence, and did not show such a phase transition. This work predicts that the thinnest layers will have a critical temperature around half that for the (100) oriented layer, although the effect of the phase transition is rapidly offset by an increase in film thickness, becoming negligible for films thicker than around 12-14 monolayers.

Octopolar reconstruction has no qualitative effect on these systems, save for the thinnest systems, and the qualitative effect is equivalent to a system about one monolayer thinner. In the case of a bilayer, this reduces to a monolayer, which is known to behave differently, due to the lack of any next

nearest neighbour interactions in the plane.

The use of UHF calculations and the Ising model that was shown to work well for rocksalt structured materials seems to work reasonably well for corundum structured sesquioxides also. Predictions based on electronic structure calculations and mean field analysis suggest Néel temperatures close to the experimental determinations for both Cr_2O_3 and Fe_2O_3. These were done under the assumption that the two possible nearest neighbour interactions were the same. Given that the Néel temperature of chromium sesquioxide is around one third that of iron sesquioxide, this is an encouraging sign. The method does appear to fail for vanadium sesquioxide, although in this case is it likely due to the incorrect prediction of an insulating state by UHF. This is similar to case for VO, where UHF predicts the incorrect magnetic ground state.

Calculation of electronic energies for a hematite film with truncated, unrelaxed surfaces gave access to a range of the possible coupling constants, including a complete set for the bulk system. These were obtained under the assumption that the surface monolayers have a different electronic structure from the rest of the film, and the rest of the film was uniform in electronic structure. This gave a slightly higher critical temperature. These coefficients also enabled an estimation of the mean field behaviour of thin films, which was predicted to be largely in line with the general quantitative trends seen for the rocksalt system. However, the determination of the bulk interaction coefficients from the film shows that the relative differences between the pairs of nearest and next nearest interaction coefficients are about the same, despite the distances the nearest neighbour interactions operate over being

almost the same.

6.1 Further work

For the stoichiometric, unreconstructed layers, the phase diagram has now been described for both the (111) layers in this work, and (100) layers in a previous work. These crystallographic orientations are the most common studied and utilised, so there are no other obvious orientations that are suggested by physical concerns. It is expected that films oriented with a (210) surface will show a splitting of phases in the AF3 region, similar to the (111) films. There are no magnetic systems, nor other systems that are analogous, known to this author, so there is no physically sourced drive to examine such a system at present.

With the reconstructed surfaces, examination of the 3/4 and 1/4 surfaces would complete the set of possible 2x2 surface textures. Whilst they have not been observed in physical systems, these, along with an examination of randomly distributed surface textures, would round out the investigation of the effect of the surface texture on the ordering within the film. It appears that the surface texture does not affect the qualitative behaviour of these systems, save where an effective reduction in film thickness produces alternate behaviour. Confirmation of this would be useful in terms of experimental results, where it would impact into the preparation needed prior to measurements - if it can be shown that the film properties are insensitive to the surface texture, then that makes experimental determination a simpler prospect. It appears that, while not totally insensitive to the surface texture,

the effect is limited.

For the corundum structured materials using some of the higher order magnetic orders to make a determination of all five terms in the Ising model would remove any ambiguity about the validity of the approximations that were made here.

Given that the (0001) layer in the corundum structure is unique, it is not expected that there is any qualitative change in behaviour within that system. However, Monte Carlo analysis is needed to confirm this and to quantify the effects of fluctuations in the system is a desirable next step from this work.

Bibliography

[1] M. N. Baibich *et al.*, Phys. Rev. Lett. **61**, 2472 (1988).

[2] P. Grunberg, Physics Today **54**, 31 (2001).

[3] S. Gardelis, C. G. Smith, C. H. W. Barnes, E. H. Linfield, and D. A. Ritchie, Phys. Rev. B **60**, 7764 (1999).

[4] L. Technologies, Lucent press release, 1998.

[5] K. O. Legg, M. Prutton, and C. Kinniburgh, J. Phys. C **7**, 4236 (1974).

[6] M. Prutton, J. A. Walker, M. R. Welton-Cook, R. C. Felton, and J. A. Ramsey, Surf. Sci. **89**, 95 (1979).

[7] V. E. Henrich and P. A. Cox, *The Surface Science of Metal Oxides* (Cambridge University Press, 1994).

[8] K. Wandelt, Surf. Sci. Rep. **2**, 1 (1982).

[9] G. W. R. Leibbrandt, L. H. Spiekman, and F. H. P. M. Hebraken, Surf. Sci. **287/288**, 250 (1993).

[10] M. Bäumer, D. Cappus, G. Illing, H. Kuhlenbeck, and H. J. Freund, Surf. Sci. **253**, 116 (1991).

[11] R. M. Jaeger *et al.*, Surf. Sci. **259**, 235 (1991).

[12] Y. C. Chung and B. J. Wuensch, J. Am. Ceram. Soc. **79**, 695 (1996).

[13] N. Uekawa and K. Kaneko, Advanced Materials **7**, 312 (1995).

[14] B. Pejova, T. Kocareva, M. Najdoski, and I. Grozdanov, App. Surf. Sci. **165**, 271 (2000).

[15] W. Weiss and G. A. Somorjai, J. Vac. Sci. Tech. **11**, 2138 (1993).

[16] T. Fujii *et al.*, Surf. Sci. **366**, 579 (1996).

[17] S. I. Yi, Y. Liang, S. Thevuthasan, and S. A. Chambers, Surf. Sci. **433**, 212 (1999).

[18] R. Lacman, Colloq. Int. CNRS **152**, 195 (1965).

[19] P. W. Tasker, J. Phys. C **12**, 4977 (1979).

[20] C. Noguera, J. Phys.: Condens. Matter **12**, R367 (2000).

[21] O. L. Warren and P. A. Thiel, J. Chem. Phys. **100**, 659 (1994).

[22] C. A. Ventrice, Jr., T. Bertrams, H. Hannemann, A. Broddle, and H. Neddermeyer, Phys. Rev. B **49**, 5773 (1994).

[23] F. Rohr *et al.*, Surf. Sci. **315**, L977 (994).

[24] D. Wolf, Phys. Rev. Lett. **68**, 3315 (1992).

[25] M. Schönnenbecka *et al.*, Surf. Sci. **347**, 337 (1996).

[26] D. Cappus *et al.*, Surf. Sci. **337**, 268 (1995).

[27] C. R. Henry and H. Poppa, Thin Solid Films **189**, 303 (1990).

[28] R. Plass *et al.*, Phys. Rev. Lett. **81**, 4891 (1998).

[29] W. C. Mackrodt *et al.*, Phil. Mag. A **68**, 653 (1993).

[30] M. D. Towler *et al.*, Phys. Rev. B **50**, 5041 (1994).

[31] H. Shaked, J. Faber, and R. L. Hittermann, Phys. Rev. B **38**, 11901 (1988).

[32] G. A. Slack, J. App. Phys. **31**, 1571 (1960).

[33] M. Catti, G. Valerio, and R. Dovesi, Phys. Rev. B **51**, 7441 (1995).

[34] M. Catti, G. Sandrone, G. Valerio, and R. Doves, J. Phys. Chem. Solids **57**, 1735 (1996).

[35] M. Catti and G. Sandrome, Far. Diss. **106**, 189 (1997).

[36] N. Erdman, O. Warschkow, D. E. Ellis, and L. D. Marks, Surf. Sci. **470**, 1 (2000).

[37] A. Barbier *et al.*, Phys. Rev. Lett. **84**, 2897 (2000).

[38] F. Finocchi, A. Barbier, J. Jupille, and C. Noguera, Phys. Rev. Lett. **92**, 136101 (2004).

[39] I. de P R Moreira, F. Illas, and R. L. Martin, Phys. Rev. B **65**, 155102 (2002).

[40] D. Ködderitzsch *et al.*, Phys. Rev. B **66**, 064434 (2002).

[41] C. de Graaf, R. Broer, and W. C. Nieuwpoort, Chem. Phys. Lett **271**, 372.

[42] G. Srinivasan and M. S. Seehra, Phys. Rev. B **29**, 6295 (1984).

[43] M. E. Lines and E. D. Jones, Phys. Rev. **139**, A1313 (1965).

[44] R. Shanker and R. A. Singh, Phys. Rev. B **7**, 5000 (1972).

[45] M. T. Hutchings and E. J. Samuelsen, Phys. Rev. B **6**, 3447 (1972).

[46] R. E. Dietz, W. F. Brinkman, A. E. Meixner, and H. J. Guggenheim, Phys. Rev. B **27**, 814 (1971).

[47] T. Oguchi, K. Terakura, and A. R. Williams, Phys. Rev. B **28**, 6443 (1983).

[48] M. Kohgi, Y. Ishikawa, and Y. Endoh, Solid State Comm. **11**, 391 (1972).

[49] B. A. Coles, J. W. Orton, and J. Owen, Phys. Rev. Lett. **4**, 116 (1960).

[50] G. E. Kugel, B. Hennion, and C. Carabatos, Phys. Rev. B **18**, 1317 (1978).

[51] W. C. Mackrodt, D. S. Middlemiss, and T. G. Owens, Phys. Rev. B **69**, 115119 (2004).

[52] M. Born and J. R. Oppenheimer, Ann. Physik **84**, 457 (1927).

[53] J. H. Monkhorst, Phys. Rev. B **20**, 1504 (1979).

[54] P. Hohenberg and W. Kohn, Phys. Rev. **136**, B864 (1964).

[55] L. H. Thomas, Proc. Camb. Phil. Soc. **23**, 542 (1927).

[56] E. Fermi, Z. Physik **48**, 73 (1928).

[57] P. A. M. Dirac, Proc. Camb. Phil. Soc. **26**, 376 (1930).

[58] J. C. Slater, Phys. Rev. **81**, 385 (1950).

[59] W. Kohn and L. J. Sham, Phys. Rev. **140**, A1133 (1965).

[60] A. D. Becke, Phys. Rev. A **38**, 3098 (1988), B3LYP hybrid paper.

[61] W. Heisenberg, Zeit. f. Phys. **49**, 619 (1928).

[62] R. Krachler, J. Alloy Compd. **189**, 169 (1992).

[63] E. Ising, Zeit. f. Phys. **31**, 253 (1925).

[64] H. A. Kramers, Physica **1**, 182 (1934).

[65] P. W. Anderson, Phys. Rev. **79**, 350 (1950).

[66] R. I. Hines, N. L. Allan, G. S. Bell, and W. C. Mackrodt, J. Phys.: Condens. Matter **9**, 7105 (1997).

[67] W. Schweika, K. Binder, and D. P. Landau, Phys. Rev. Lett. **65**, 3321 (1990).

[68] R. Lipowsky, J. App. Phys. **55**, 2485 (1984).

[69] D. Alders *et al.*, Phys. Rev. B **57**, 11623 (1998).

[70] D. P. Landau and K. Binder, Phys. Rev. B **41**, 4633 (1990).

[71] H. Bethe, Z Phys **71**, 205 (1931).

[72] L. Onsager, Phys. Rev. **65** (1944).

[73] B. Kaufman, Phys. Rev. **76** (1949).

[74] N. Metropolis, A. Rosenbluth, M. Rosenbluth, A. Teller, and E. Teller, J. Chem. Phys. **21**, 1087 (1953).

[75] D. P. Landau and K. Binder, *A Guide to Monte Carlo Simulation in Statistical Physics* (Cambridge Universtiy Press, 2000).

[76] D. E. Knuth, *The art of computer programming, Vol 2: Semi numerical algorithms* (Addison-Wesley, 1969).

[77] K. Koike and T. Furukawa, Phys. Rev. Lett. **77**, 3921 (1996).

[78] W. C. Mackrodt and C. Noguera, To be submitted .

[79] A. Berbier *et al.*, Phys. Rev. Lett. **84**, 2897 (2000).

[80] C. Noguera and W. C. Mackrodt, (100) rocksalt monte carlo code, (test1.f), 1999.

[81] L. Pauling and S. B. Hendricks, J. Am. Chem. Soc. **47**, 781 (1925).

[82] Y. J. Kim, Y. Gao, and S. A. Chambers, Surf. Sci. **371**, 358 (1997).

[83] P. W. Tasker, Adv Ceram **10**, 176 (1984).

[84] J. Guo, D. E. Ellis, and D. J. Lam, Phys. Rev. B **45**, 13647 (1992).

[85] W. C. Mackrodt, R. J. Davey, S. N. Black, and R. Docherty, J Cryst Growth **80**, 441 (1987).

[86] I. Manassidis and M. J. Gillan, Surf. Sci. **285**, L517 (1993).

[87] I. Manassidis and M. J. Gillan, J Am Ceram Soc **77**, 335 (1994).

[88] M. Causa, R. Dovesi, C. Pisani, and C. Roetti, Surf. Sci. **215**, 259 (1989).

[89] G. Renaud, Surf. Sci. Rep **32**, 1 (1998).

[90] C. Rehbein, N. M. Harrison, and A. Wander, Phys. Rev. B **54**, 14066 (1996).

[91] P. J. Lawrence, PhD thesis, University of Bath, 1989, Cr2O3 relaxation by shell model calculations, predicts -59, + 13, -54, +31, 0 by layer spacing.

[92] F. Rohr *et al.*, Surf. Sci. **372**, L291 (1997).

[93] F. Alvarez-Ramirez, J. M. Martinez-Magadan, J. R. B. Gomes, and F. Illas, Surf. Sci. **558**, 4 (2004).

[94] S. Gota, E. Guiot, M. Henroit, and M. Gautier-Soyer, **60**, 14387 (1999).

[95] C. W. Searle and G. W. Dean, Phys. Rev. B **1**, 4337 (1970).

[96] L. M. Levinson, Phys. Rev. B **3**, 3965 (1971).

[97] H. Chow and F. Keffer, Phys. Rev. B **10**, 243 (1974).

[98] S. S. Hanna, J. Heberle, G. J. Perlow, R. S. Preston, and D. H. Vincent, Phys. Rev. Lett. **4**, 513 (1960).

[99] C. J. Song, J. Trooster, N. Benczer-Koller, and G. M. Rothberg, Phys. Rev. Lett. **29**, 1165 (1972).

[100] C. J. Song, J. Trooster, and N. Benczer-Koller, Phys. Rev. B **9**, 3854 (1974).

[101] T. Yang, A. Krishnan, and N. Benczer-Koller, Phys. Rev. B **30**, 2438 (1984).

[102] G. Rollman, A. Rohrbach, P. Entel, and J. Hafner, Phys. Rev. B **69**, 165107 (2004).

[103] L. M. Sandratskii and J. Kübler, EuroPhys. Lett **33**, 447 (1996).

[104] V. R. Saunders *et al.*, *CRYSTAL98 User's Manual*, 1998.

[105] S. Geller, Acta Cryst. B **27**, 821 (1971), Source for Jahn-Teller distortion on Mn2O3.

[106] J. B. Goodenough, *Magnetism and the chemical bond* (Interscience publishers, 1963).

[107] N. W. Ashcroft and N. D. Mermin, *Solid state physics* (Harcourt, Inc., 1976).

Appendix

This section contains important fragments of Fortran computer code, developed during the course of the research.

Variable list

Table 6.1 lists some of the important variable in the code fragments.

Name	Type	Purpose
nc	Integer	Number of layers
l	Integer	Length of slab in the plane
nsp	Integer	Total number of atoms ($nc \cdot l^2$)
n1(xy, z)	Integer Array	No. of direct neighbours of the spin (xy, z)
n1c(i, xy, z)	Integer Array	Z coordinate of i'th neighbour of (xy,z)
n1p(i, xy, z)	Integer Array	XY coordinate of i'th neighbour of (xy, z)
n2, n2c, n2p	Integer Arrays	Equivalents of n1 etc. for the super exchange
p(n1, n2)	Real Array	Energetics for spin flips
t	Real	Reduced temperature, temp $= \frac{k_B \cdot T}{2J_{se}}$
X	Real	Ratio $\frac{J_d}{J_{se}}$

Table 6.1: Selected important variables

Neighbour list routines

This is an example of one the the neighbourlist calcluation routines, for the direct interactions in (111) rocksalt structures. This section of code was written for clarity, on the basis that it is run only once, it was better to be as clear as possible, rather than worry about execution time.

```
      subroutine voisins1
      implicit real*8 (a-h,o-z)
      parameter (lmax = 60, nspmax=lmax*lmax,ncmax=lmax,ntmax=50)
      common /dim/l,nc,nsp
      common /v1/n1p(12,nspmax,ncmax),n1c(12,nspmax,ncmax)
      common /v11/n1(nspmax,ncmax)

        INTEGER :: x, y
        INTEGER, EXTERNAL :: combine
! Variables are initialised to zero (Abridgement)                    10

      do ij=1,nc
      do k = 1, nsp
! Translate to x and y, then combine back again
        x = mod(k-1,l)
        y = ((k-1)/l)
        kk=1
! FIRST NEIGHBOURS IN PLANE COUNTING CLOCKWISE
! NEIGHBOUR 1
        n1p(kk,k,ij) = combine(x+1, y)                               20
        n1c(kk,k,ij) = ij
        kk=kk+1
```

```
! NEIGHBOUR 2 to 5 (Abridged)
! NEIGHBOUR 6
        n1p(kk,k,ij) = combine(x+1, y-1)
          n1c(kk,k,ij) = ij
!
! il existe un plan au=dessus
! FIRST NEIGHBOURS ABOVE PLANE COUNTING CLOCKWISE
         if(ij.eq.nc)then                                          30
! Do nothing
           else
            ij1=ij+1
! NEIGHBOUR 1
        kk=kk+1
        n1p(kk,k,ij) = combine(x-1, y)
        n1c(kk,k,ij) = ij1
        kk=kk+1
! NEIGHBOUR 2
        n1p(kk,k,ij) = combine(x, y)                               40
        n1c(kk,k,ij) = ij1
        kk=kk+1
! NBEIGHBOUR 3
        n1p(kk,k,ij) = combine(x, y-1)
        n1c(kk,k,ij) = ij1
        end if
!
! il existe un plan en=dessous
! FIRST NEIGHBOURS BELOW PLANE COUNTING CLOCKWISE
        if(ij.eq.1)then                                            50
! Do nothing
          else
```

```
          ij1=ij-1
! NEIGHBOUR 1
        kk=kk+1
        n1p(kk,k,ij) = combine(x+1, y)
        n1c(kk,k,ij) = ij1
        kk=kk+1
! NEIGHBOUR 2
        n1p(kk,k,ij) = combine(x, y)                                    60
        n1c(kk,k,ij) = ij1
        kk=kk+1
! NEIGHBOUR 3
        n1p(kk,k,ij) = combine(x, y+1)
        n1c(kk,k,ij) = ij1
        end if
!
          n1(k,ij)=kk
!
      enddo                                                             70
      enddo
      end subroutine voisin1
```

The function "combine" abstracts out the boundary conditions from the inherent geometry of the crystal. Should it be desired to extend the code to handle systems other than periodic in two dimensions (such as 3D bulk, as was done for testing purposes), or to implement other forms of periodic boundaries such as a screw periodicity, only this function need be changed. Thus the nature and orientation of the crystal is de-coupled from it's size and shape, a very useful property.

```
      INTEGER FUNCTION combine (i, j)
      IMPLICIT NONE
      INTEGER, INTENT(IN) :: i, j

      INTEGER :: l, nc, nsp
      COMMON /dim/ l, nc, nsp
! *******************************************************
      combine = mod(i+l,l) + l*mod(j+l,l) + 1
      RETURN
      END FUNCTION combine                                    10
```

Transition energy calculation

The various possible energies for transitions were collected in a lookup table. Strictly, this represents an optimisation, not an algorithmic nessecity. However, due to the time taken to evaluate an exponential function, this optimisation becomes a practical nessecity. It is a straight forward modification to change the array lookup to be a function call to a direct calculation - the core of that routine would be the same as the array population code presented.

```
      subroutine probas(t,X)
      implicit real*8 (a-h,o-z)
      common /prob/p(-12:12,-6:6)
      do i = -12,12
        do j = -6,6
          p(i,j)=dexp((i*X-j)/t)
        end do
```

```
      end do
      return
      end                                                          10
```

Main Monte-Carlo loop

The key section of this code is between lines 50 and 70. The first part counts the sum of the neightbouring spins, in the direct and super-exchange, which are used as indicies into the energies array in the second part.

```
      PROGRAM Ising_monte_carlo
! Variable Decleration (Abridgment)
! Initialise some variables (Abridgment)
! Reading in parameters (Abridgment)
!
      time=cputime()
!
      call voisins1
      call voisins2
      call condinit(init)                                          10
      if(nprint1.gt.0)then
        call print_neighbour_lists(nprint1)
      endif
!
      write(6,*) ' '
      do it=1,ntemp
        call probas(t(it),X)
        call spcorr1(sro1,sro1paral,sro1perp)
        call spcorr2(sro2,sro2paral,sro2perp)
```

```
      call AF21ro(AAF2)                                                    20
      call Ferrolro(FFerro)
!
      if(it.eq.1)then
       write(6,110) aaf2,fferro
110 format(/5x,'INITIAL ORDER PARAMETERS', &
       /5x,'----------------------------', &
       //5x,'AF2',1x,f7.4, &
       /5x,'FM',2x,f7.4)

       if(nprint2.gt.0)then                                                30
        call print_order_by_layer(nprint2)
       end if
      end if
!
      call srand(iseed)
!
!  Initialse remaingin variables to zero (Abridgment)
! DEBUT RUNS MC
      do nr = 1, nruns
                                                                           40
! DEBUT ESSAIS RETOURNEMENTS DE SPINS
!
            do j=1,nc
                  do i = 1, nsp
!
! na1 : NOMBRE DE PREMIERS VOISINS SPIN UP DE L'ATOME(i,j)
! na2 : NOMBRE DE SECONDS VOISINS SPIN UP DE L'ATOME(i,j)
```

```
                na1 = ltype( n1p(1, i, j), n1c(1, i, j) )                    50
                do k = 2, n1(i,j)
                      na1 = na1 + ltype( n1p(k, i, j), n1c(k, i, j))
                end do

                na2 = ltype( n2p(1, i, j), n2c(1, i, j) )
                do k = 2, n2(i,j)
                      na2 = na2 + ltype( n2p(k, i, j), n2c(k, i, j))
                end do

! L'ATOME I EST-IL up or down?                                               60
! ltype(i,j).eq.1 correspond au spin up
! ALGORTIHME DE Metropolis

                if ( ltype(i,j) .ne. 1 ) then
                      if( rand() .le. p(na1, na2)) then
                            ltype(i, j) = 1
                      end if
                else
                      if( rand() .le. p(-na1, -na2)) then
                            ltype(i, j) = -1                                 70
                      end if
                end if
          end do
!  FIN boucle sur i (les sites du plan)
          end do
!  FIN boucle sur j (les couches)
!
         if (nr.gt.n0) then
!
```

```
        call spcorr1(sro1,sro1paral,sro1perp)                          80
        call spcorr2(sro2,sro2paral,sro2perp)
        call AF2lro(AAF2)
        call Ferrolro(FFerro)

      do k=1,nc
!      arotot(k) = arotot(k) +das(AF2lrop(k))
!      crotot(k) = crotot(k) +dabs(Ferrolrop(k))
       arotot(k) = arotot(k) +AF2lrop(k)
       crotot(k) = crotot(k) +Ferrolrop(k)
      end do                                                           90

      af2tot=af2tot+aaf2
      ferrotot=ferrotot+fferro
       sro1tot=sro1tot+sro1
       sro1paraltot=sro1paraltot+sro1paral
       sro1perptot=sro1perptot+sro1perp
       sro2tot=sro2tot+sro2
       sro2paraltot=sro2paraltot+sro2paral
       sro2perptot=sro2perptot+sro2perp
       utot=utot+(-x*sro1+sro2)                                       100
       u2tot=u2tot+(-x*sro1+sro2)*(-x*sro1+sro2)
       chiAF2tot=chiAF2tot+AAF2*AAF2
       chiFerrotot=chiFerrotot+FFerro*FFerro
       end if

    end do
!   FIN boucle sur nr (runs Monte Carlo)

    ntotal=(nruns-n0)
```

```
! Normalise statistics by ntotal (Abridged)                                    110
      u(it)=utot
      cv(it)=(u2tot-utot**2)/(t(it)*t(it))
      chiAF2(it)=(chiAF2tot-BAF2(it)**2)/t(it)
!     chiAF1(it)=(chiAF1tot-BAF1(it)**2)/t(it)
      chiFerro(it)=(chiFerrotot-BFerro(it)**2)/t(it)


        end do
!
!  FIN boucle sur temperature
! Write main output (Abridged)                                                  120
!
      time=cputime()
      write(6,300) time
 300  format(//5x,'END OF CALCULATION',2x,f8.1,1x,'SECONDS')
      stop
      end program Ising monte carlo
```

Octopolar reconstruction

```
      IMPLICIT NONE

! layer specifices which layer to reconstruct, and does no checking that
! it is actually at the surface.
! Type specifies which termination. 0 is oxygen terminated, i.e. remove 1/4 metal
! and type of 1 says metal terminated so remove 3/4 metal

      INTEGER, INTENT(IN) :: layer, type
```

```
      INTEGER, PARAMETER :: lmax = 50, ntmax = 36
      INTEGER, PARAMETER :: nspmax = lmax * lmax, ncmax = lmax          10
! XMAT: This must be increased for further interactions types.
      INTEGER, PARAMETER :: nmatmax = 2, nintermax = nmatmax*nmatmax + nmatmax
      INTEGER :: l, nc, nsp
      INTEGER, DIMENSION(nspmax, ncmax) :: ltype
      COMMON /dim/ l, nc, nsp
      COMMON /typ/ ltype

      INTEGER, EXTERNAL :: combine

      INTEGER :: i, j, k, x, y                                          20
! ****************
! do the system by assuming the following order
!
!    o x o x o x o x o x
!   o o o o o o o o o o
! o x o x o x o x o x
!o o o o o o o o o o
!
! **********

                                                                        30
      if(type .eq. 0) then
            do i = 0, l-1
                  do j = 0, l-1
                        if((mod(i, 2) .eq. 1) .AND. (mod(j, 2) .eq. 1)) then
                              ltype(combine(i, j), layer) = 0
                        end if
                  end do
            end do
```

```
else if(type .eq. 1) then                                          40
      do i = 0, l-1
            do j = 0, l-1
                  if((mod(i, 2) .eq. 1) .AND. (mod(j, 2) .eq.1)) then
                        ! we are at one of the x sites
                        ! so do nothing
                  else
                        ltype(combine(i, j), layer) = 0
                  end if
            end do
      end do                                                       50

else
      ! Error in type parameter
end if

END SUBROUTINE reconstruct
```

Acknowledgements

The author would like thank Dr William C. Mackrodt for his guidence and supervision throughout the course of this work, and for his help and patience in understanding the subtle concepts involved in this work.

The author would also like to thank Derek S. Middlemiss for very many interesting and enligtening conversations during his time at St Andrews, and to Gemma L. Holliday and Thomas G. Owens for similar during their projects.

Financial support for this work was provided by EPSRC.